Fluorene based π-Conjugated System for Multifunctional Applications

Jinjia XU

August 2016

Fluorene based π-Conjugated System for Multifunctional Applications

Jinjia XU

Doctoral Program in Materials Science and Engineering

Submitted to the Graduate School of
Pure and Applied Sciences
in Partial Fulfilment of the Requirements
for the Degree of Doctor of Philosophy in
Engineering
at the
University of Tsukuba

Table of Contents

General Introduction 2

Chapter 1. Phosphorescence Emission from Pure Organic Fluorene Derivative in Solution at Room Temperature 17

Chapter 2. RGB Trichromophoric Nanoparticle with Dual FRET: Highly Sensitive Fluorogenic Response toward Polyanions 40

Chapter 3. Multiple Emissions from Indenofluorenedione in Solution and in Polymer Film 85

Conclusions 111

List of publications 113

Acknowledgments 115

General Introduction

The π-conjugated system

The π-conjugated organic materials have been extensively employed to design and utilize for various functional materials, including organic optoelectronic devices,[1] organic light-emitting diodes (OLEDs),[2] organic thin film transistors (OFETs),[3] organic solar cells,[4] sensing and imaging[5] owing to their excellent luminescent properties, various structures, versatile modification, good photostability and processability. The chemical structures of typical conjugated polymer building blocks were illustrated in Scheme 1.

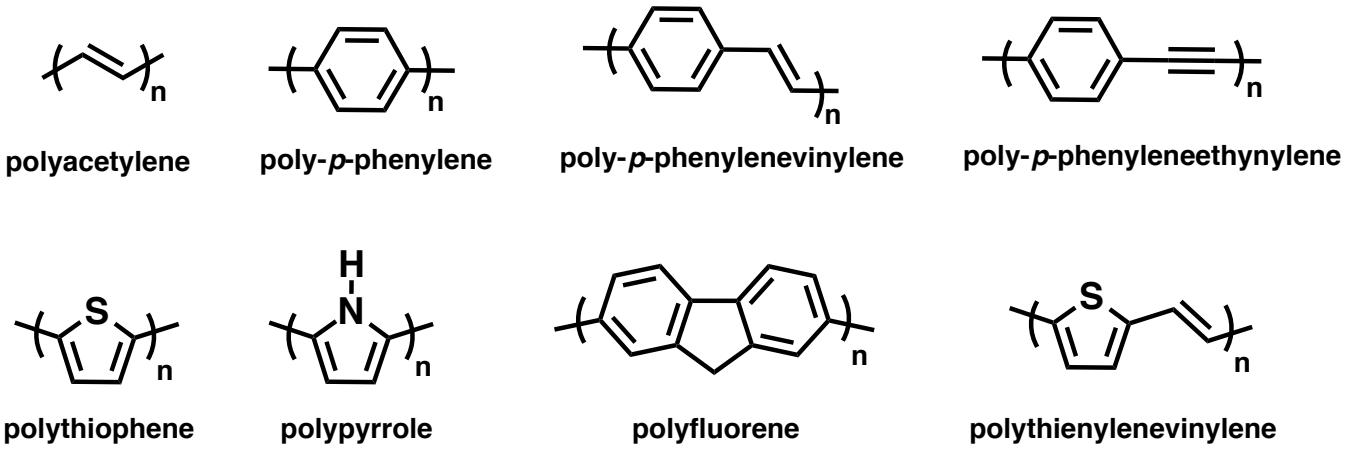

Scheme 1. Chemical structures of typical conjugated polymer building blocks.

The fluorene based π-conjugated building blocks

As one of promising materials, fluorene based materials have attractive and advantageous properties such as rigid and planar structures, easy modification through synthetic methods, thermal and oxidative stability as well as high photoluminescence quantum yield.[6] Therefore, the π-conjugated system based on fluorene building blocks is of great importance in various applications, such as organic electronic and photonic devices, chemo- or bio-sensing, imaging, and supramolecular assembly.[7] Particularly, the fluorene-based π-conjugated system with interesting and unique luminescent properties are wildly investigated in optoelectronic devices[8] and bio-related sensing, imaging and labeling applications.[9] Typical examples are illustrated in Scheme 2.

Chemo-sensor

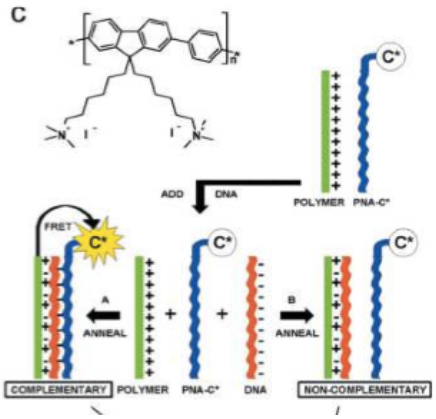

Organic Semiconductor

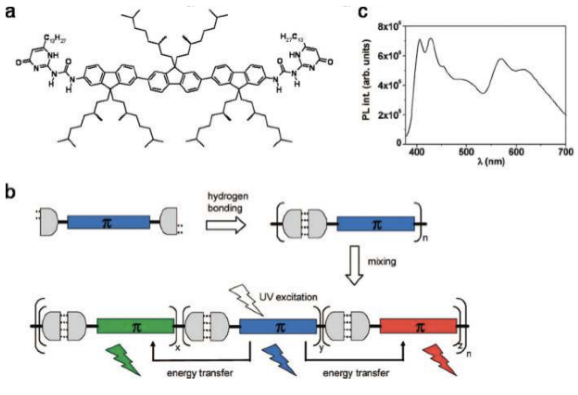

Supramolecular Organization

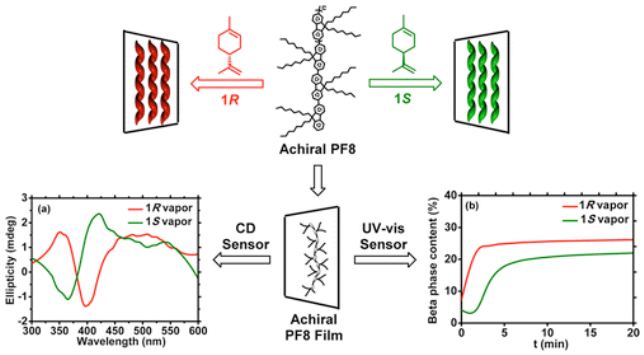

Bio-imaging

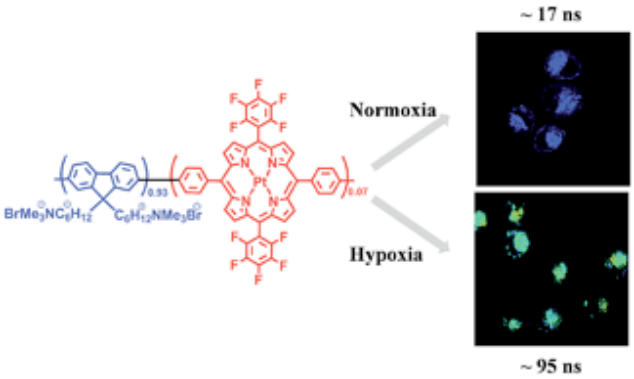

Scheme 2. Illustration of fluorene-based materials utilized in chemo-sensing, bio-imaging, supramolecular organization and organic semiconductors.

From the structural points of view, fluorene is a common polycyclic aromatic hydrocarbon with rigid and planar structure and well known for intense fluorescence.[10] The decoupling provided by bonding groups to fluorene's 9-position is also noteworthy, as these groups are placed at 109° angles to the π-conjugated system comprising fluorene molecules (Figure 1).[11] This allows solubility and aggregation behavior of fluorene compounds to be modulated independently of their electronic properties. These properties have been exploited extensively in many fluorene derivatives that have grown to be a major field in organic electronic and photonics, exhibiting efficient polarized lighting emission,[12] long-lasting blue electroluminescence,[13] impressive lasing gain,[14] and promising performance in organic solar cells.[15]

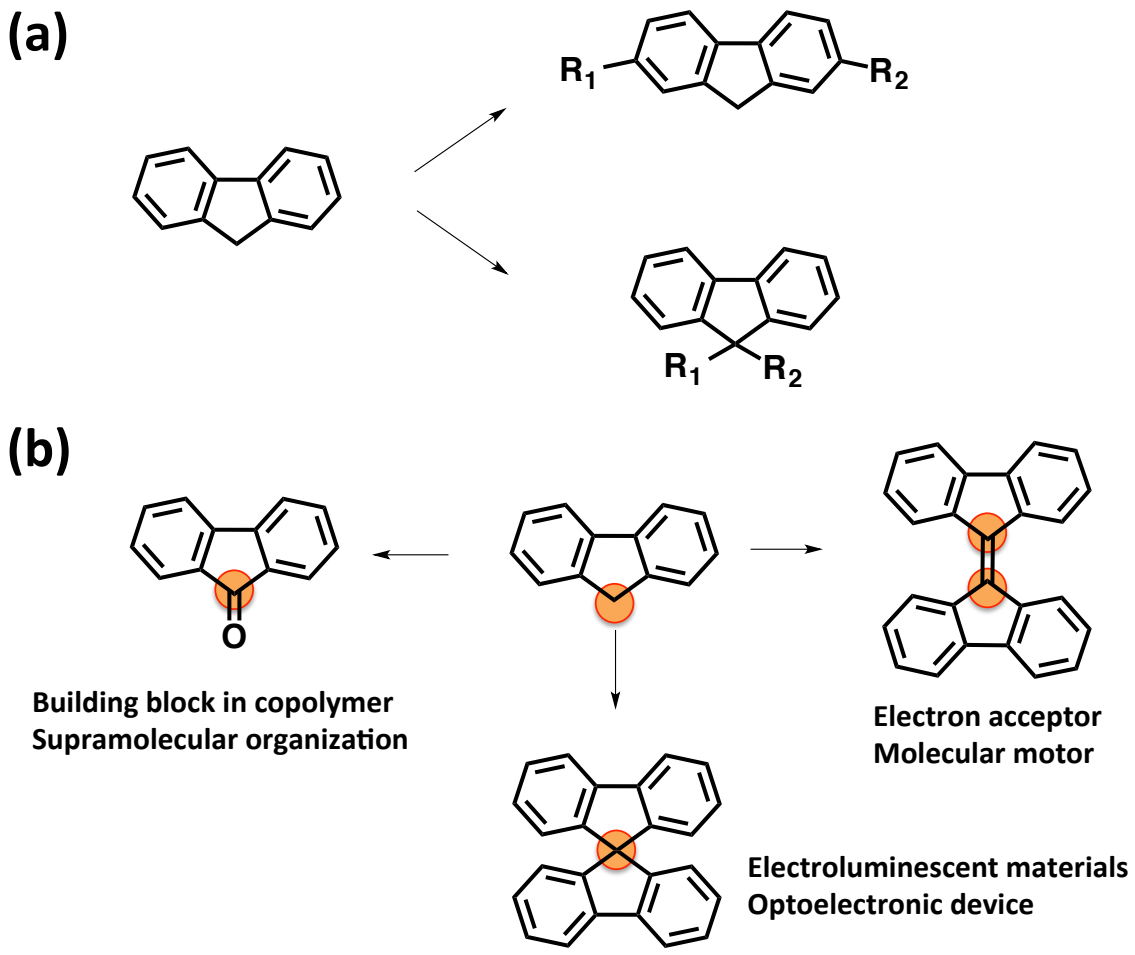

Figure 1. (a) Schematic illustration of two most commonly used synthetic strategies to functionalize the fluorene derivatives; (b) examples of extended building blocks based on fluorene π-conjugated system.

The optical and electronic properties of fluorene-based materials are highly dependent on both the chemical structures and supramolecular organization.[16] Moreover, photophysical properties of π-conjugated systems are generally known to be very sensitive to local environments. Fluorescence phenomena that involve fluorescent resonance energy transfer, intra-/inter-molecular charge transfer, intermolecular photon transfer, excimer/exciplex formation are highly affected by relative distance or orientation of fluorophores, conformation of individual fluorophores and local environments. In this thesis, our concern is to develop the new fluorene-based luminescent materials with unique properties and interesting functionalities via control over the deactivation pathways.

- **Control over the deactivation pathways toward developing the new luminescent materials with unique properties and interesting functionalities**

(a) Enhance the efficient intersystem crossing to generate metal-free room temperature **phosphorescence**

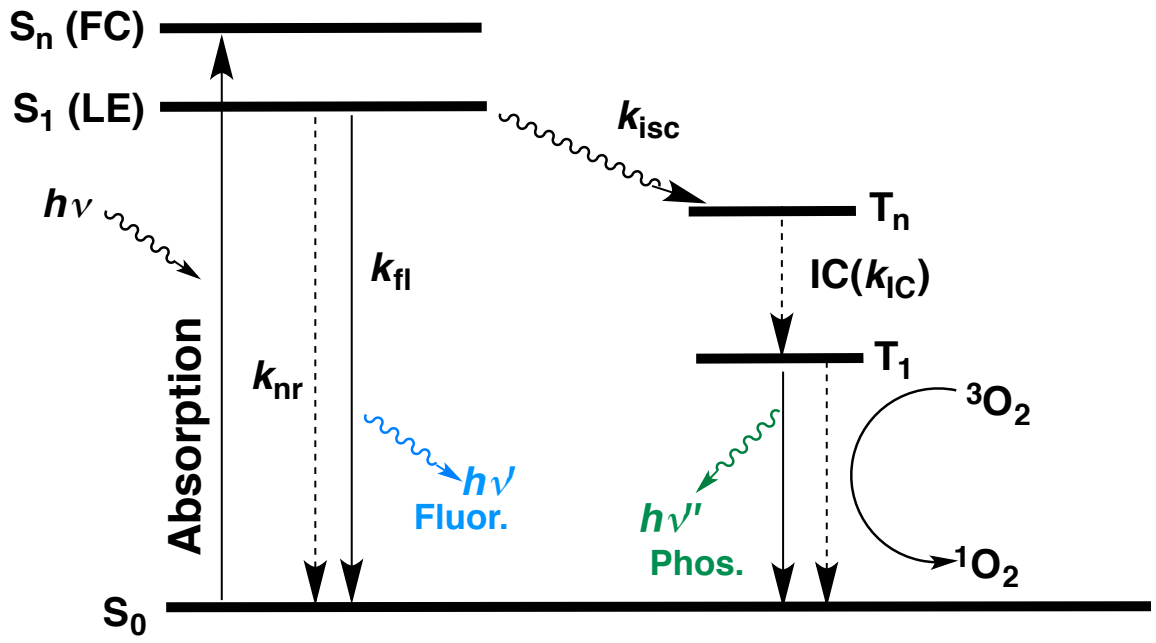

Figure 2. Schematic illustration of phosphorescence based on Jablonski energy diagram. (S_0: ground state, S_1: excited singlet state, T_1: excited triplet state, IC: Internal Conversion, ISC: Intersystem Crossing, LE: locally excited state, FC: Frank Condon, K_{nr}: non-radiative decay constant, K_{fl}: fluorescent decay constant, K_{IC}: internal conversion constant, K_{ISC}: intersystem crossing constant)

Luminescence, the emission of light by electronically excited states of the molecules, can be formally divided into two categories, namely, fluorescence and phosphorescence, according to the nature of the excited states. In excited singlet state, the electron in the excited orbital is paired to the other electron in the ground state orbital. Consequently, return to the ground state is spin-allowed and occurs rapidly by emission of a photon, resulting in fluorescence. On the other hand, phosphorescence is emission of light from excited triplet states, in which the electron in the excited orbital has the same spin orientation as the ground state electron. Transition to the ground state is forbidden and the emission rates are slow, so that phosphorescence lifetime is typical milliseconds to seconds (Figure 2). On the other hand, different from rapidly radiative decay from singlet excited state yielding prompt fluorescence, direct radiative decay from triplet excited state resulted in phosphorescence. Owing to

association with triplet state during the radiative decay process, phosphorescence possesses two characteristic features that long photoluminescence lifetime, typically in the microsecond to millisecond range, and easily quenched by di-oxygen.[17] There is a great deal of interest in development of phosphorescence materials, due to their potential applications in display, lasing, optical storage and sensing because theoretically they could realize 100 % external electroluminescence efficiencies that is three-fold higher than fluorescence alternatives.[18] In general, there are two critical prerequisites for facilitating phosphorescence: (1) spin-flipping from an excited singlet state to an excited triplet state and (2) efficient radiative decay from the excited triplet state to the ground state compared with non-radiative decays.[19] Accordingly, many efforts have been devoted to developing the materials that undergo significant spin-orbital coupling to harvest triplet excitons through intersystem crossing. However, the range of such materials has narrowed to include only organometallic complexes, particularly platinum and iridium.[20] The metal-free pure organic phosphorescence materials are still limited, because the highly bonded nature of electrons in metal-free organic materials leaves them little freedom and less impetus to emit from triplet state.[21] Therefore, metal-free pure organic phosphors under practical conditions are highly desirable in order to compete with relatively high-cost and less stable organometallic counterparts. Recently, metal-free pure organic materials exhibiting phosphorescence have been reported in crystalline systems, probably attributable to aromatic carbonyls, the heavy atom effect, and halogen bonding.[22] In this materials design, these three prerequisites presumedly promote spin-orbital coupling and suppress vibrational loss of excited triplet state at the same time by strict order of the crystal structures. Although these findings are promising breakthroughs for the development of metal-free phosphors under ambient conditions, there still reminds many limitations, such as no phosphorescence observed in solution and high quality requirements for crystal growth leading to difficulties in large-scale device fabrication and processing. Herein, **chapter 1** of this thesis described one novel and meaningful phenomenon that the metal-free pure organic fluorene derivative bearing the bromide and aldehyde groups unexpectedly exhibited phosphorescence in solution or within host matrix at room temperature. This fascinating serendipity makes it an ideal complement to reported crystalline-induced phosphorescence system to furnish fundamental insight into the development of metal-free pure organic phosphors under ambient conditions to compete with organometallic counterparts that have been systematically investigated.

(b) White light emissive nanoparticle assisted by **FRET** towards polyanoinic sensing

In general, the strategies for tuning fluorescence emission spectra and emissive colors of π-conjugated organic materials mainly focus on changing substituents or π-conjugated length[23] and controlling molecular stacking modes or intra- and intermolecular interactions.[24] One outstanding method for fine-tuning fluorescence emission spectra and colors is involvement of fluorescence resonance energy transfer (FRET).[25-27] FRET is a physical phenomenon occurring in natural photosynthetic systems where excitation energy from an excited donor is non-radiatively transferred to a proximal ground-state energy acceptor (donor and acceptor here refer to energy donor and energy acceptor) through long-range dipole-dipole interaction (Figure 3).

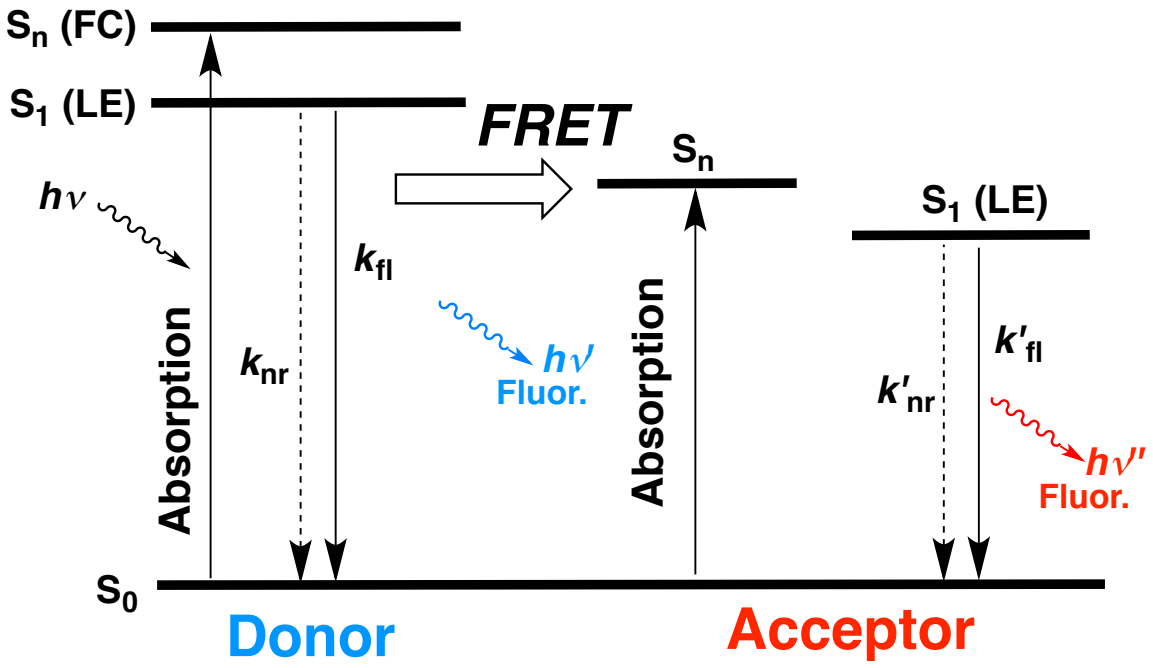

Figure 3. Schematic illustration of the process of fluorescence resonance energy transfer (FRET) based on Jablonski energy diagram. (S_0: ground state, S_1: excited singlet state, LE: locally excited state, FC: Frank Condon, K_{nr}: non-radiative decay constant of energy donor, K_{fl}: fluorescent decay constant of energy donor, K'_{nr}: non-radiative decay constant of energy acceptor, K'_{fl}: fluorescent decay constant of energy acceptor)

The efficiency of FRET is highly dependent on three factors: spatial distance, molecular orientation, and the extent of spectra overlap of donors and acceptors.[26b] In solution, the transition orientation of molecule is random, thus orientation factor is approximated to be 2/3, which is an average of the values

for the donors and acceptors randomized through rotational diffusion prior to energy transfer.[25] The extent of spectral overlap integral between absorption of acceptor and emission of donor has been considered to control the FRET in some donor-acceptor systems.[26] Moreover, the spatial distance dependence of FRET has been widely used as a "spectroscopic ruler" capable of measuring the donor-to acceptor distance in the range of 20-100 Å, and to study conformational distribution and dynamics of bio-macromolecules. Therefore, much more attention has been paid into controlling the spatial distance between donor and acceptor aiming at modulation of FRET.[27] Among the various FRET-controlled fluorescence color tuning systems explored so far, use of nanoparticle scaffolds encapsulating acceptors are regarded as one fascinating method to ensure the spatial proximity of well-defined donor-acceptor molecules and thus facilitate the highly efficient FRET.[28] As a result, the fluorescent organic nanoparticles derived from π-conjugated systems such as oligofluorene derivatives as a donor scaffold for efficient FRET are crucial, which provides a simple and efficient strategy to improve fluorescence efficiency and tune emission colors. Several methods are available for the preparation of nanoparticle in water, of which reprecipitation is the most simple and commonly used one, where a solution of oligomer or polymer dissolved in organic solvents, is rapidly injected into a large excess of water under stirring.[29] The size of resultant nanoparticle is dependent on the initial concentration of the organic solution. Therefore, it is possible to tune the size of nanoparticles over a wide range of diameters for various applications, for example, optimization of conditions to obtain dispersions of nanoparticles around 100 nm in diameter with narrow size distributions is accessible if biological applications are expected.[16d] Moreover, nanoparticles typically show brightness and better photostability than small organic fluorophores, because of the large numbers of chromophores per particle.[30a, 30b] Additionally, nanoparticles, built from organic building blocks, show good dispersion in water and can be surface-modified, thus allowing specific binding affinity towards various bio-related materials in aqueous medium.[30e] This unique supramolecular design provides us an approach to construct unprecedented RGB nanoparticle system with dual FRET feature in aqueous medium towards practical bio-macromolecular detection or sensing with low detection limit and visibly sensitive response.

(c) Unusual multicolor emissions from intramolecular charge transfer (**ICT**) molecules

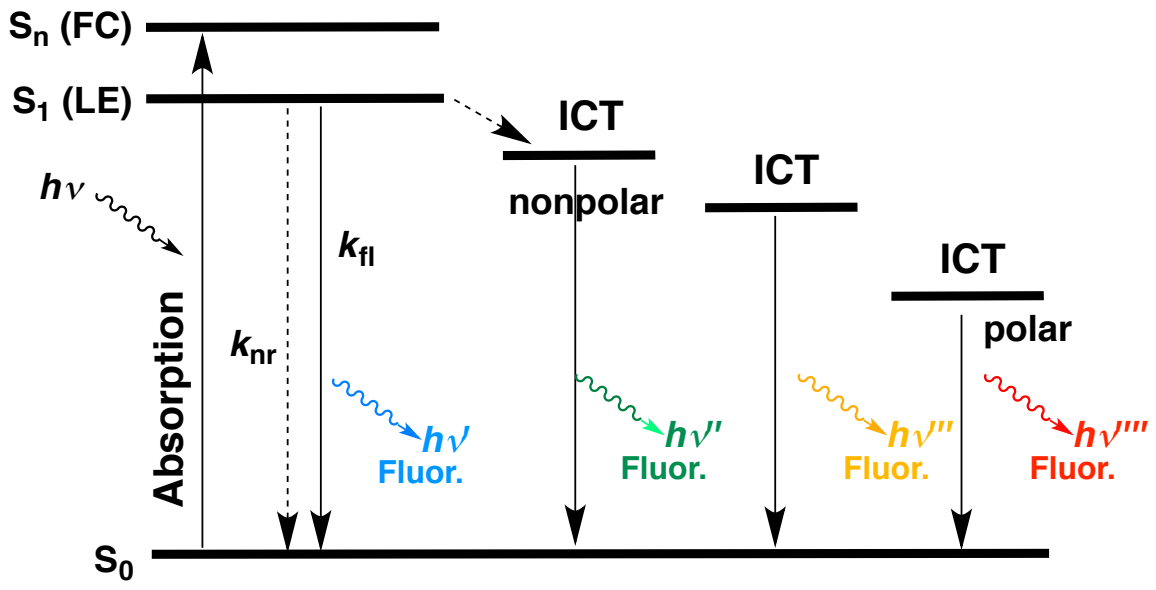

Figure 4. Schematic illustration of the process of intramolecular charge transfer (**ICT**) based on Jablonski energy diagram. (S_0: ground state, S_1: excited singlet state, LE: locally excited state, FC: Frank Condon, K_{nr}: non-radiative decay constant, K_{fl}: fluorescent decay constant)

Intramolecular charge transfer (**ICT**) is a relatively common phenomenon in molecules that consist of a D–A (D and A are defined as charge transfer electron donating or accepting groups rather than excitation energy donors or acceptors), in which an electron transfer process that occurs upon photo-excitation in molecules that usually consist of a donor and acceptor part linked by a single bond.[31] Charge transfer processes include the aforementioned excimer and exciplex formation, which are short-lived excimer or exciplex of which at least one molecule is at the excited state. While the aforementioned processes all reflect relative arrangements of fluorophores, fluorescence phenomena governed by intramolecular charge transfer (**ICT**) involve interaction of an individual fluorophore. **ICT** state returns to the ground state either through red-shifted emission or by nonradiative relaxation (Figure 4). The emission properties are potentially environment-dependent, which makes **ICT**-based fluorophores ideal sensors for solvents, viscosity, and chemical species. Recently, several **ICT**-based materials have been discovered to become fluorescent upon aggregation. Furthermore, various recent studies in organic optoelectronics, non-linear optics and solar energy conversions utilised the concept of **ICT** to modulate the electronic-state mixing and coupling on charge transfer states. In polar

environments, such fluorophores undergo fast intramolecular electron transfer from the donor to the acceptor part of the molecule. The equilibration between charge transfer state from the individual entities showing red-shifted emission and locally excited state from the monomer's emission results in dual fluorescence from a high energy band through relaxation of the locally excited (**LE**) state and from a lower energy band due to emission from the **ICT** state. Since the relaxation pathways can easily be modulated by substituents, local polarity and steric restrictions, the **ICT** process can be exploited for novel design strategies of functional molecules. Therefore, **ICT** fluorescence holds great promise in applications such as OLEDs, chemo- sensors, and photovoltaic devices.

Herein, this thesis described several molecular design strategies to achieve fluorene-based multifunctional materials aiming at exploring unique photo-physical properties and control over supramolecular organizations of fluorene-based oligomers and polymers (Scheme 3).

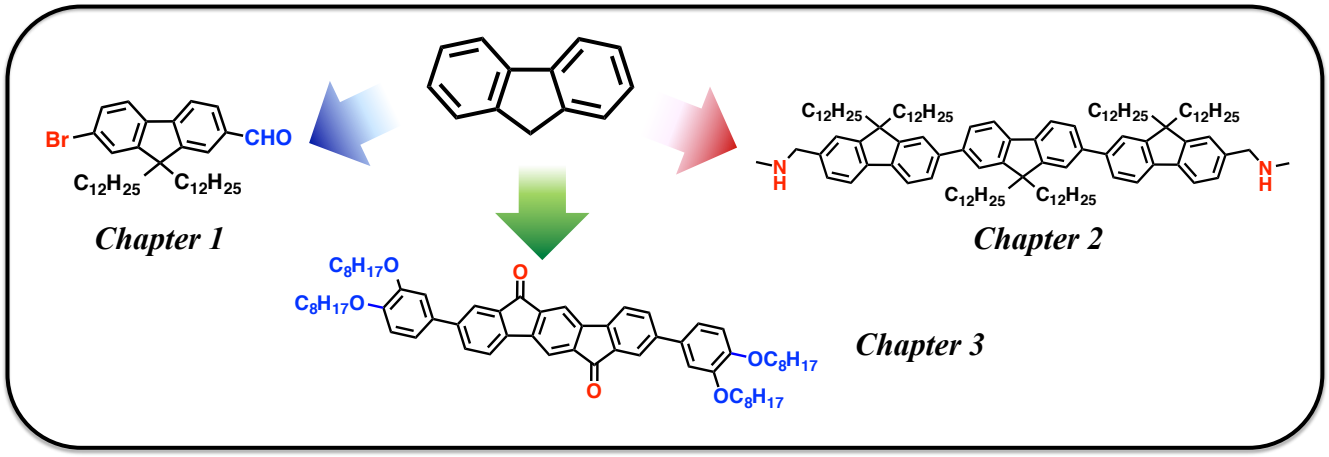

Scheme 3. Schematic illustration of fluorene-based π-conjugated system for photo- and electro-active materials.

1) Enhance the Efficient Intersystem Crossing to Generate the Metal-free Room Temperature Phosphorescence

In chapter 1, one unique phenomenon was discovered and discussed that a pure organic fluorene derivative, 7-bromo-9,9-didodecylfluorene-2-carbaldehyde (**Br–FL–CHO**), exhibited phosphorescence in both solution and film states at 298 K. In this molecular design, heavy atom effect is implemented by the directly-linked bromo and formyl substituents may promote the intersystem crossing from the single excited state to the triplet excited state. Furthermore, the rigidity of fluorene framework helps suppress non-radiative process. The characteristic emission bands at 358 nm and 500 nm were

observed in degassed $CHCl_3$ at 298 K; the emission band at 500 nm completely quenched by dioxygen, whereas the emission band at 358 nm remained constant. We confirmed that the emission at 500 nm has neither significant solvent- nor concentration-dependent characteristics. The lifetimes monitored at 358 nm and 500 nm were determined to be 1.05 ns and 355 μs, respectively; these results revealed that the emission at 358 nm is attributed to fluorescence, whereas the emission at 500 nm was phosphorescence. The absolute phosphorescence quantum yield was 5.9% at 298 K in degassed $CHCl_3$ and enhanced up to 35% at 77 K in glass 2-methyl tetrahydrofuran. The TD–DFT calculations showed a good agreement with the observed experimental results. This property makes this system versatile because it can be embedded into any polymer matrixes; as a result, phosphorescence in film state (PMMA matrix) was observed upon illumination of 254 nm and remained for several months even exposure to air. This fascinating serendipity not only makes it an ideal complement to the reported crystalline-induced phosphorescence systems to furnish fundamental insight into the development of metal-free pure organic phosphors under ambient conditions, but also offers a great platform toward the development of practical optoelectronic devices and dioxygen-sensors based on purely organic phosphors under ambient conditions.

2) White Emission from RGB Trichromophoric Nanoparticle Assisted by Dual FRET: Highly Sensitive Fluorogenic Response toward Polyanions

We designed the oligofluorene (**OF**), which was functionalized with 9,9'-dodecyl chains and *N*-methylaminomethyl end groups. By reprecipitation method, the dodecyl-substituted **OF** typically affords nanoparticles through self-assembly and the *N*-methylaminomethyl end groups would be protonated in aqueous medium (p*K*a ~ 10.7), leading to the nanoparticles (**OFN**) with positive charge on the surface. The intense blue emitting **OFN** can be utilized as a donor scaffold for fluorescence resonance energy transfer (FRET) studies. **In chapter 2**, we describe a facile strategy to fabricate RGB trichromophoric fluorescent **OFN** in aqueous medium where two distinct FRET events occur through spatial organization of a donor scaffold and two acceptor molecules. Consequently, the blue emitting cationic **OFN** acted as an energy donor scaffold to undergo FRET to the red emitting dye embedded in the nanoparticle (interior FRET) and to the green emitting dye adsorbed on the surface through electrostatic interaction (exterior FRET). Each FRET event occurs independently and is free from sequential FRET, thus dual FRET (in combination of interior and exterior FRET) system was constructed, exhibiting multicolor emission including white in aqueous solution and film state. We also demonstrated that the cationic trichromophoric **OFN** acts as a highly sensitive ratiometric and

colorimetric sensor toward polyanionic species. In particular, a white emissive nanoparticle, which has low background in terms of colorfulness, is beneficial for sensing anionic species, exhibiting the remarkable emission color changes in a ratiometric manner. As a result, the characteristic white emissive nanoparticle showed perceived visible response upon perturbation of the exterior FRET efficiency by the acceptor displacement, leading to highly sensitive response toward various poly-anions. Specifically, our system exhibits high sensitivity toward heparin amoung other anionic analytes with extremely low detection limit.

3) Multicolour Emissions in Solution and Polymer Matrix with Unusual Solvatochromic Behavior Driven by Solvent Dependent Fluorescent Channel Switching

The indenofluorenedione building block with extension of π-conjugation lengths compared with fluorenone, has electron–accepting ability with rigid and planar aromatic configuration, the lowest excited n-π^* and π-π^* states of which are lying very close to each other in non-polar solvents, and the character of the lowest excited state becomes π-π^* transition dominantly in polar solvents. **In chapter 3**, we describe the unusual solvatochromic behavior from new indenofluorenedione bearing D–A–D framework (**IFO**), which is based on indenofluorenedione core as an electron-accepting unit, dialkyloxy phenyl groups as weak electron donating species. Typically, a fluorescent band at 436 nm was observed in DMF attributable to the transition from locally excited state (**LE**), while two emission peaks at 530 nm and 610 nm were observed in *p*-xylene. We inferred that in non-polar solvents, the lowest excited state is n-π^* forbidden transition. Consequently, excited deactivation pathway of **IFO** is actively switched onto the **CT** channels (including intra and inter molecular charge transfers), leading to the low-energy fluorescence with solvent-dependent characteristics. Interestingly, the character of the lowest excited state of **IFO** changed to allowed π-π^* transition in polar medium. In this case, the **CT** band was not as favorably active as in non-polar solvents probably due to electron donating ability of dialkyloxy phenyl groups. Instead, the **LE** with π-π^* character played a major role in excited-state deactivation mechanism. The dual fluorescent channels namely the **LE** and **CT** states can be controllably switched on and off by changing solvent, resulting in environmental polarity sensitive multi-luminescence. This unusual solvatochromic behavior enables us to generate white emission in DMF with *p*-xylene binary solvent mixtures. Furthermore, a single organic emitter, **IFO**, showed high sensitivity towards micro-environmental polarity even embedded in the polymer matrix and have visible discrimination of polar solvents from common organic solvents.

Reference

1 Selected reviews: (*a*) T. W. Kelly, P. F. Baude, C. Gerlach, D. E. Ender, D. Muyres, M. A. Haase, D. E. Vogel, S. D, Theiss, *Chem. Mater.*, 2004, **16**, 4413; (*b*) S. R. Forrest, M. E. Thompson, *Chem. Rev.*, 2007, **107**, 923; (*c*) A. Facchetti, *Chem. Mater.*, 2011, **23**, 733; (*d*) Q. H. Wang, K. K. Zadeh, A. Kis, J. N. Coleman, M. S. Strano, *Nat. Nanotechnol*, 2012, **7**, 699.

2 Selected reviews: (*a)* B. W. D'Andrade, S. R. Forrest, *Adv. Mater.,* 2004, **16**, 1585; (*b*) K. T. Kamterkar, A. P. Monkman, M. R. Bryce, *Adv. Mater.,* 2010, **22**, 572.

3 Selected reviews: (*a*) G. Horowitz, *Adv. Mater.,* 1999, **10**, 365; (*b*) H. Sirringhaus, *Adv. Mater.,* 2005, **17**, 2411; (*c*) J. Zaumseil, H. Sirringhaus, *Chem. Rev.*, 2007, **107**, 1296; (*d*) N. Tessler, Y. Preezant, N. Rappaport, Y. Roichman, *Adv. Mater.,* 2009, **21**, 2741.

4 Selected reviews: (*a*) Y.-J. Cheng, S.-H. Yang, C.-S. Hsu, C*hem. Rev.*, 2009, **109**, 5868; (*b*) M. O. Neill, S. M. Kelly, *Adv. Mater.,* 2011, **23**, 566; (*c*) J.-T. Chen, C.-S. Hsu, *Polym. Chem.,* 2011, **2**, 2707; (*d*) L. Lu, T. Zheng, Q. Wu, A. M. Schneider, D, Zhao, L. Yu, C*hem. Rev.*, 2015, **115**, 1266.

5 Selected reviews: (*a*) D. T. McQuade, A. E. Pullen, T. M. Swager, C*hem. Rev.*, 2000, **100**, 2537; (*b*) S. W. Thomas, G. D. Joly, T. M. Swager, C*hem. Rev.*, 2007, **107**, 1339.

6 (*a*) U. Scherf, E. J. W. List, *Adv. Mater.,* 2002, **14**, 477; (*b*) R. Abbel, A. P. H. J. Schenning, E. W. Meijer, *J. Polym. Sci. A: Polym. Chem.,* 2009, **47**, 4215; (c) C.-L. Ho, Z.-Q. Yu, W.-Y. Wong, C*hem. Rev.*, 2016, **DOI:** 10.1039/C6CS00226A.

7 (a) B. S. Gaylord, A. J. Heeger, G. C. Bazan, *Proc Natl Acad Sci USA*, 2002, **99**, 10954; (b) R. Abbel, C. Grenier, M. J. Pouderoijen, J. W. Stouwdam, P. E. L. G. Leclere, R. P. Sijbesma, E. W. Meijer, A. P. H. J. Schenning, *J. Am. Chem. Soc.*, 2009, **131**, 833; (c) Y. Zhao, N. A. A. Rahim, Y. Xia, M. Fujiki, B. Song, Z. Zhang, W. Zhang, X. Zhu, *Macromolecules*, 2016, **49**, 3214.

8 *(a)* I. D. W. Samuel, G. A. Turnbull, *Chem. Rev.*, 2007, **107**, 1272; *(b)* A. C. Grimsdale, K. L. Chan, R. E. Martin, P. G. Jokisz, A. B. Holmes, *Chem. Rev.*, 2009, **109**, 897; *(c)* P. M. Beaujuge, J. R. Reynolds, *Chem. Rev.*, 2010, **110**, 268.

9 S. W. Thomas, G. D. Joly and T. M. Swager, *Chem. Rev.*, 2007, **107**, 1339.

10 M. Leclerc, *J. Polym. Sci. Part A: Polym. Chem.*, 2001, **39**, 2867.

11 S. Setayesh, A. C. Grimsdal, T. Weil, V. Enkelmann, K. Mullen, F. Meghdadi, E. J. List, G. Leising, *J. Am. Chem. Soc.*, 2001, **123**, 946.

12 *(a)* M. Grell, D. D. C. Bradley, M. Inbasekaran, E. P. Woo, *Adv. Mater.*, 1997, **9**, 798; *(b)* A. C. Chen, S. W. Culligan, Y. Geng, S. H. Chen, K. P. Klubek, K. M. Vaeth, C. M. Tang, *Adv. Mater.*, 2004, **16**, 783.

13 *(a)* A. Duarte, K.-Y. Pu, B. Liu and G. C. Bazan, *Chem. Mater.*, 2011, **23**, 501; *(b)* L. Xiao, Z. Chen, B. Qu, J. Luo, S. Kong, Q. Gong and J. Kido, *Adv. Mater.*, 2011, **23**, 926; *(c)* D. Yu, Y. Zhao, H. Xu, C. Han, D. Ma, Z. Deng, S. Gao and P. Yan, *Chem. Eur. J.*, 2011, **17**, 2592.

14 *(a)* R. Xia, G. Heliotis, D. D. C. Bradley, *App. Phys. Lett.*, 2003, **82**, 3599; *(b)* G. Heliotis, R. Xia, G. A. Turnball, P. Andrew, W. L. Barnes, I. D. W. Samuel, D. D. C. Bradley, *Adv. Func. Mater.*, 2004, **14**, 91.

15 *(a)* S. Beaupre, P.-L. T. Boudreault and M. Leclerc, *Adv. Mater.*, 2010, **22**, E6; *(b)* J. Zhang, H.-B. Li, S.-L. Sun, Y. Geng, Y. Wu and Z. M. Su, *J. Mater. Chem.*, 2012, **22**, 568; *(c)* G. marzari, J. Durantini, D. Minudri, M. Gervaldo, L. Otero, F. Fungo, G. Pozzi, M. Cavazzini, S. Orlandi and S. Quici, *J. Phys. Chem. C* 2012, **116**, 21190.

16 J. Schill, A. P. H. J. Schenning, L. Brunsveld, *Macromol. Rapid Commun*. 2015, **36**, 1306.

17 *Modern Molecular Photochemistry*, N. J. Turro, 1999.

18 *(a)* C. W. Tang, A. S. Vanslyke, *Appl. Phys. Lett.*, 1987, **51**, 913; *(b)* M. A. Baldo, D, F, O'Brien, Y. You, A. Shoustikov, S. Sibley, M. E. Thompson and S. R. Forrest, *Nature* 1998, **395**, 151; *(c)* C. Adachi, M. A. Baldo, M. E. Thompson and S. R. Forrest, *Appl. Phys. Lett.*, 2000, **77**, 904; *(d)* Y. You, Y. Han, Y.-M. Lee, S. Y. Park, W. Nam, S. J. Lippard, *J. Am. Chem. Soc.*, 2011, **133**, 11488.

19 D. Lee, O. Bolton, B. C. Kim, J. H. Youk, S. Takayama and J. Kim, *J. Am. Chem. Soc.*, 2013, **135**, 6325.

20 *(a)* C. L. Ho, W. Y. Wong, *Coord. Chem. Rev.* 2006, **250**, 2627; *(b)* C. L. Ho, W. Y. Wong, *Acc. Chem. Rev.* 2010, **43**, 1246; *(c)* S. Goeb, V. Prusakova, X. Wang, A. Vezinat, M. Salle, F. N. Castellano, *Chem. Commun.*, 2011, **47**, 4397; *(d)* G. J. Zhou, W. Y. Wong, *Chem. Rev.* 2011, **40**, 2541; *(e)* J.-S. Chen, G.-J. Zhou, T. R. Cook, K.-L. Han and P. J. Stang, *J. Am. Chem. Soc.*, 2013, **135**, 6694; *(f)* K. Li, G. Cheng, C. Ma, X. Guan, W.-M. Kwok, Y. Chen, W. Lu and C.-M. Che, *Chem. Sci.*, 2013, **4**, 2630.

21 *(a)* S. Hoshino and H. Suzuki, *Appl. Phys. Lett.*, 1996, **69**, 224; *(b)* A. Kohler, J. S. Wilson and R. H. Friend, *Adv. Mater.*, 2002, **14**, 701.

22 *(a)* G. Zhang, J. Chen, S. J. Payne, S. E. Kooi, J. N. Demas and C. L. Fraser, *J. Am. Chem. Soc.*, 2007, **129**, 8942; *(b)* W. Z. Yuan, X. Y. Shen, H. Zhao, J. W. Y. Lam, L. Tang, P. Lu, C. Wang, Y.

Liu, Z. Wang, Q. Zheng, J. Z. Sun, Y. Ma and B. Z. Tang, *J. Phys. Chem. C*, 2010, **114**, 6090; *(c)* O. Bolton, K. Lee, H. J. Kim, K. Y. Lin and J. Kim, *Nat. Chem.*, 2011, **3**, 205; *(d)* G. P. Yong, Y. M. Zhang, W. L. She, Y. Z. Li, *J. Mater. Chem.*, 2011, **21**, 18520.

23 *(a)* A. Wakamiya, K. Mori, S. Tamaguchi, *Angew. Chem. Int. Ed.*, 2007, **46**, 4273; *(b)* E. Ishow, A. Brosseau, G. Clavier, K. Nakatanim, P. Tauc, C. T.-Debuisschert, S. Neveu, O. Sandre, A. Leaustic, *Chem. Mater.*, 2008, **20**, 6597; *(c)* E. Kim, S. B. Park, *Chem. Asian J.*, 2009, **4**, 1646; *(d)* Z. Zhang, B. Xu, J. Su, L. Shen, Y. Xie, H. Tian, *Angew. Chem. Int. Ed.*, 2011, **50**, 11654; *(e)* B. Liu, Z. Wang, N. Wu, M. Li, J. You, J. Lan, *Chem.-Eur. J.*, 2012, **18**, 1599.

24 *(a)* H. Y. Zhang, Z. L. Zhang, K. Q. Ye, J. Y. Zhang, Y. Wang, *Adv. Mater.*, 2006, **18**, 2369; *(b)* N. S. S. Kumar, S. Varghese, C. H. Suresh, N. P. Rathm, S. Das, *J. Phys. Chem. C* 2009, **113**, 11927; *(c)* S. P. Anthony, S. Varughese, S. M. Draper, *Chem. Commun.*, 2009, **48**, 7500; *(d)* D. Yan, A. Delori, G. O. Lloyd, T. Friscic, G. M. Day, W. Jones, J. Lu, M. Wei, D. G. Evans, X. Duan, *Angew. Chem. Int. Ed.*, 2011, **50**, 12483; *(e)* T. Hinoue, M, Miyata, I. Hisaki, N. Tohnai, *Angew. Chem. Int. Ed.*, 2012, **51**, 155; *(f)* T. Hinoue, Y. Shigenoi, M. Sugino, Y. Mizobe, I. Hisaki, M. Miyata, N. Tohnai, *Chem.-Eur. J.*, 2012, **18**, 4634.

25 *(a)* L. Giribabu, A. A. Kumar, V. Neeraja, B. G. Maiya, *Angew. Chem. Int. Ed.*, 2001, **40**, 3621; *(b)* F. D. Lewis, L. Zhang, X. Zuo, *J. Am. Chem. Soc.*, 2005, **127**, 10002; *(c)* K. Borjesson, S. Preus, A. H. El-Sagheer, T. Brown, B. Albinsson, L. M. Wilhelmsson, *J. Am. Chem. Soc.*, 2009, **131**, 4288; *(d)* J. A. Riddle, X. Jiang, J. Huffman and D. Lee, *Angew. Chem. Int. Ed.*, 2007, **46**, 7019; *(e)* S. Ogi, K. Sugiyasu and M. Takeuchi, *Bull. Chem. Soc. Jpn*, 2011, **1**, 40; *(f)* S. Ogi, K. Sugiyasu and M. Takeuchi, *ACS Macro Lett.*, 2012, **1**, 1199.

26 *(a)* T. Sagawa, S. Fukugawa, T. Yamada and H. Ihara, *Langmuir*, 2002, **18**, 7223; *(b)* X. Zhang, S. Rehm, M. M. S.-Sempere and F. Wurthner, *Nat. Chem.*, 2009, **1**, 623.

27 *(a)* A. Adronov, S. L. Gilat, J. M. J. Frechet, K. Ohta, F. V. R. Neuwahl, G. R. Fleming, *J. Am. Chem. Soc.*, 2000, **122**, 1175; *(b)* J. R. Lakowicz, *Principles of Fluorescence Spectroscopy*, Springer New York, 2006; *(c)* N. Bruns, K. Pustelny, L. M. Bergeron, T. A. Whitehead, D. S. Clark, *Angew. Chem. Int. Ed.*, 2009, **48**, 5666; *(d)* S. Karthikeyan, R. P. Sijbesma, *Macromolecules* 2009, **42**, 5175; *(f)* Y. Sun, H. Wallrabe, S.-A. Seo and A. Periasamy, *Chemphyschem*, 2011, **12**, 462.

28 *(a)* A.-D. Peng, D.-B. Xiao, Y. Ma, W.-S. Yang and J.-N. Yao, *Adv. Mater.*, 2005, **17**, 2050; *(b)* L. Kang, Y. Chen, D. Xiao, A. Peng, F. Shen, X. Kuang, H. Fu and J. Yao, *Chem. Commun.*, 2007, 2695; *(c)* Y. S. Zhao, H. Fu, F. Hu, A. Peng, W. Yang and Y. Yao, *Adv. Mater.*, 2008, **20**, 79; *(d)*

X. Li, Y. Qian, S. Wang, S. Li and G. Yang, *J. Phys. Chem. C* 2009, **113**, 3862; *(e)* S. Kim, S.-J. Yoon and S. Y. Park, *J. Am. Chem. Soc.*, 2012, **134**, 12091; *(f)* L. Cerdan, E. Enciso, V. Martin, J. Banuelos, I. L.-Arbeloa, A. Costela and I. G.-Moreno, *Nature Photonics*, 2012, **6**, 621.

29 *(a)* N. Kurokawa, H. Yoshikawa, N. Hirora, K Hyodo, H. Masuhara, *ChemPhysChem*, 2004, **5**, 1609; *(b)* C. Wu, C. Szymanski and J. McNeill, *Langmuir*, 2006, **22**, 2956; *(c)* C. Wu, Y. Zheng, C. Szymanski and J. McNeill, *J. Phys. Chem. C* 2008, **112**, 1772; *(d)* C. Wu, B. Bull, C. Szymanski, K. Christensen and J. McNeill, *ACS Nano*, 2008, **11**, 2415; *(e)* C. Wu, B. Bull, K. Christensen and J. McNeill, *Angew. Chem. Int. Ed.*, 2009, **48**, 2741; *(f)* J. Xu, C. Wu, S. Sahu, L. Fernando, C. Szymanski and J. McNeill, *Nano Lett.*, 2012, **12**, 1300.

30 *(a)* X. J. Zhao, R. P. Bagwe, W. H. Tan, *Adv. Mater.*, 2004, **16**, 173; *(b)* H. Ow, D. R. Larson, M. Srivastava, B. A. Baird, W. W. Webb, U. Wiesner, *Nano Lett.*, 2005, **5**, 113; *(c)* A. Kaeser, A. R. H. J. Schenning, *Adv. Mater.*, 2010, **22**, 2985; *(d)* C. Cordovilla, T. M. Swager, *J. Am. Chem. Soc.*, 2012, **134**, 6932; *(e)* C. Wu. D. T. Chiu, *Angew. Chem. Int. Ed.*, 2013, **52**, 2.

31 (*a*) Z. R. Grabowski, K. Rotkiewicz, *Chem. Rev.*, 2003, **103**, 3899; (*b*) S. Sasaki, G. P. C. Drummen, G. Konishi, *J. Mater. Chem. C*, 2016, **4**, 2731.

Chapter 1
Phosphorescence Emission from Pure Organic Fluorene Derivative in Solution at Room Temperature

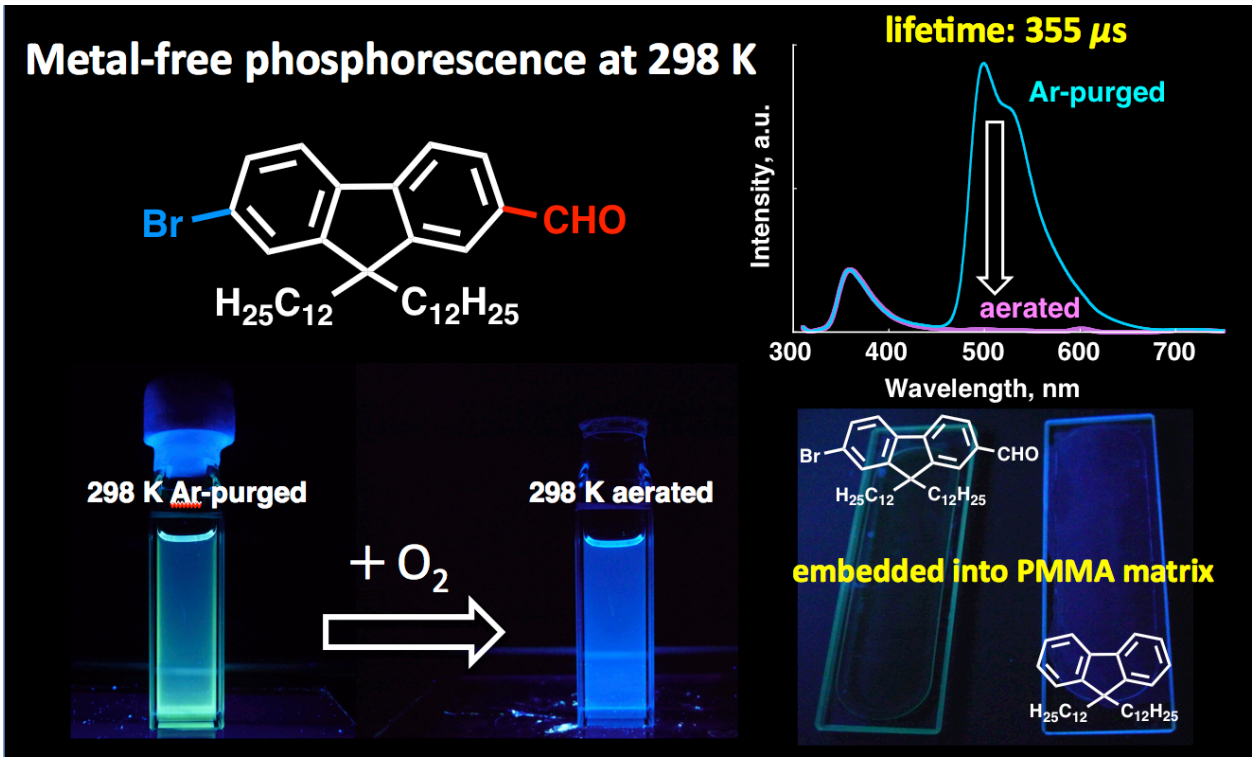

Abstract

Metal free pure organic compound, a fluorene derivative bearing bromo and formyl groups, 7-bromo-9,9-didodecylfluorene-2-carbaldehyde (**Br–FL–CHO**), unanticipatedly exhibited phosphorescence emission in solution and film states at room temperature. The phosphorescence lifetime was determined to be as long as 355 μs. The absolute phosphorescence quantum yield reached to 5.9% in chroloform at 298 K and enhanced up to 35% in glass 2-methyl tetrahydrofrane (2-MeTHF) at 77 K. The phosphorescence emission was observed for over five days even under air at 298 K when embedded in poly(methyl methacrylate) matrix. The time-dependent density functional theory (TD-DFT) calculation was performed to elucidate the plasusible mechanism of this phenomenon further, which is consistent with experimental results.

Introduction

Recent advance in luminescent materials using pure organic compounds have provided low-cost, easily-handled and thermally stable platforms for optoelectronic devices,[1] chemosensors,[2] or photoresponsive switches.[3] Fluorene and its derivatives are one of the most attractive planar π-conjugated compounds which exhibit excellent fluorescent and electrical properties.[4] Polyfluorenes and fluorene-based copolymers have been used as fluorescent chromophores in organic light-emitting diodes and dye-sensitized solar cells.[5]

On the other hand, materials that show phosphorescence and delayed fluorescence via reverse intersystem crossing (ISC) from the triplet excited state have attracted much attention, because electro-luminescence efficiency of these materials is 100% in principle, which is four times larger than that of conventional fluorophores (25%).[6,7] Coordination complexes containing transition metals such as Pt and Ir have so far been extensively investigated for use as phosphorescent materials.[2,6,8] Although many efforts have also been devoted to develop pure organic phosphors toward practical applications,[9] most of the phosphorescence emission of pure organic compounds are observed under specific conditions (e.g., in crystals and in solid states at 77 K),[10] which hampers the development of prospective phosphorescent materials. Hence, there is a strong incentive to look for metal-free organic phosphorescent materials in solution or in host maxtrix under ambient conditions. We report herein that a versatile fluorene derivative, 7-bromo-9,9-didodecylfluorene-2-carbaldehyde (**Br–FL–CHO**), exhibits phosphorescence under ambient conditions: in solutions and doped films at room temperature. It has been demonstrated that aromatic carbonyls exhibited a degree of spin-orbit coupling through intersystem crossing, giving

rise to triplet generation.[9a] The bromine that affords heavy atom effect strongly induces singlet-triplet conversion by enhancing spin-orbit coupling. Moreover, the rigid framework of fluorene serves to lower internal conversion as well as restrict vibrational loss of excited triplet state, making triplet emission active.[9d]

In this chapter, a series of fluorene derivatives were synthesized and characterized (Schemes 1-1 and 1-2) to compare the effect of substituents on photophysical properties.[11] The chacterastic features of phosphorescence were observed and confirmed in organic solvents at 298 K by the means of emission spectroscopy as well as the time-revoled photoluminescence study under Ar atmosphere. The quantum chemical calculation results were found to be in accordance with experimental results. We further investigated emission behaviors of the fluorene derivatives incorporated in films of poly(methyl methacrylate), PMMA, whose oxygen permeability is relatively low at room temperature.[12]

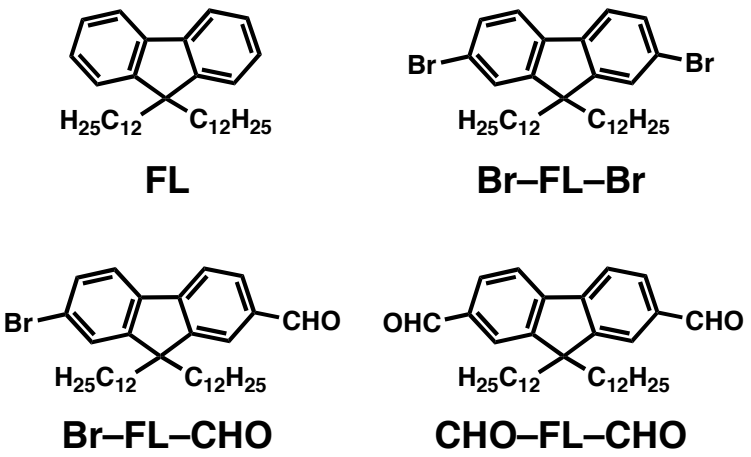

Scheme 1-1. Structures of **FL**, **Br–FL–Br**, **Br–FL–CHO**, **CHO–FL–CHO** under study.

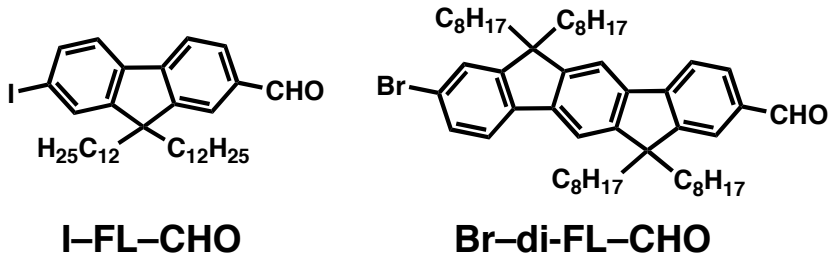

Scheme 1-2. Structures of **I–FL–CHO** and **Br–di-FL–CHO** for comparison.

Results and discussions

UV–Vis absorption spectra of fluorene derivatives (**FL**, **Br–FL–Br**, **Br–FL–CHO**, **CHO–FL–CHO**) were measured in chloroform ($CHCl_3$) and shown in Figure 1-1. The lowest energy absorption bands of all fluorene derivatives in $CHCl_3$ are assigned to π-π* transition, which are consistent with other fluorene derivatives.[13]

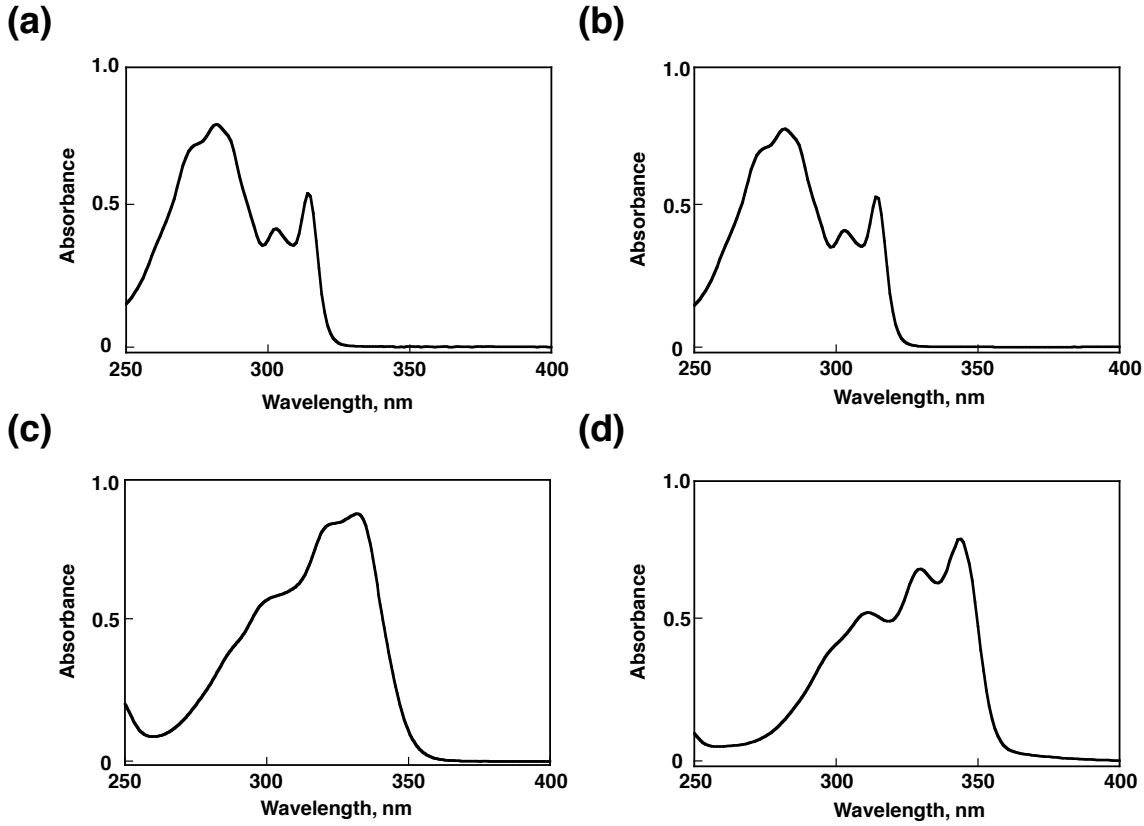

Figure 1-1. Normalized UV–vis absorption spectra of (a) **FL**, (b) **Br–FL–Br**, (c) **Br–FL–CHO**, (d) **CHO–FL–CHO** at 4×10^{-5} M in $CHCl_3$ at 298 K.

Figure 1-2 showed emission spectra of fluorene derivatives (**FL**, **Br–FL–Br**, **Br–FL–CHO**, **CHO–FL–CHO**) measured in $CHCl_3$ under air (dash black) and argon (Ar) atmospheres (red line) at 298 K. Compared with the emission spectra observed under air, no additonal peaks observed under Ar in emission spectra for **FL**, **Br–FL–Br** and **CHO–FL–CHO** as shown in Figure 1-2. On the contrary, the characteristic dual emission bands at 358 nm and 500 nm for **Br–FL–CHO** were observed under Ar as shown in Figure 1-2c. Interestingly, the emission band at 500 nm completely

disappeared in the presence of dioxygen (red line in Figure 1-2c). In contrast, the emission at 358 nm remained constant both under air and Ar.

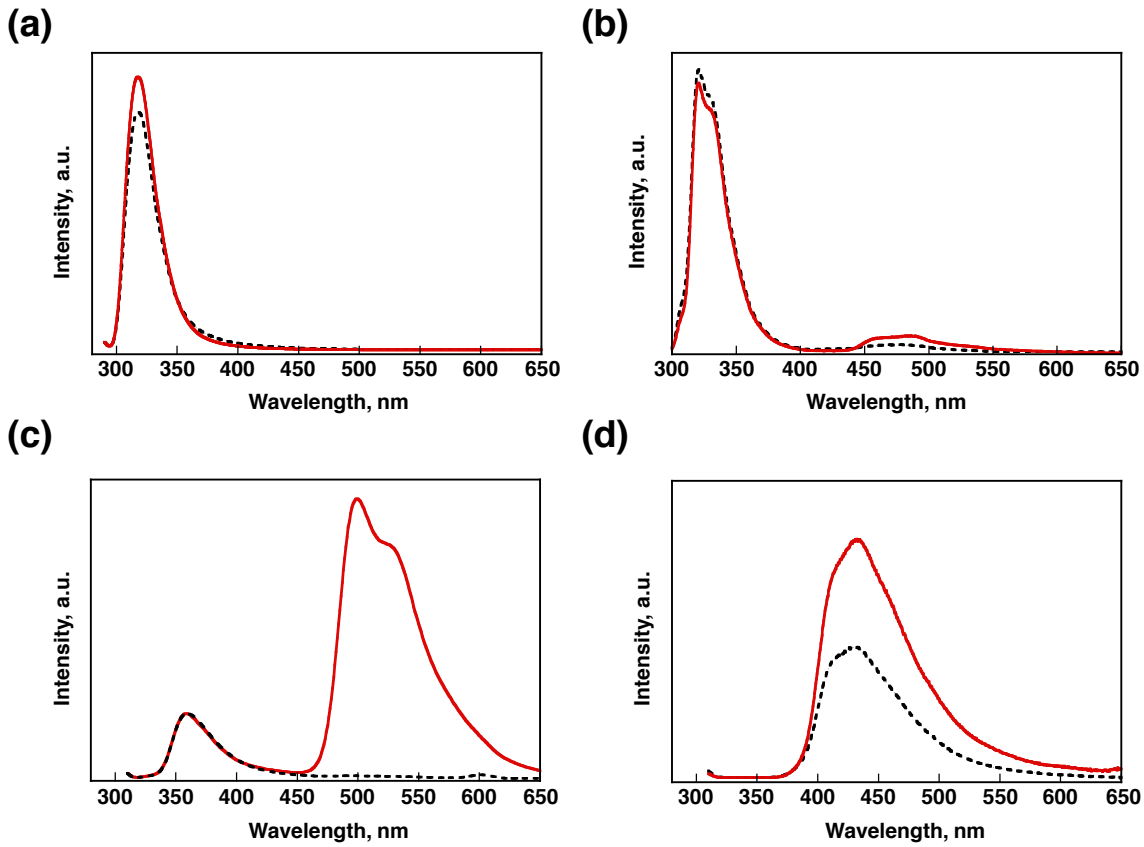

Figure 1-2. Normalized fluoresence spectra of (a) **FL**, (b) **Br–FL–Br**, (c) **Br–FL–CHO**, (d) **CHO–FL–CHO** at 4×10^{-5} M under air (dash black) and Ar (red line) in $CHCl_3$ at 298 K. Excitation wavelength is 280 nm for **FL**; 300 nm for **Br–FL–Br**, **Br–FL–CHO** and **CHO–FL–CHO**.

Simultaneously, the emission color change of **Br–FL–CHO** from blue to green was observed under air and Ar in $CHCl_3$ as shown in Figure 1-3. Such color change occurs immediately and completely reversible by exposure to air and bubbling of Ar gas.

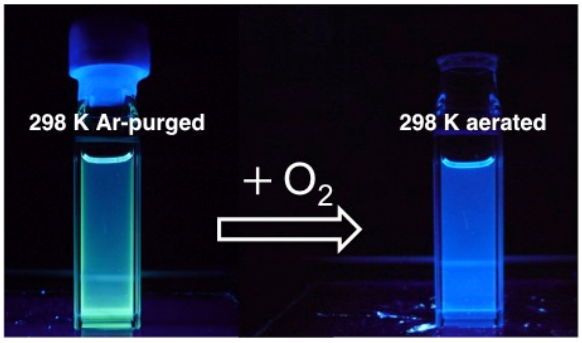

Figure 1-3. Photographs of **Br–FL–CHO** with Ar purged (left) and under air (right) in $CHCl_3$

Figure 1-4 showed that the excitation spectrum of **Br–FL–CHO** monitered at 500 nm is identical to that of UV-Vis spectrum. This result suggests that 500 nm emission is from **Br–FL–CHO**, not from any inpurities leading to additional emission peaks.

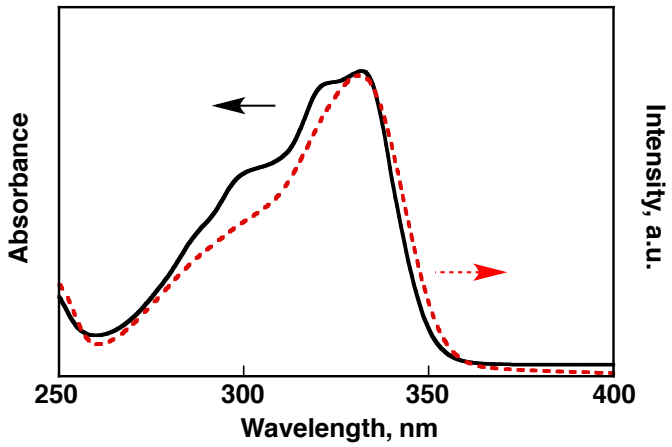

Figure 1-4. UV-Vis absorption (black line) and excitation spectra (red dash) of **Br–FL–CHO** at 4 $\times 10^{-5}$ M in $CHCl_3$ at 298K. (λ_{moni} = 500 nm)

Moreover, the emission spectra of **Br–FL–CHO** were also measured in various organic solvents with different polarities as shown in Figure 1-5. The results showed that the emission band at 500 nm was always observed without additional peak or peak shift regardless of the solvent polarity, indicating that the possibilites of emission from the charge tranfer state which has significant sovlent dependence, can be ruled out.

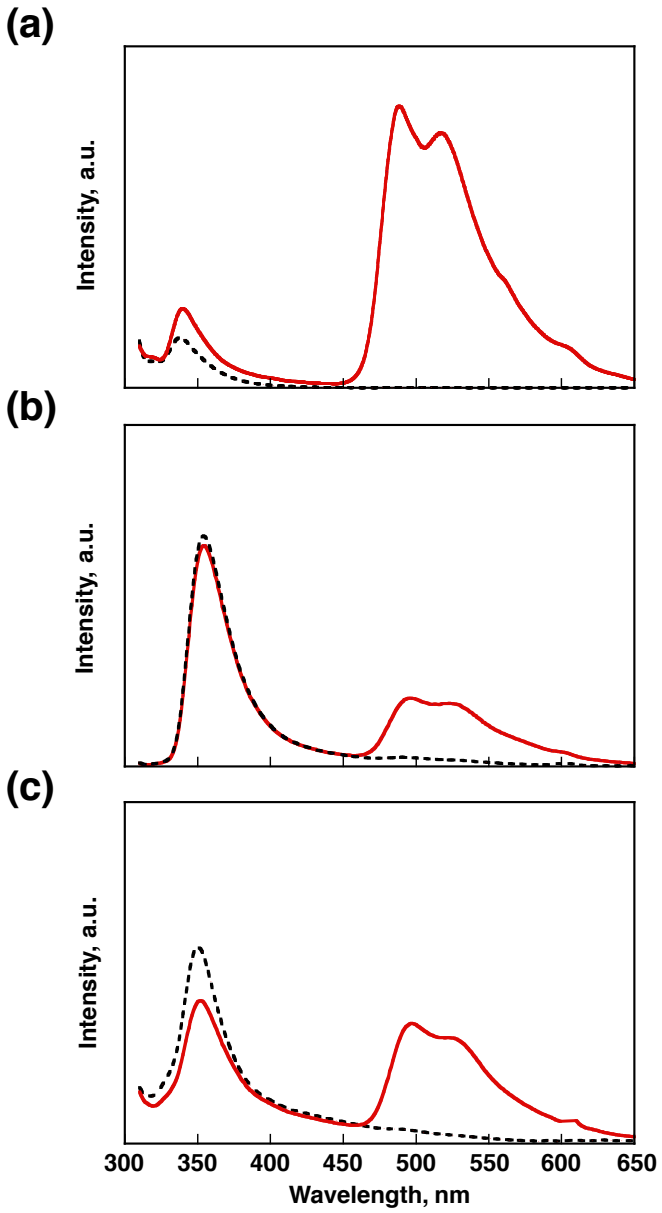

Figure 1-5. Normalized fluoresence spectra of **Br–FL–CHO** in (a) Hexene, (b) DMF, (c) DMSO under air (dash black) and under Ar (red line) at 298 K. (λ_{ex} = 300 nm)

The time-revoled photoluminescence study was investigated. The decay at 500 nm obeys mono-exponential function with an emission lifetime of 355 μs, as shown in Figure 1-6b. The lifetime of phosphorescence emission is usually much longer than that of fluorescence as the result of a spin-forbidden radiative process.[9b] The emission at 358 nm for **Br–FL–CHO** decays with an emission lifetime 1.05 ns (Figure 1-6a). These results suggest that exicted singlet state rapidly decays by intersystem crossing with a rate constant estimated to be about 9.5×10^8 S^{-1} to the excited triplet

state, which is two orders of magnitude faster than prompt fluorescence with a approximate rate constant of 4.3×10^6 S^{-1}, resulting in additional emission peak at 500 nm abserved under Ar.

Based on these observations above, we thus assign the emission at 358 nm to fluorescence, whereas the emission at 500 nm is attribute to phosphorescence which was completely quenched in the presence of dioxygen and undergoes much longer lifetime of 355 μs.

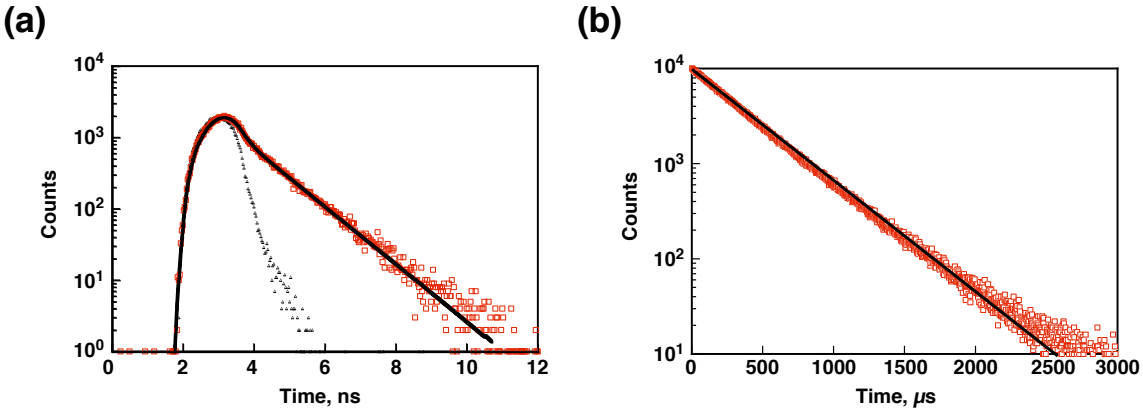

Figure 1-6. Emission lifetime of **Br–FL–CHO** (a) excited at 330 nm, monitored at 370 nm under air in $CHCl_3$ at 298 K and (b) excited at 300 nm, monitored at 500 nm under Ar in $CHCl_3$ at 298 K.

In order to investigate the origin of phosphorescence of **Br–FL–CHO** (halogen-bonding induced or monomeric property), the concentration dependence of UV-Vis absorption and emission spetra of **Br–FL–CHO** were also studied (Figure 1-7). We found that the absorbance increased linerly with increasing concentrations, suggesting no tendency of aggregation (Figure 1-7a). Furthermore, the intensity of phosphorescence emission at 500 nm was found to be proportional to the corresponding concentration in $CHCl_3$ ranging from 10^{-6} M to 10^{-5} M as shown in Figures 1-7b and 1-7c. Quenching of fluorensence intensity due to relatively high concentrations is usually inevitable. Therefore, concentration dependent ^{1}H NMR was complementally invesitigated for high concentrated chroloform solutions of **Br–FL–CHO** (10^{-4} M to 10^{-2} M) as shown in Figures 1-8a and 1-8b. The results showed that no obvious signal shifts in 7.5–10.2 ppm range even when the solution was two orders of magnitude concentrated (from 10^{-4} M to 10^{-2} M). Foregoing observations indicated that phosphorescence emission originates from monomeric **Br–FL–CHO** species, rather than from aggregation of **Br–FL–CHO**. Therefore, halogen-bonding is not indispensable under experimental conditions for **Br–FL–CHO** to achieve room temperature

phosphorescence, which is distinct from the case recently published results.[10b]

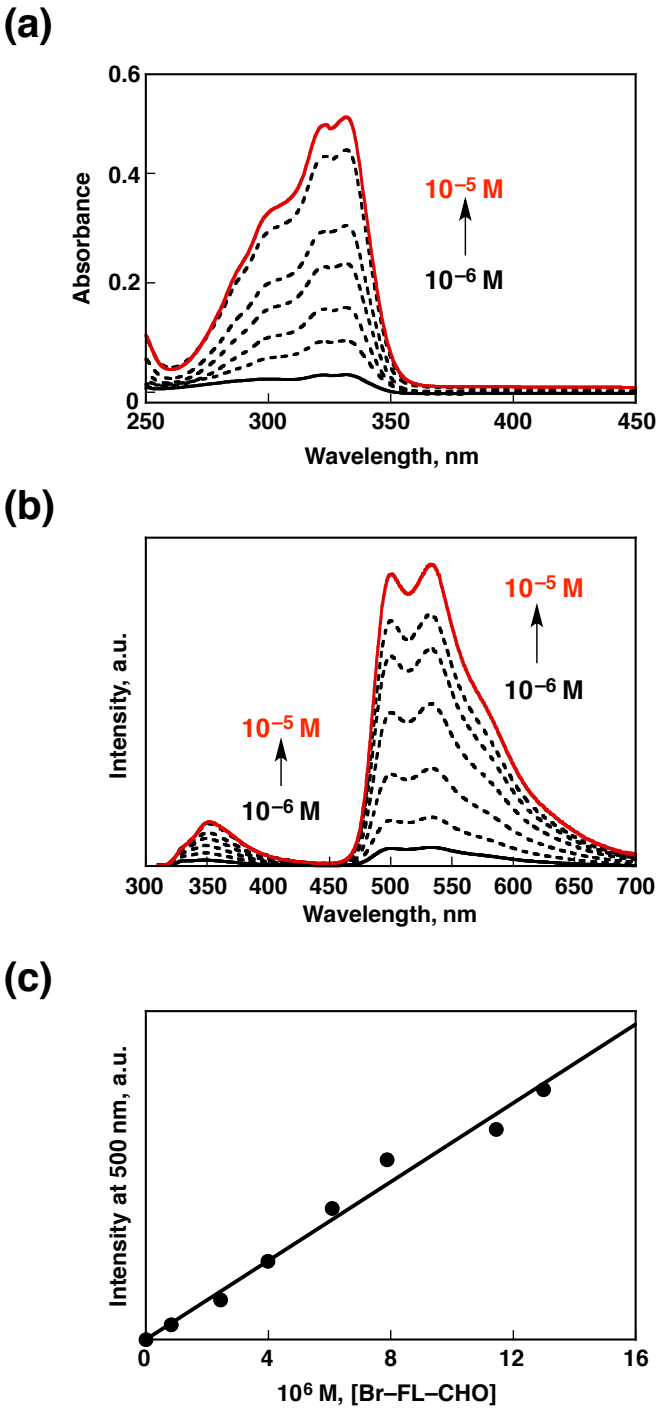

Figure 1-7. Concentration dependence of (a) UV-vis absorption, (b) fluorescence spectrum and (c) phosphorescence intensity at 500 nm for **Br–FL–CHO** measured under Ar in $CHCl_3$ at 298 K. (λ_{ex} = 300 nm).

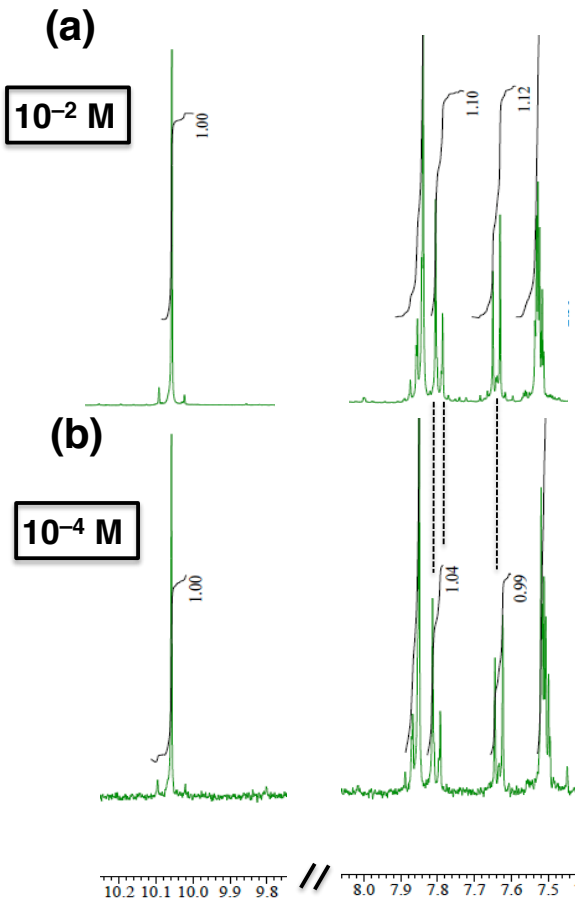

Figure 1-8. Concentration dependence of ^{1}H NMR for **Br–FL–CHO** with concentration of (a) 10^{-2} M, (b) 10^{-4} M, in $CDCl_3$ at 298 K.

The absolute phosphorescence quatumn yield of **Br–FL–CHO** was calculated to be 5.9% in chroloform at 298 K. The phosphorescence emission intensity at 500 nm was enhanced with absolute phosphorescent quatumn yield as high as 35% in deaerated glass 2-methyl tetrahydrofrane (2–MeTHF) at 77 K as shown in Figure 1-9. The observation of strong phosphorescence at 77 K results from depression of nonradiative deactivation process from the triplet excited state (T_1) to the ground state of **Br–FL–CHO**.

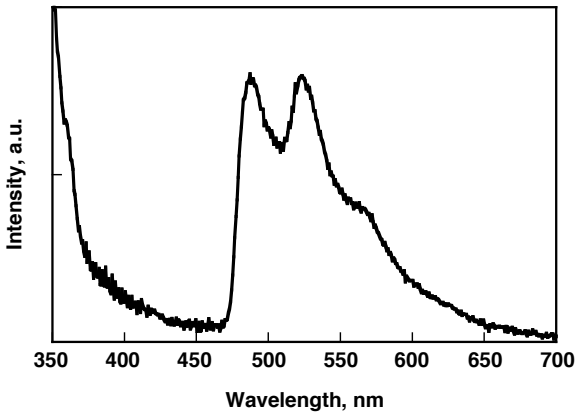

Figure 1-9. Phosphorescence spectrum of **Br–FL–CHO** in 2-Me-THF at 77 K.(λ_{ex} = 300 nm)

Photophysical properties of all fluorene derivatives (**FL**, **Br–FL–Br**, **Br–FL–CHO** and **CHO–FL–CHO**) are summarized and shown in Table 1-1. On the contrary to the case of **Br–FL–CHO**, no characteristic phosphorescence emission but only fluorescence emissions were observed for the other fluorene derivatives in $CHCl_3$ under Ar. These results indicated that the combination of the bromo and the formyl groups plays important roles to exhibit room temperature phosphorescence.

Table 1-1. Photophysical data of fluorene derivatives in $CHCl_3$ at 298 K under air.

	λ_{abs}[nm] (logε)	λ_{em} [nm]	τ_f [ns][b]	Φ_f (%)[c]
FL	282 (4.3)	318	0.48	3.2
Br–FL–CHO	332 (4.6)	358, 500[a]	1.05	0.5
Br–FL–Br	282 (4.6)	320	0.38	0.5
CHO–FL–CHO	344 (4.6)	432	1.18	0.2

[a]Observed only under Ar atomosphere. [b]Excited at 280 nm and monitered at emission maxmum. [c]Absolute fluorescence quantum yield determined under Air.

For the comparison, we also designed and synthesized **I–FL–CHO**, in which the iodine is acting as the heavy atom instead of bromide. The same experimental conditions were used to invesigate the possiblity for the generation of room temperature phosphorescence. The introduction of iodine in replacement of bromine turned out to be failure to facilitate phosphoresence in solution at room temperature. As shown in the Figure 1-10, the absorption spectra of **I–FL–CHO** was identical to that of **Br–FL–CHO**, indicating that heavy atom did not greatly contribute to the electronic ground state. However, no additional emission peaks appeared when measured under Ar, indicating that **I–FL–CHO** did not exhibit phosphorescence. Although the idoine acting as a heavy atom is theorically responsible for enhancing intersystem crossing from excited single state into excited triplet state, it could presumedly introduce addtional fast chemical deactivation pathways as well, leading to quenching of phosphoresence at 298 K.

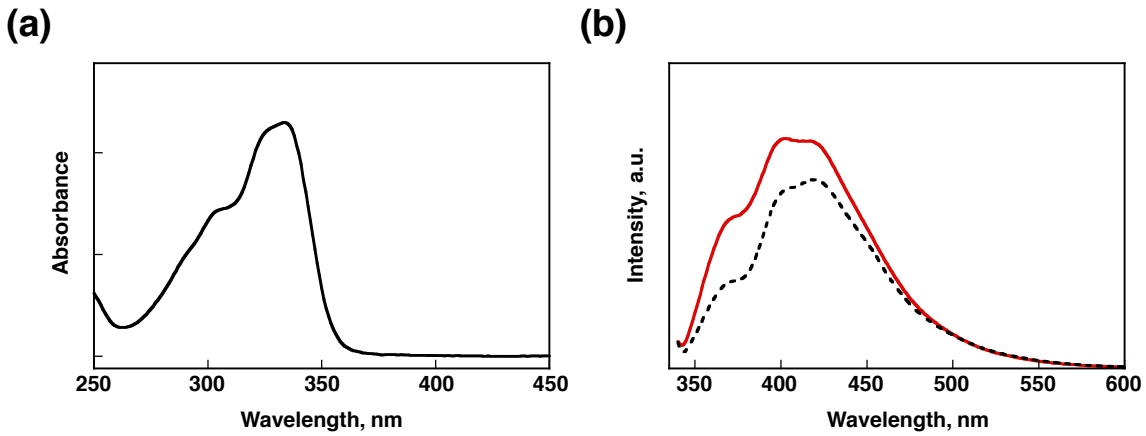

Figure 1-10. Normalized (a) UV-vis absorption and (b) fluoresence spectra of I–FL–CHO in $CHCl_3$ at 298 K under air (dash black) and under Ar (red line). (λ_{ex} = 332 nm)

It is possible to modify and improve the macrosopic emission characteristics such as emission colour and photoluminescence quantum yield by controlling the π-conjugated length. Accordingly, we designed and synthesized 2-aldehyde-8-bromo-6,12-dihydro-6,6,12,12-tetroctyl-indeno [1,2-b] fluorene (**Br–di-FL–CHO**). The **Br–di-FL–CHO** displays extended π-conjugated plannar structure. As a result, enhanced photoluminesence quantum yield and emission feature change could be expected, which is beneficial from lowering internal conversion as well as restrict vibrational loss of excited state. The preliminary results of UV-Vis absorption and fluorescence spetra of **Br–di-FL–CHO** were presented in Figure 1-11. We found that **Br–di-FL–CHO** showed characteristic fluorescence properties without the generation of phosphorescence. This result

indicated that combination of bromo and aldehyde as well as the conjugated length is indispensable to facilitate phosphoresence in solution at room temperature.

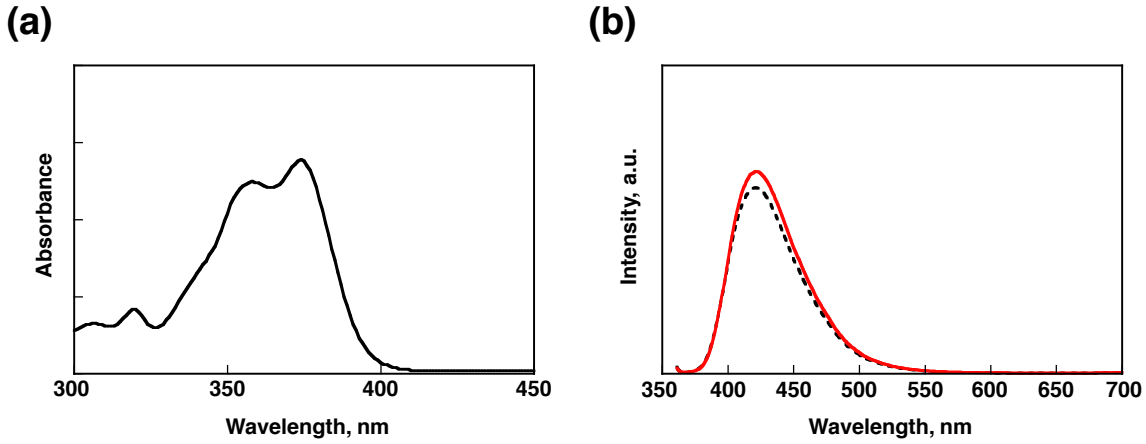

Figure 1-11. Normalized (a) UV-vis absorption and (b) fluoresence spectra of **Br–di-FL–CHO** in $CHCl_3$ at 298 K under air (dash black) and under Ar (red line). (λ_{ex} = 332 nm)

In order to gain deeper insight into mechanism of this novel and unanticipated phenomenon, the time-dependent density functional theory (TD-DFT) based on B3LYP/6-31G* basis set calculation has been performed at respective optimized S_0 ground state, S_1 excited singlet state and T_1, T_2 excited triplet state geometries of **Br–FL–CHO** as shown in Figure 1-12a. The identical calculations were conducted for **CHO–FL–CHO** for comparisons. Involvement of unusual intersystem crossing from singlet excited state into triplet excited state is indispensible for occurrence of phosphorescence. In most of cases, the singlet and tripet transition is forbidden without spin-orbit coupling (SOC), because the electric dipole moment is independent of an electron spin.[9b] But SOC is allowed between states of different symmetries and electronic configurations according to El-Sayed' rule.[14a] The results presented that S_1 and T_2 of **Br–FL–CHO** are assigned to $^1(n, \pi^*)$ and $^3(\pi, \pi^*)$ respectively as shown in Figure 1-12a and Table 1-2. Consequently, the different symmetries and electronic configurations between S_1 and T_2 make SOC between them theoretically achievable; transition from T_2 $^3(\pi, \pi^*)$ to T_1 $^3(n, \pi^*)$ through internal conversion was followed by radiative decay from T_1 $^3(n, \pi^*)$ to S_0 ground state, resulting in detectable phosphorescence under ambient conditions. What is the reason for this luminesecent behavior instead of phosphorescence quenching at 298 K? We infer that, relatively less possibilities for occurrence of internal conversion between T_1 $^3(n, \pi^*)$ and ground state (S_0) is attributed to small vibrational overlap integral.[14b] Therefore, non-radiative deactivation from T_1 $^3(n,$

π^*) to ground state was inhibited to some extents and in turn radiative decay was predominate. It has been successfully demonstrated that the TD-DFT quantum chemistry calculation results are well in accordance with the experimental results. The efficency of intersystem crossing of **CHO–FL–CHO** from excited singlet state into triplet stae is relatively low, due to the same configuration between them, which accounts for no observation of phosphoresecence under experimental conditions.

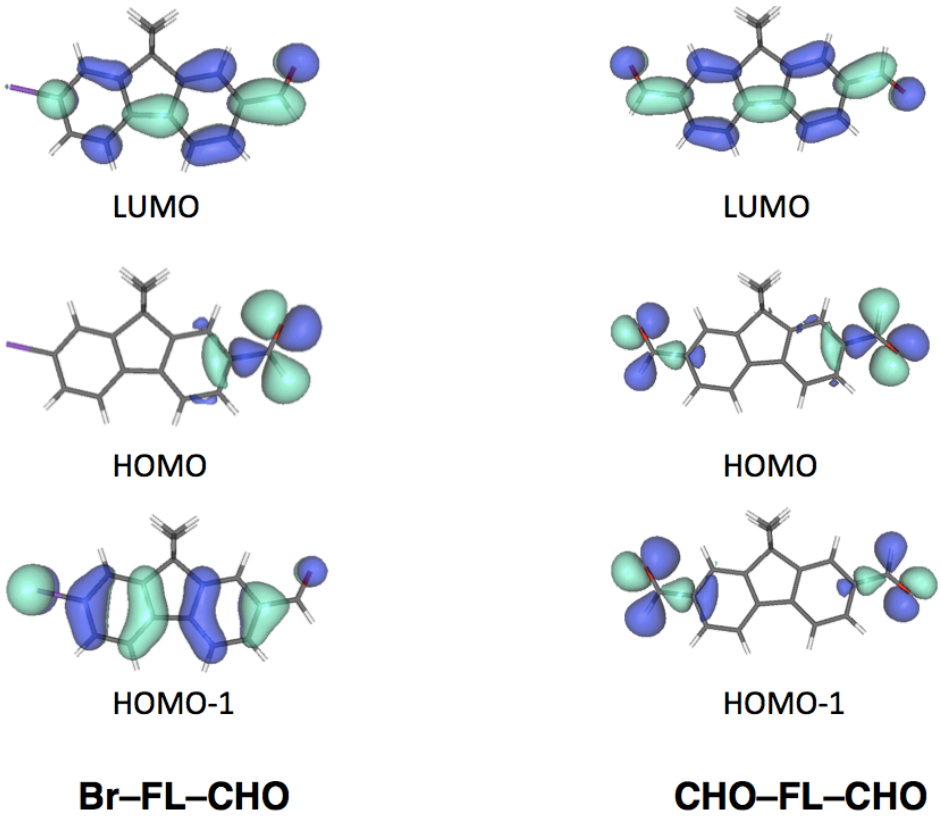

Figure 1-12. Diagrams of the molecular orbitals of **Br–FL–CHO** (left) and **CHO–FL–CHO** (right).

Table 1-2. Calculated excited state of **Br–FL–CHO** and **CHO–FL–CHO** by TD–DFT calculation.

Compound	State	Transition	E/nm (eV)	Configuration
Br–FL–CHO	S_1	HOMO → LUMO	345 (3.59)	(n, π^*)
	S_2	HOMO → LUMO+1	316 (3.92)	(π, π^*)
	T_1	HOMO → LUMO	464 (2.67)	(n, π^*)
	T_2	HOMO → LUMO+1	404 (3.07)	(π, π^*)
CHO–FL–CHO	S_1	HOMO → LUMO	355 (3.49)	(n, π^*)
	S_2	HOMO-1 → LUMO	352 (3.52)	(n, π^*)
	T_1	HOMO → LUMO	488 (2.54)	(n, π^*)
	T_2	HOMO-1 → LUMO	412 (3.01)	(n, π^*)

Based on TD–DFT calculations, the plausible mechanism of this phenomenon is elucidated as shown in Figure 1-13.

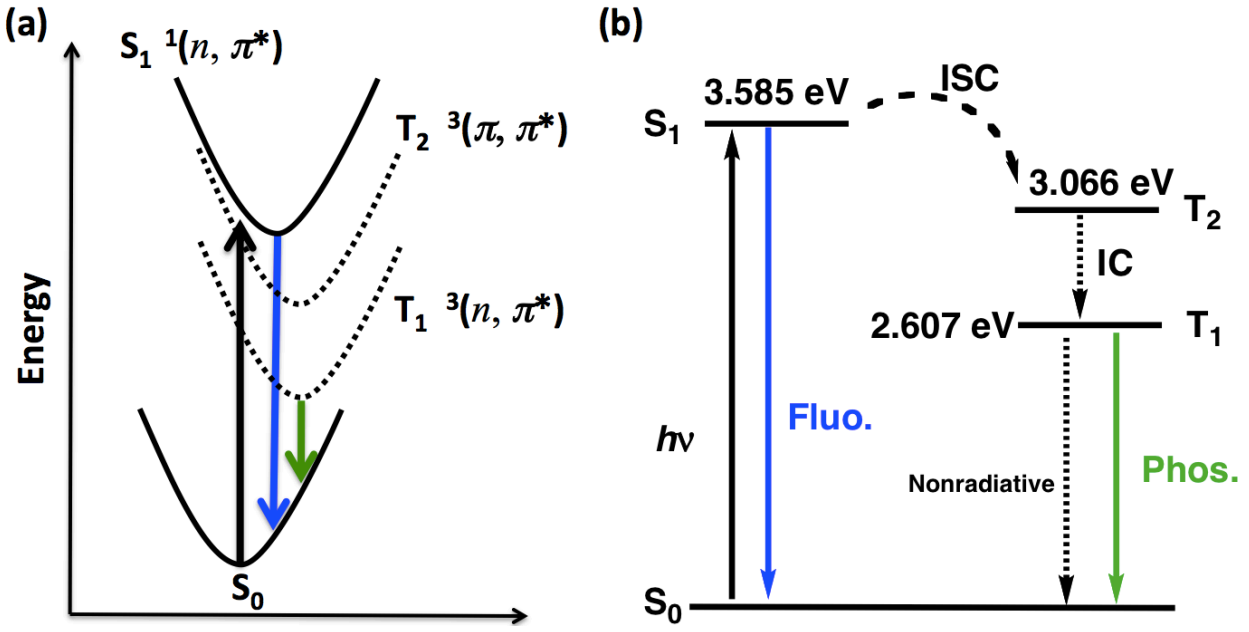

Figure 1-13. (a) Sketch of the potential energy surfaces and vertical transition energies for S_1, T_1 and T_2 states of **Br–FL–CHO**. (b) Modified Jablonski diagram based on TD-DFT calculation, illustrating plausible mechanism for observation of phosphoresence under experimental conditions. (ISC: Intersystem Crossing, IC: Internal Conversion)

It is of great importance to achieve phosphorescence in various common organic solutions at room temperature. This novel property makes this system more versatile and practical because it can be embedded into any polymer matrixs to make a fabrication of film easily by solution processing. This time we chose PMMA as polymer matrix due to its relatively low permeability of oxygen.[12] Films of **Br–FL–CHO** and **FL** doped in PMMA were fabricated by drop-casting of $CHCl_3$ solution containing the corresponding fluorene derivatives and PMMA (5 wt%) onto the surface of quartz cell. The corresponding emission spectra and photoimage of PMMA films of **Br–FL–CHO** and **FL** are shown in Figure 1-14. The emission maximum at 500 nm of **Br–FL–CHO**-doped PMMA film corresponds perfectly to the phosphorescence emission in organic solvents. In addition, the **Br–FL–CHO**-doped PMMA film displays green emission upon illumination of 254 nm, whereas blue

emission was observed for **FL**-doped PMMA film. Surprisingly, the PMMA film of **Br–FL–CHO** showed emission at 500 nm for over five days even under air, as shown in Figure 1-14.

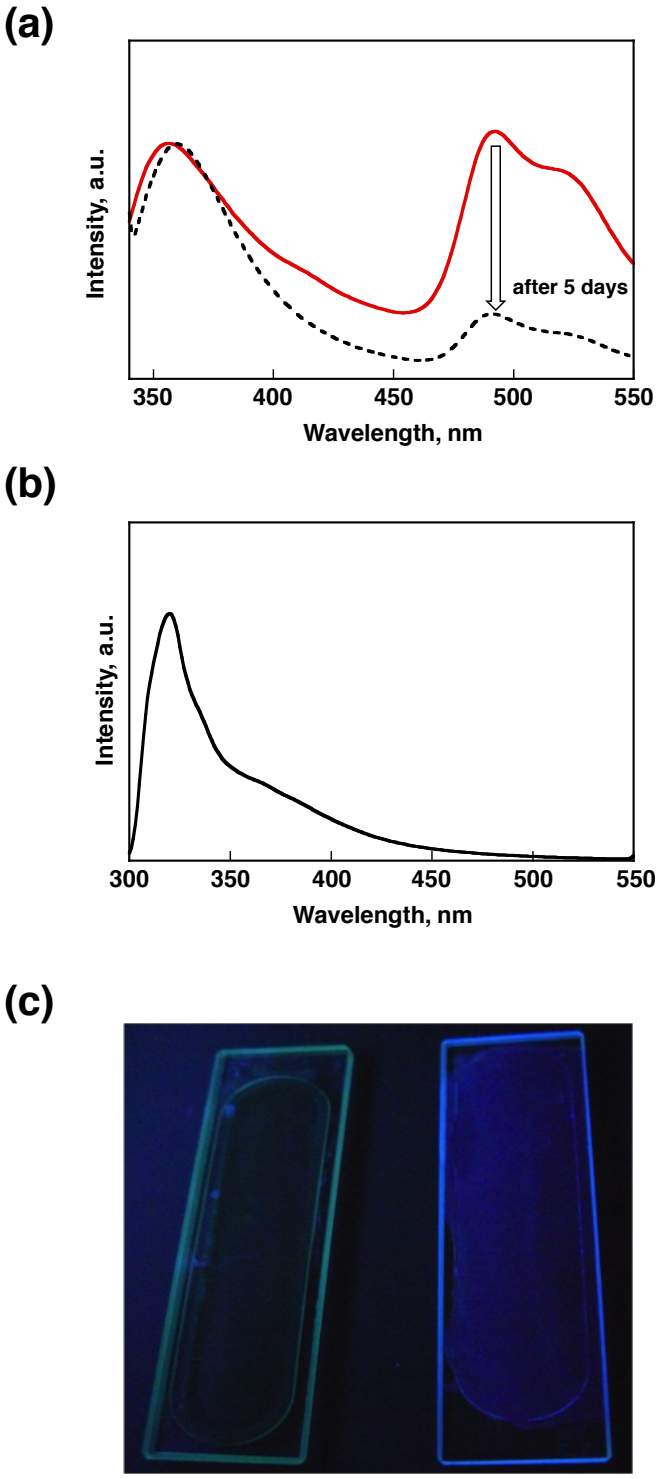

Figure 1-14. Fluorescence spectra of PMMA films of (a) **Br–FL–CHO** (red line: just after fablicating the film, black dash: after 5 days) and (b) **FL** at 298 K. The excitation wavelengths are

300 nm and 280 nm, respectively. (c) Photographic image of PMMA-based **Br–FL–CHO** (left) and **FL** (right) upon UV-light irradiation at 254 nm under air at 298 K.

This result suggests that **Br–FL–CHO** inside the PMMA matrix is molecularly dispersed and shielded from dioxygen to exhibit phosphorescence emission at 500 nm as well as fluorescence emission at 358 nm. Low permeability of dioxygen in PMMA film assists the efficient phosphorescence emission of **Br–FL–CHO** even under air.

Conclusions

In conclusion, the well-known fluorescent material surprised us with novel and unanticipated phenomenon that a pure organic fluorene derivative bearing bromo and formyl groups exhibited phosphorescence emission in solution at room temperature. The **Br–FL–CHO**-doped PMMA film also showed phosphorescence emission for several days at room temperature even upon exposure to dioxygen. We believe that this unanticipatedly new finding will surely offer a great platform toward the development of practical optoelectronic devices and dioxygen-sensors based on purely organic phosphors under ambient conditions.

Experimental Sections

Chemicals and Reagents.

All chemicals were purchased from Aldrich, Kanto Chemicals, TCI or Wako and used as received. Chloroform ($CHCl_3$), anhydrous Dimethylformamide (DMF), Dimethyl sulfoxide (DMSO), 2-MeTHF and hexane spectroscopic grade (Wako Pure Chemical Industries, Ltd.) were used for analysis. Fluorene derivatives were synthesized according to the literature procedures.[11]

Instrumentation.

^{1}H NMR spectra were recorded on a Biospin DRX-600 spectrometer (600 MHz); chemical shifts are expressed in ppm relative to TMS (0 ppm). UV-Vis absorption spectra, fluorescence spectra were obtained on a Hitachi U-2900 spectrophotometer and Hitachi F-7000 spectrophotometer, respectively. Absolute fluorescence and phosphorescence quantum yields were obtained on a Hamamatsu Photonics, Absolute PL Quantum Yield Measurement System, C9920-02G. The fluorescence and phosphorescence lifetimes of the fluorene derivatives were measured by a Horiba FluoroCube time-correlated single-photon-counting (TCSPC) system equipped with a pulse laser. The decay profile simulations were performed by a nonlinear least-squares method.

Synthesis of 9,9-didodecylfluorene-2,7-dicarbaldehyde (CHO–FL–CHO).

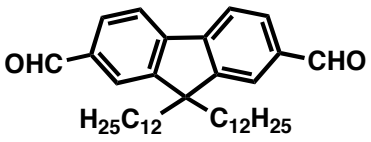

To a stirred solution of 2,7-Dibromo-9,9-didodecylfluorene (5 g, 7.6 mmol) in anhydrous ether (50 mL) at –78 °C, 2.5 M n-BuLi solution in hexane (7.6 mL, 19.0 mmol) was added dropwise under argon atmosphere and continued stirring for 30 min. Then the reaction mixture was warmed to room temperature and kept stirring for another 30 min. It was cooled again to –78 °C, following by addition of DMF (2.1 mL, 27.1 mmol) to room temperature gradually. Aqueous HCl solution (2 M, 80 mL) was added and continued stirring for another 2 h. The reaction mixture was extracted with ether and washed with water and brine. The organic extracts were dried over anhydrous Na_2SO_4. The solvent was evaporated under reduced pressure to give white solid. Yield: 83%; ^{1}H NMR (600 MHz, $CDCl_3$): δ [ppm] 0.53–0.57 (m, 4H), 0.86 (t, J = 7.2 Hz, 6H), 1.02–1.31 (m, 36H), 2.05–2.11 (m, 4H), 7.90–7.94 (m, 6H), 10.10 (s, 2H).

Synthesis of 2,7-Diodo-9,9-didodecylfluorene (I–FL–I).

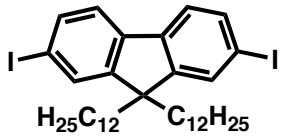

To a solution of 9,9-didodecylfluorene (3 g, 6.1 mmol), iodine (1.13 g, 4.43 mol), iodic acid (0.5 g, 2.85 mmol), concentrated sulfuric acid (1 mL) and carbon tetrachloride (2 mL) in acetic acid (8 mL) was warmed to 80 ^{o}C for 5 h. The resulting precipitate was filtered and dissolved in dichloromethane; the solution was then washed with aqueous sudium thiosulfate (0.1 M), dried over Na_2SO_4 and evaporated to dryness to yield a white power (3.2 g, 70%), which gave, by recrystallisation from ethyl acetate. ^{1}H NMR (600 MHz, $CDCl_3$): δ [ppm] 0.53–0.57 (m, 4H), 0.89 (t, J = 12 Hz, 6H), 1.03–1.28 (m, 36H), 1.87–1.96 (m, 4H), 7.25–7.43 (m, 3H), 7.64–7.69 (m, 3H).

Synthesis of 7-iodo-9,9-didodecylfluorene-2-carbaldehyde (I–FL–CHO).

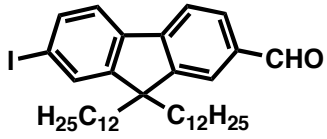

To a stirred solution of 2,7-Diodo-9,9-didodecylfluorene (1g, 1.33 mmol) in anhydrous ether (mL) at –78 °C, 2.5 M *n*-BuLi solution in hexane (0.66 mL, 1.66 mmol) was added dropwise under argon atmosphere and continued stirring for 30 min. Then the reaction mixture was warmed to room temperature and kept stirring for another 30 min. It was cooled again to –78 °C, following by addition of DMF (0.26 mL, 3.3 mmol) to room temperature gradually. Aqueous HCl solution (2 M, 8 mL) was added and continued stirring for another 2 h. The reaction mixture was extracted with ether and washed with water and brine. The organic extracts were dried over anhydrous Na_2SO_4. The solvent was evaporated under reduced pressure to give white solid. Yield: 35%; ^{1}H NMR (600 MHz, $CDCl_3$): δ [ppm] 0.56–0.59 (m, 4H), 0.85–0.89 (m, 6H), 1.02–1.13 (m, 36H), 1.56–2.03 (m, 4H), 7.38–7.40 (m, 3H), 7.83–7.87 (m, 3H), 10.06 (s, 1H).

Synthesis of 2-aldehyde-8-bromo-6,12-dihydro-6,6,12,12-tetroctyl-indeno[1,2-b] fluorene (Br–di-FL–CHO).

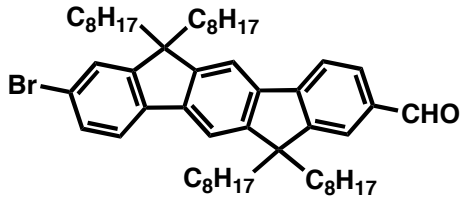

To a stirred solution of 2,8-Dibromo-6,12-dihydro-6,6,12,12-tetraoctyl-indeno [1,2-b] fluorene (50 mg, 0.058 mmol) in anhydrous ether (1 mL) at –78 °C, 0.25 M *n*-BuLi solution in hexane (1.6 mL, 0.638 mmol) was added dropwise under argon atmosphere and continued stirring

for 30 min. Then the reaction mixture was warmed to room temperature and kept stirring for another 30 min. It was cooled again to −78 °C, following by addition of DMF (1.12 mL, 14.47 mmol) to room temperature gradually. Aqueous HCl solution (2 M, 2 mL) was added and continued stirring for another 2 h. The reaction mixture was extracted with ether and washed with water and brine. The organic extracts were dried over anhydrous Na_2SO_4. The solvent was evaporated under reduced pressure to give white solid. Yield: 62%; ^{1}H NMR (600 MHz, CD_2Cl_2): δ [ppm] 0.57–0.59 (m, 8H), 0.74–0.79 (m, 12H), 1.02–1.12 (m, 40H), 1.97–2.12 (m, 8H), 7.44–7.50 (m, 2H), 7.62–7.64 (d, J = 7.2 Hz, 1H), 7.67 (s, 1H), 7.72 (s, 1H), 7.82–7.89 (m, 3H), 10.02 (s, 1H).

Theoretical Calculation.

The time dependent density functional theory (TD-DFT) calculations based on geometry optimization was carried out using the Becke 3LYP functional and 3-21G(*) basis set with the Gaussian 03 program, revision.

Preparation of Fluorene-Doped Films.

The fluorene derivatives (5 mmol) and PMMA (500 mg) were dissolved in 10 mL of $CHCl_3$, and the film was prepared by drop-casting the solution onto the surface of quartz cell. The transparent PMMA films of the fluorene derivatives were obtained by slow evaporation of $CHCl_3$.

Reference

1 *(a)* Y. Shirota, *J. Mater. Chem.*, 2000, **10**, 1; *(b)* A. C. Grimsdale, K. L. Chan, R. E. Martin, P. G. Jokisz and A. B. Holmes, *Chem. Rev.*, 2009, **109**, 897; *(c)* L. X. Xiao, Z. J. Chen, B. Qu, J. X. Luo, S. Kong, Q. H. Gong and J. J. Kido, *Adv. Mater.*, 2011, **23**, 926.

2 Q. Zhao, F. Y. Li and C. H. Huang, *Chem. Soc. Rev.*, 2010, **39**, 3007.

3 *(a)* C. Y. Park, J. Lim, M. Y. Yun and C. Kim, *Angew. Chem., Int. Ed.*, 2008, **47**, 2959; *(b)* A. Jana, K. S. P. Devi, T. K. Maiti and N. D. P. Singh, *J. Am. Chem. Soc.*, 2012, **134**, 7656; *(c)* A. Gopal, M. Hifsudheen, S. Furumi, M. Takeuchi and A. Ajayaghosh, *Angew. Chem., Int. Ed.*, 2012, **51**, 10505.

4 *(a)* J. Liu, Z. Xie, Y. Cheng, Y. Geng, L. Wang, X. Jing and F. Wang, *Adv. Mater.*, 2007, **19**, 531; *(b)* K. Y. Pu, K. Li and B. Liu, *Adv. Mater.*, 2010, **22**, 643; *(c)* K. Y. Pu, K. Li and B. Liu, *Chem. Mater.*, 2010, **22**, 6736; *(d)* D. Yu, Y. Zhao, H. Xu, C. Han, D. Ma, Z. Deng, S. Gao and P. Yan, *Chem. Eur. J.*, 2011, **17**, 2592; *(e)* P. Robert, A. Bolduc and W. G. Skene, *J. Phys. Chem. A*, 2012, **116**, 9305.

5 *(a)* M. Leclerc, *J. Polym. Sci., Part A: Polym. Chem.*, 2001, **39**, 2867; *(b)* U. Scherf and E. J. W. List, *Adv. Mater.*, 2002, **14**, 477; *(c)* S. Beaupre, P. L. T. Boudreault and M. Leclerc, *Adv. Mater.*, 2010, **22**, E6; *(d)* C. H. Chen, Y. C. Hsu, H. H. Chou, K. R. J. Thomas, J. T. Lin and C. P. Hsu, *Chem. Eur. J.*, 2010, **16**, 3184; *(e)* J. Zhang, H. B. Li, S. L. Sun, Y. Geng, Y. Wu and Z. M. Su, *J. Mater. Chem.*, 2012, **22**, 568.

6 *(a)* M. A. Baldo, D. F. O'Brien, Y. You, A. Shoustikov, S. Sibley, M. E. Thompson and S. R. Forrest, *Nature*, 1998, **395**, 151; *(b)* Yersin, H. *Top. Curr. Chem.*, 2004, **241**, 1.

7 *(a)* K. Goushi, K. Yoshida, K. Sato and C. Adachi, *Nat. Photonics*, 2012, **6**, 253; *(b)* Q. Zhang, J. Li, K. Shizu, S. Huang, S. Hirata, H. Miyazaki and C. Adachi, *J. Am. Chem. Soc.*, 2012, **134**, 14706; *(c)* T. Nakagawa, S. Y. Ku, K. T. Wong and C. Adachi, *Chem. Commun.*, 2012, **48**, 9580; *(d)* G. Méhes, H. Nomura, Q. Zhang, T. Nakagawa and C. Adachi, *Angew. Chem., Int. Ed.*, 2012, **51**, 11311; *(e)* H. Uoyama, K. Goushi, K. Shizu, H. Nomura and C. Adachi, *Nature*, 2012, **492**, 234.

8 *(a)* C. Wu, B. Bull, K. Christensen and J. McNeill, *Angew. Chem., Int. Ed.*, 2009, **48**, 2741; *(b)* Y. You and S. Y. Park, *Dalton Trans*., 2009, **8**, 1267; *(c)* J. R. Sommer, A. H. Shelton, A. Parthasarathy, I. Ghiviriga, J. R. Reynolds and K. S. Schanze, *Chem. Mater.*, 2011, **23**, 5296; *(d)* H. Sun, H. Guo, W. Wu, X. Liu and J. Zhao, *Dalton Trans*., 2011, **40**, 7834; *(e)* M. T. Whited, P. I. Djurovich, S. T. Roberts, A. C. Durrell, C. W. Schlenker, S. E. Bradforth and M .E. Thompson, *J. Am. Chem. Soc.*, 2011, **133**, 88; *(f)* W. Lu, W-M. Kwok, C. S. Ma, C. T.-L, Chan, M.-X. Zhu and

C.-M. Che, *J. Am. Chem. Soc.*, 2011, **133**, 14120; *(g)* Z. M. Hudson, C. Sun, M. G. Helander, Y. L. Chang, Z. H. Lu and S. Wang, *J. Am. Chem. Soc.*, 2012, **134**, 13930.

9 *(a)* D. R. Kearns and W. A. Case, *J. Am. Chem. Soc.*, 1966, **88**, 5087; *(b)* K. Kalyanasundaram, F. Grieser and J. K. Thomas, *Chem. Phys. Lett.*, 1977, **51**, 501; *(c)* N. J. Turro, K. C. Liu, M. F. Chow and P. Lee, *Photochem. Photobiol.*, 1978, **27**, 523; *(d)* N. J. Turro, V. Ramamurthy and J. C. Scaianon *Modern Molecular Photochemistry of Organic Molecules*, University Science Books: Sausalito, 2010.

10 *(a)* G. Zhang, J. Chen, S. J. Payne, S. E. Kooi, J. N. Demas and C. L. Fraser, *J. Am. Chem. Soc.*, 2007, **129**, 8942; *(b)* W. Z. Yuan, X. Y. Shen, H. Zhao, J. W. Y. Lam, L. Tang, P. Lu, C. Wang, Y. Liu, Z. Wang, Q. Zheng, J. Z. Sun, Y. Ma and B. Z. Tang, *J. Phys. Chem. C*, 2010, **114**, 6090; *(c)* O. Bolton, K. Lee, H. J. Kim, K. Y. Lin and J. Kim, *Nat. Chem.*, 2011, **3**, 205; *(d)* G. P. Yong, Y. M. Zhang, W. L. She, Y. Z. Li, *J. Mater. Chem.*, 2011, **21**, 18520; *(e)* S. Menning, M. Kramer, B. A. Coombs, F. Rominger, A. Beeby, A. Dreuw and U. H. F. Bunz, *J. Am. Chem. Soc.*, 2013, **135**, 2160.

11 C. Vijaykumar, K. Sugiyasu and M. Takeuchi, *Chem. Sci.*, 2011, **2**, 291.

12 *(a)* W. J. Koros and M. Moaddeb, in *Polymeric Materials Encyclopedia*: *Synthesis, Properties, and Applications*, ed. J. C. Salamone, CRC Press, Boca Raton 1996; *(b)* S. Hess, A. Becker, S. Baluschev, V. Yakutkin and G. Wegner, *Macromol. Chem. Phys.*, 2007, **208**, 2173.

13 Z. Chen, J. Bouffard, S. E. Kooi and T. M. Swager, *Macromolecules*, 2008, **41**, 6672.

14 *(a)* M. Baba, *J. Phys. Chem. A*, 2011, **115**, 9514; *(b)* G. Bergamini, A. Fermi, C. Botta, U. Giovanella, S. Motta, F. Negri, R. Peresutti, M. Gingras and P. Ceroni, *J. Mater. Chem. C*, 2013, **1**, 2717.

Chapter 2.
RGB Trichromophoric Nanoparticle with Dual FRET: Highly Sensitive Fluorogenic Response toward Polyanions

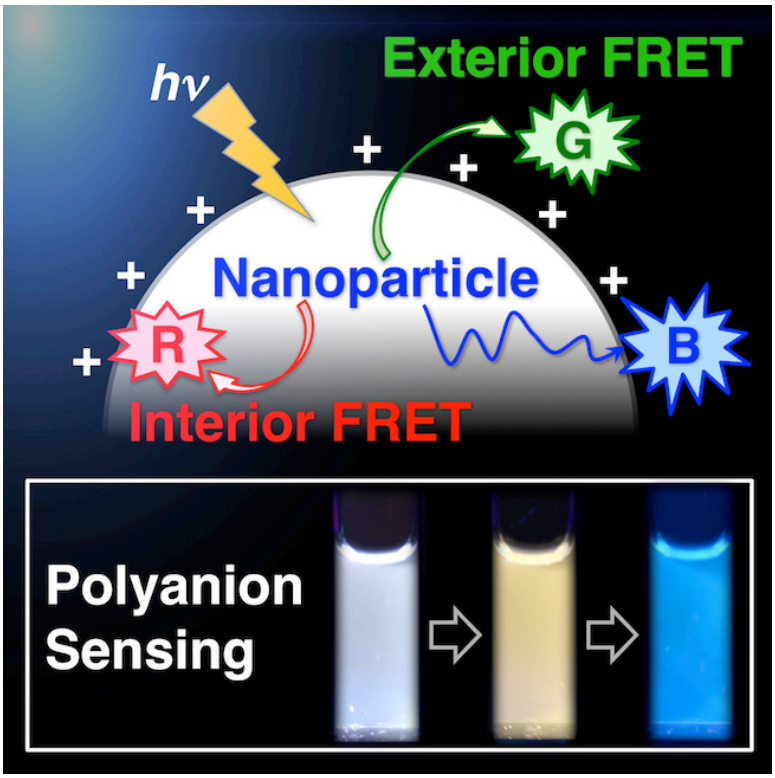

Abstract

A red-green-blue (RGB) trichromophoric fluorescent organic nanoparticle exhibiting multicolor emission was constructed; the blue emitting cationic oligofluorene nanoparticle acted as an energy donor scaffold to undergo FRET to the red emitting dye embedded in the nanoparticle (interior FRET) and to the green emitting dye adsorbed on the surface through electrostatic interaction (exterior FRET). Each FRET event occurs independently and is free from sequential FRET, thus the resultant dual FRET system exhibits multicolor emission including white in aqueous solution and film state. A characteristic white emissive nanoparticle showed perceived visible response upon perturbation of the exterior FRET efficiency by the acceptor displacement, leading to highly sensitive response toward polyanions in a ratiometric manner. Specifically, our system exhibits high sensitivity toward heparin with extremely low detection limit.

Introduction

Multichromophoric luminescent assemblies have found widespread use in biological, polymeric, and sensory materials chemistry, exhibiting multiple emissions to generate perceived colors for lightning, imaging, sensing, and so forth.[1] An efficient strategy for tuning emissions from multichromophoric assemblies is use of fluorescence resonance energy transfer (FRET) among chromophores, which has extensively been investigated in organogel,[2] nanofiber,[3] nanoparticle,[4] supramolecular polymer,[5] and so forth.[6] Among them, fluorescent organic nanoparticles have recently been regarded as a powerful platform for spatial control over the molecular organization of energy donor/acceptor constituents.[7–9] The advantages of such fluorescent organic nanoparticle systems are the relatively high fluorescent quantum yield, the capability of surface modification and incorporation of additives, and the potential use as light-harvesting antennas exhibiting effective exciton or energy migration among constituents. It thus occurred to us that if one can construct a multichromophoric system based on a fluorescent organic nanoparticle scaffold (energy donor) with one energy acceptor within the nanoparticle and the other on the surface, the multiple emissions would be readily possible by regulating dual signaling pathways without interfering each other. Such a "dual FRET" system should be sensitive to perturbations of either signaling pathway induced by an analyte, giving rise to highly sensitive sensory system with color changes.We herein describe a facile strategy to fabricate red-green-blue (RGB) trichromophoric fluorescent nanoparticles in aqueous medium where two distinct FRET events occur

through spatial-organization of a donor scaffold and two acceptor molecules for exhibiting multicolor emission in the whole visible range. We also demonstrate that the cationic trichromophoric nanoparticle suspension acts as a highly sensitive ratiometric and colorimetric sensor toward polyanionic species. In particular, a white emissive nanoparticle, which has low background in terms of colorfulness,[10] is beneficial for sensing an anionic polysaccharide, heparin, exhibiting the remarkable emission color changes and low detection limit comparable or even superior to a conventional heparin binder, hexadimethrine bromide, under the conditions we used here.

Results and discussions

To construct the RGB trichromophoric assembled nanoparticle system, we chose a blue emitting cationic oligofluorene (**OF**) acting as an energy donor nanoparticle scaffold, a red emitting neutral dye 4-(dicyanomethylene)-2-methyl-6-(4-dimethylamino-styryl)-4H-pyran (**DCM**) encapsulated within the nanoparticle for interior FRET, and a green emitting anionic dye perylene-3,4,9,10-tetracarboxylate tetrapotassium salt (**PS**) adsorbed on the nanoparticle for exterior FRET. The chemcial structures of **OF**, **DCM** and **PS** were shown in Scheme 2-1.

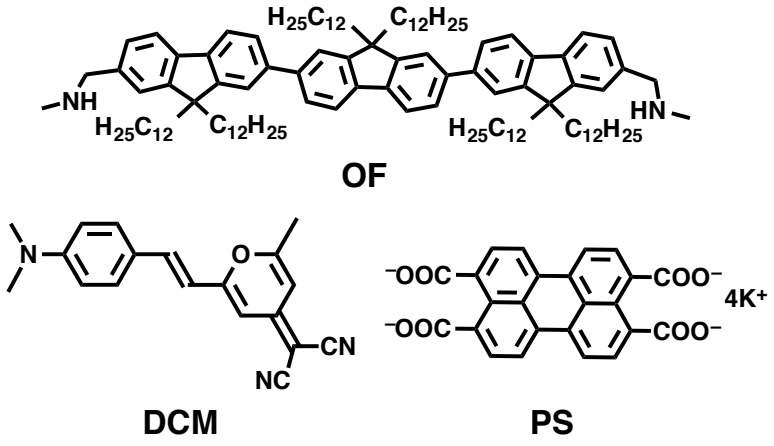

Scheme 2-1. Chemical structures of **OF** (energy donor), **DCM** (energy acceptor**)**, and **PS** (energy acceptor).

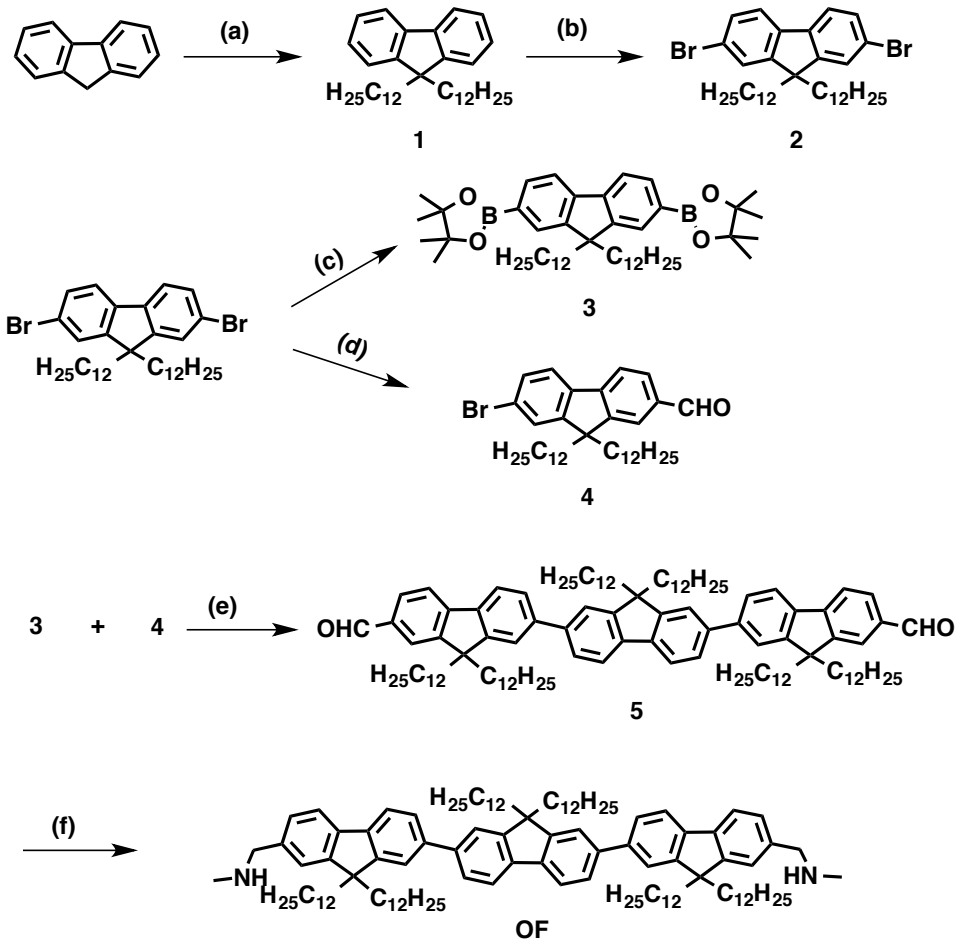

Scheme 2-2. Reagents and conditions: (a) *n*–BuLi, THF, $C_{12}H_{25}Br$, –78 °C to r.t, 5h; (b) bromine, iodine, CH_2Cl_2, r.t, 20 h; (c) *n*–BuLi, 2–isopropoxy–4,4,5,5–tetramethyl–1,3,2–dioxaborolane, THF, –78 °C to r.t, 24 h; (d) *n*–BuLi, diethylether, –78 °C and r.t, 1 h; DMF, –78 °C to r.t, 8 h; (e) $Pd(PPh_3)_4$, K_2CO_3, THF–water, 90 °C, 2 h; (f) CH_3NH_2, $NaBH_4$, MeOH, CH_2Cl_2, r.t, 1 h.

The dodecyl-substituted **OF** typically affords nanoparticles through self-assembly.[11] The *N*-methylaminomethyl end groups would be protonated in aqueous medium ($pK_a \sim 10.7$), leading to the cationic nanoparticles. The oligofluorene derivative **OF** functionalized with 9,9'-dodecyl chains and *N*-methylaminomethyl end groups was synthesized according to the steps shown in Scheme 2-2.

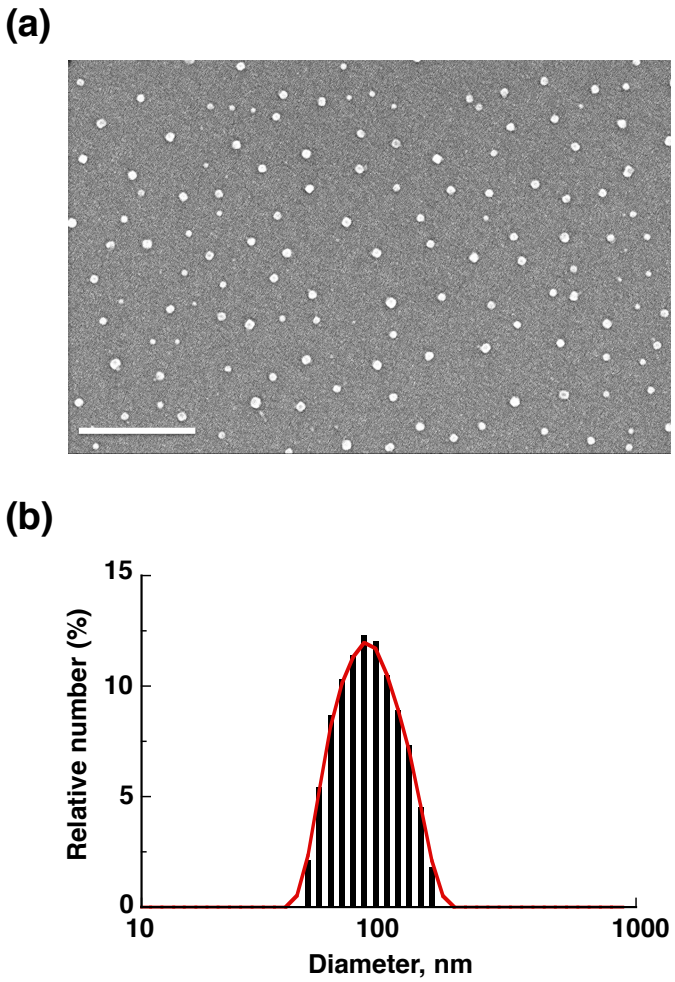

Figure 2-1. (a) A SEM image of **OFN** drop-casted from aqueous suspension on a silicon substrate (scale bar equivalent to 500 nm). (b) Size distribution profile from DLS analysis ([**OF**] = 1×10^{-5} M). The average diameter varies about ± 5 nm.

One of simple and straightforward approaches for the preparation of nanoparticles is reprecipitation method by injecting THF solution of **OF** into water under vigorous stirring. No stabilizer or surfactant was added during the preparation. Indeed, upon rapid injection of THF solution of **OF** into water under vigorous stirring, a nanoparticle suspension of **OF** (**OFN**) was obtained as a macroscopically homogeneous and well-dispersed solution without formation of agglomerated precipitates.[12]

We used fresh nanoparticles for each experiment, and the nanoparticles in this study are thermally and photochemically stable. Scanning electron microscope (SEM) and dynamic light scattering (DLS) studies revealed that the resultant **OFN**s are approximately spherical shapes with the average diameter of 83 nm, as shown in Figures 2-1a and 2-1b. Zeta (ξ) potential measurement showed that the surface

of the nanoparticle was positively charged. The ξ-potential of the nanoparticle was found to be + 37 mV indicating good stability for the colloidal dispersion, which means that agglomeration and precipitation of the particles did not take place. The charged particle can move under the influence of an applied external electric field (electrophoresis) with excellent electrophoretic mobility of 3.42×10^{-4} $cm^2\ V^{-1}\ s^{-1}$.

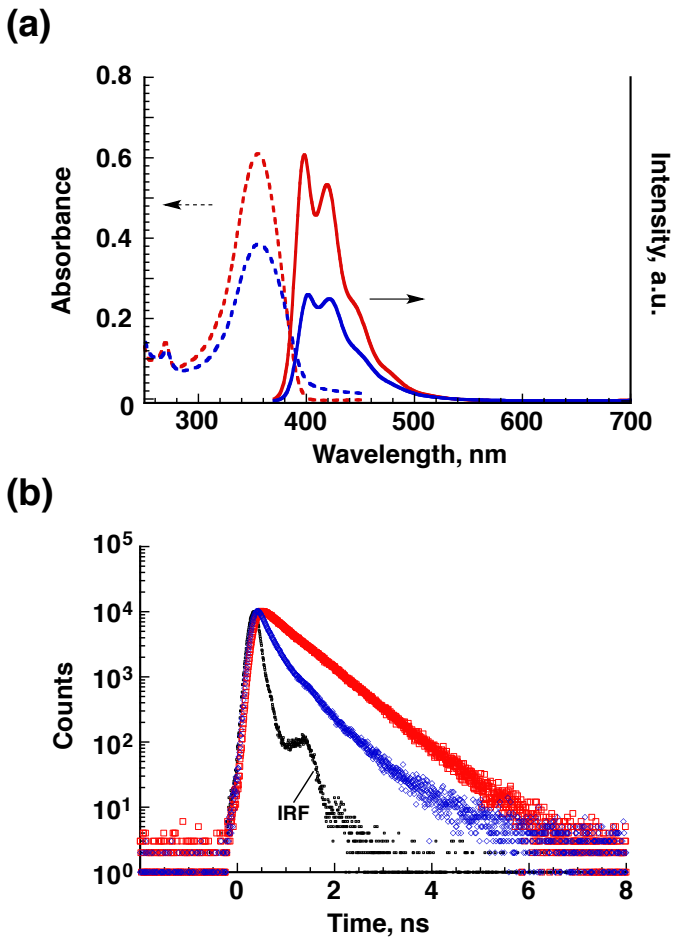

Figure 2-2. (a) Absorption (dash line) and emission (solid line) spectra of **OF** in THF solution (red, 1×10^{-5} M) and **OFN** dispersion (blue, 1×10^{-5} M). Excitation wavelength is 355 nm. (b) Lifetime decay profile (λ_{ex} = 375 nm) of **OF** monitored at 420 nm in THF solution (red) and **OFN** dispersion (blue) (IRF: Instrumental Response Function). The fluorescence lifetime of molecularly dissolved **OF** in THF solution was measured to be 0.69 ns (red) with mono-exponential fluorescence decay. On the other hand, **OFN** suspension presented biexponential decay (blue) having lifetime of 0.24 ns (74.39%) and 0.71 ns (25.61%).

Absorption and emission spectra of **OF** in THF showed the characteristic features of molecularly dissolved species as shown in Figure 2-2 in red line. The absorption maximum was observed at 355 nm with molar extinction coefficient (ε) of $1.05 \times 10^5\ M^{-1}\ cm^{-1}$. The emission spectrum displayed two structured sharp peaks at 398 nm and 418 nm with absolute fluorescence quantum yield Φ_f of 72%. On the other hand, the absorption spectrum of the **OFN** in aqueous medium showed decrease in ε ($0.56 \times 10^5\ M^{-1}\ cm^{-1}$) and a marginal red shift in the absorption maximum (λ_{max} = 356 nm). The nanoparticles emit bright, steady blue fluorescence with subsequent red-shifted in emission maximum and reduced intensity when compared to THF solution as shown in Figure 2-2 in blue line. In accordance with the decrease in the fluorescence intensity, the absolute quantum yield of **OFN** was dramatically reduced to 29%.

Moreover, the fluorescence lifetime of **OF** in THF solution was found to be 0.69 ns with a mono-exponential fluorescence decay indicating only one emitting species as shown in Figure 2-2b. On the other hand, the decay became multi-exponential with an average lifetime of 0.48 ns in **OFN** as shown in Figure 2-2b, which suggests that a significant portion of the excited energy lost in non-radiative ways. The observation of red-shift in the absorption and emission maximum, reduction in the absorption and emission intensities along with decrease in the fluorescent quantum yield and fluorescence decay lifetime in **OFN**, supported the fact that the nano-aggregation occurred, facilitating the formation of the **OFN** in the aqueous medium. All of photo-physical properties of **OF** in THF and aqueous medium are summarized in Table 2-1.

Table 2-1. Photophysical parameters such as absorption maxima, emission maxima, extinction coefficients (ε), absolute fluorescence quantum yield (Φ_f) and fluorescence lifetime (τ_f) of **OF** in THF and **OFN** in aqueous medium.

	Absorption		**Emission**		
	λ_{max} (nm)	$\varepsilon \times 10^5$ ($M^{-1}\ cm^{-1}$)	λ_{max} (nm)	Φ_f (%)	τ_f (ns)
OF in THF	355	1.05	398, 418	72	0.69
OFN in water	356	0.56	402, 421	29	0.48

Interior particle FRET

Facile and efficient tuning of emission colors is one of the most interesting and useful features of organic nanoparticles. Doping techniques based on energy transfer to a fluorescent molecule or dye have been found to be an effective method to tune the emission colour of organic nanoparticles. In several cases, the nanoparticle assembly acts as a donor scaffold for the encapsulated acceptor. Fluorene-based oligomers and polymers are known to be efficient FRET donors because of their suitable energy levels and excellent fluorescence quantum yields.

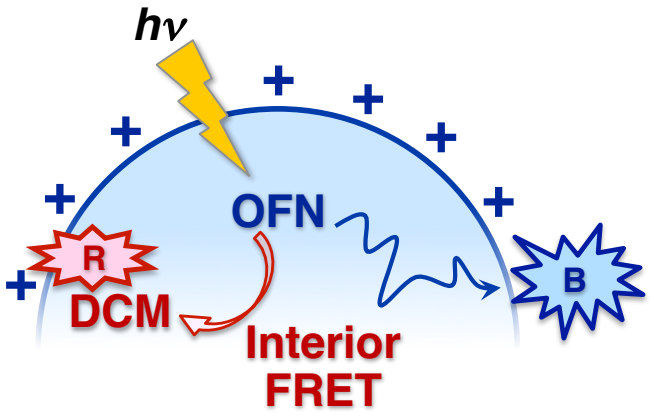

Scheme 2-3. Schematic illustration of interior FRET from **OFN** to **DCM**.

We studied co-assembled nanoparticle composed of **OF** and a red emitting neutral dye (**DCM**) as illustrated in Scheme 2-3. The six dodecyl chains and three fluorene units of **OF** facilitate to incorporate **DCM**, which results in the formation of energy donor-acceptor co-assembled nanoparticles. In order to make the **DCM** encapulated within the **OFN**, the THF solution with mixture of **OF** and **DCM** was rapidly injected into the stirring water as shown in Scheme 2-4.

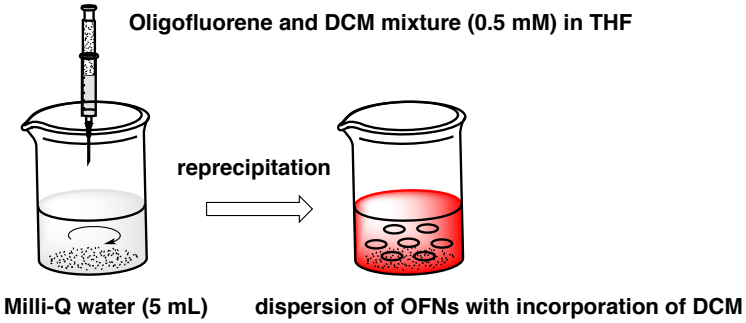

Scheme 2-4. The illustration of the preparation of co-assembled nanoparticle in corporation of **OFN** with **DCM**.

The **OF** satisfied the requirements of a supramolecular donor–acceptor system with **DCM** for FRET studies. For example, there were significant spectral overlaps observed between the donor (**OF**) emission and the acceptor (**DCM**) absorption in the nanoparticle state as shown in Figure 2-3a. The UV/Vis absorption spectra of the donor molecules showed no additional peaks or peak shift on addition of the acceptor, which is an indication of the absence of any ground-state interactions between the donor and acceptor molecules (Figure 2-3b). Direct excitation of the acceptor at the excitation wavelength of the donor was negligible, especially at low acceptor concentrations (Figure 2-3c).

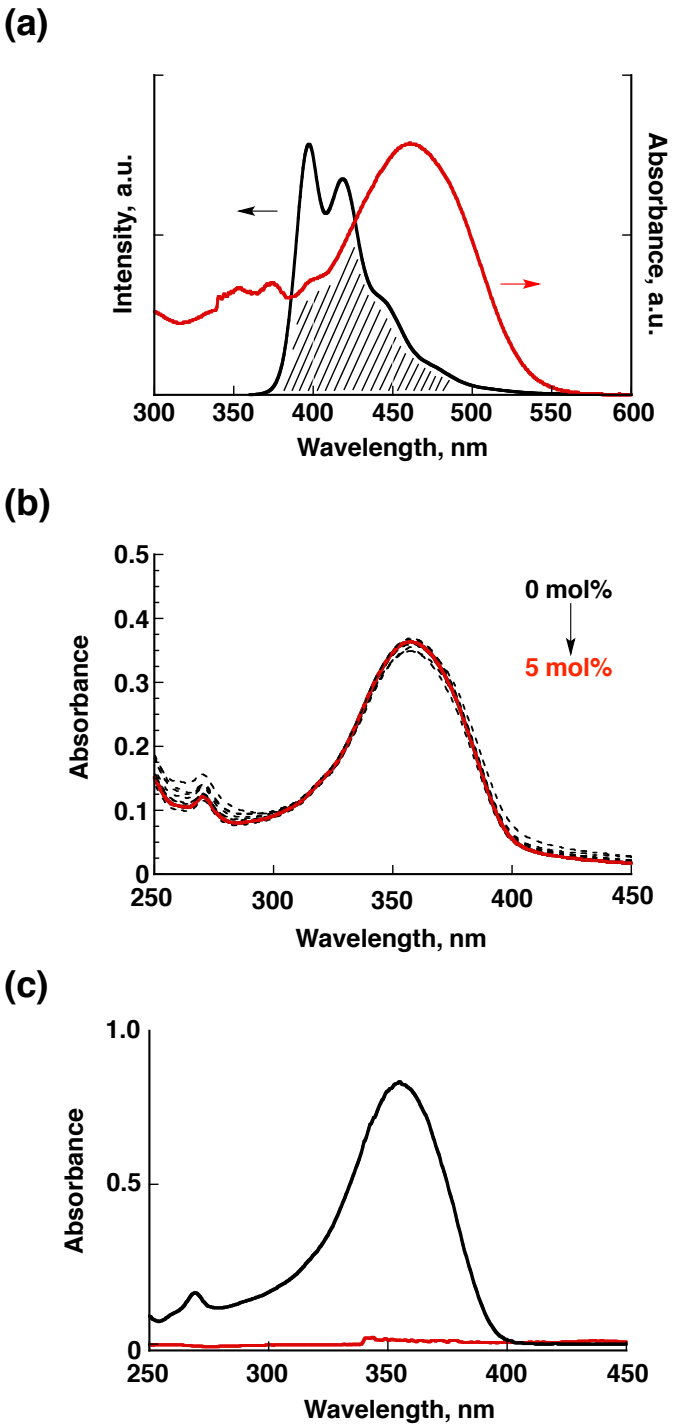

Figure 2-3. (a) Spectral overlap between the absorption of **DCM** energy acceptor (red) and the emission of **OFN** energy donor (black) at room temperature (5×10^{-6} M, λ_{ex} = 355 nm, $J(\lambda) = 1.3 \times 10^{15}$ M^{-1} cm^{-1} nm^4); (b) UV/Vis absorption spectra of **OFN** in the absence and the presence of neutral dye **DCM** (0–5 mol%). Only a little spectral change upon addition of 5 mol% **DCM** was observed, probably because of minimal incorporation of **DCM**; (c) comparison of individual absorption spectra

of **OFN** (black line, [**OF**] = 5×10^{-6} M) and **DCM** (red line, 2×10^{-7} M, which is 4 mol% with respect to the **OFN** concentration), indicating that **OFN** energy donor can be selectively excited at 355 nm.

The identical co-assembled nanoparticles (**OFN–DCM**) were formed reproducibly, as confirmed by UV/Vis absorption and fluorescence spectra. The **OFN–DCM** suspension is stable for one day enough to carry out all the experiments. The averaged size and ξ potential of the resultant **OFN–DCM** (83 nm, +35 mV) were almost the same as those of **OFN** alone because of the minimal incorporation of **DCM** (5 mol%, Figure 2-4).

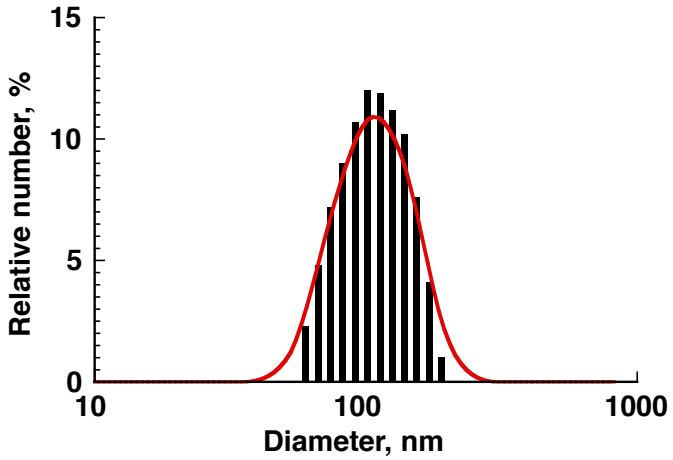

Figure 2-4. Particle size distribution profile of **OFN–DCM** in the presence of 4 mol% **DCM** obtained from DLS analysis. The average diameter is 83 ± 5 nm.

The FRET properties were analyzed by monitoring the **OFN** emission on excitation with UV light in the presence of increasing amounts of the **DCM**. Efficient interior FRET from **OFN** to **DCM** was confirmed by quenching emission from **OFN** along with the appearance of **DCM** emission upon selective excitation of **OFN** at 355 nm (Figure 2-5). The FRET event was visibly recognized; the emission color of the **OFN–DCM** was red in contrast to the blue color from prinstine **OFN**.

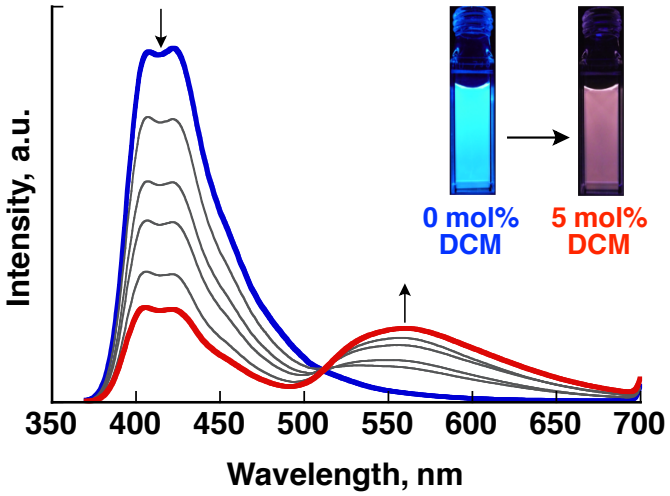

Figure 2-5. Fluorescence spectral changes of **OFN** suspensions upon addition of increasing amounts of **DCM** (λ_{ex} = 355 nm). Insets: fluorescent color images of the nanoparticle suspension in the absence and presence of **DCM** under 365 nm UV-illumination.

The excitation spectra of **OFN–DCM** in the presence of 4 mol% **DCM** was performed and monitored at 600 nm (emission from **DCM**) is consistent with the absorption of **OFN** (Figure 2-6). This results indicated that the emission from **DCM** is originating from the absorption of **OFN**.

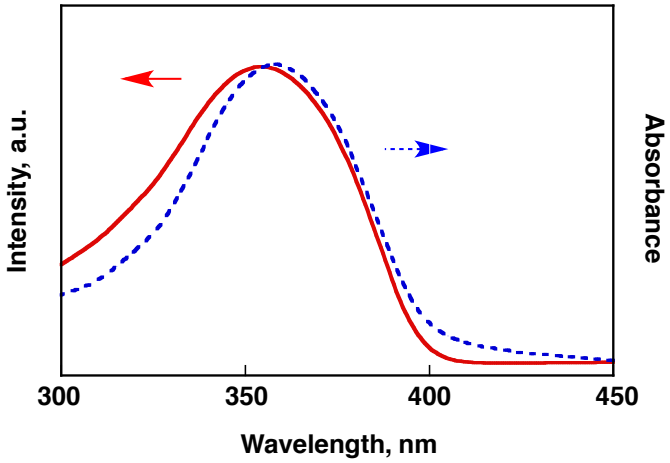

Figure 2-6. Excitation (green) and absorption spectra (blue) of **OFN–DCM** suspension in the presence of 4 mol% **DCM** (λ_{moni} = 600 nm) in aqueous medium.

Time-correlated single photon counting experiments also support the fact that the interior and exterior particle FRET processes efficiently took place (Figure 2-7).

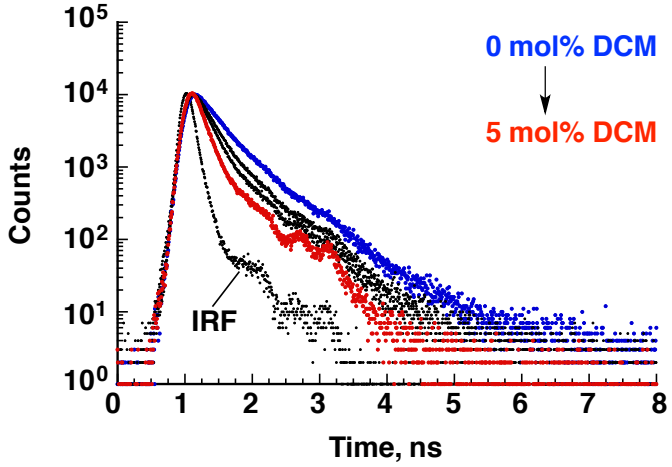

Figure 2-7. Lifetime decay profiles of **OFN–DCM** suspension with increasing amounts (0–5 mol%) of **DCM** (λ_{ex} = 375 nm, λ_{moni} = 420 nm; IRF: Instrumental Response Function).

Exterior particle FRET

We also investigated exterior co-assembling formation of **OFN** with a green emitting dye (**PS**). Because of the positive ξ potential value of the **OFN** surface, **PS** can be physically adsorbed on the surface of **OFN**s through electrostatic interaction to form **OFN–PS** composites where exterior FRET can occur as illustrated in Scheme 2-5.

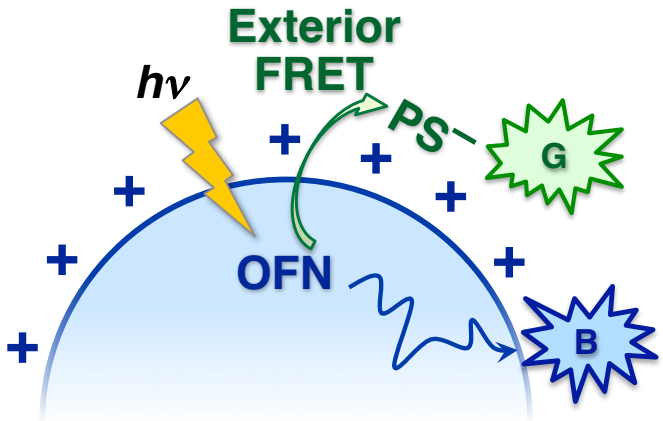

Scheme 2-5. Schematic illustration of exterior FRET from **OFN** to **PS**.

Surface adsorption of **PS** on the **OFN** surface was achieved by adding **PS** in water to the pre-assembled **OFN** suspension at the appropriate concentration as shown in Scheme 2-6.

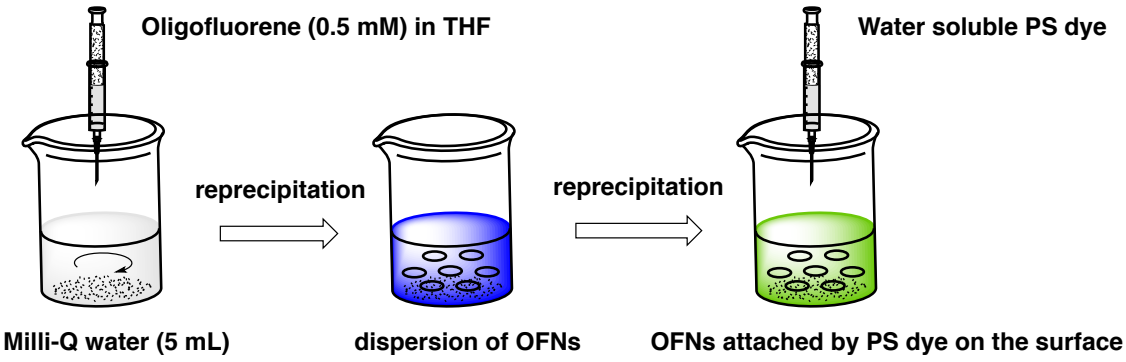

Scheme 2-6. The illustration of the preparation of co-assembled nanoparticle in corporation of **OFN** with **PS**.

The UV-Vis absorption spectra of the donor molecules showed no additional peaks or peak shift on addition of the acceptor, which is an indication of the absence of any ground-state interactions between the donor and acceptor molecules. (Figure 2-8) The **OF** satisfied the requirements of a supramolecular donor–acceptor system with **PS** for FRET studies. For example, there were significant spectral overlaps observed between the donor (**OF**) emission and the acceptor (**PS**) absorption in the nanoparticle state as shown in Figure 2-8a. Direct excitation of the acceptor at the excitation wavelength of the donor was negligible, especially at low acceptor concentrations. (Figure 2-8c)

The identical co-assembled nanoparticles (**OFN–PS**) were formed reproducibly, as confirmed by UV-Vis absorption and fluorescence spectra. The **OFN–PS** suspension is stable for one day enough to carry out all the experiments. The formation of **OFN–PS** was substantiated from the zeta potential and DLS measurements; the ξ-value decreased from +37 mV to +6.1 mV in the presence of 5 mol% of **PS** owing to the cancelation of the **OFN** surface charge, and the average size of **OFN–PS** (105 nm) became larger as compared to that of the original **OFN** (83 nm, Figure 2-9).[14]

The absorption spectrum of **OFN** ([**OF**] = 10^{-5} M) showed a little change upon addition of varying amounts of **PS** (0–5 mol%), as shown in Figure 2-8b, whereas the significant change in the emission spectrum of **OFN** was observed. The blue emission from **OFN** gradually decreased along with increasing green emissions (485 and 520 nm) from **PS** (Figure 2-10).

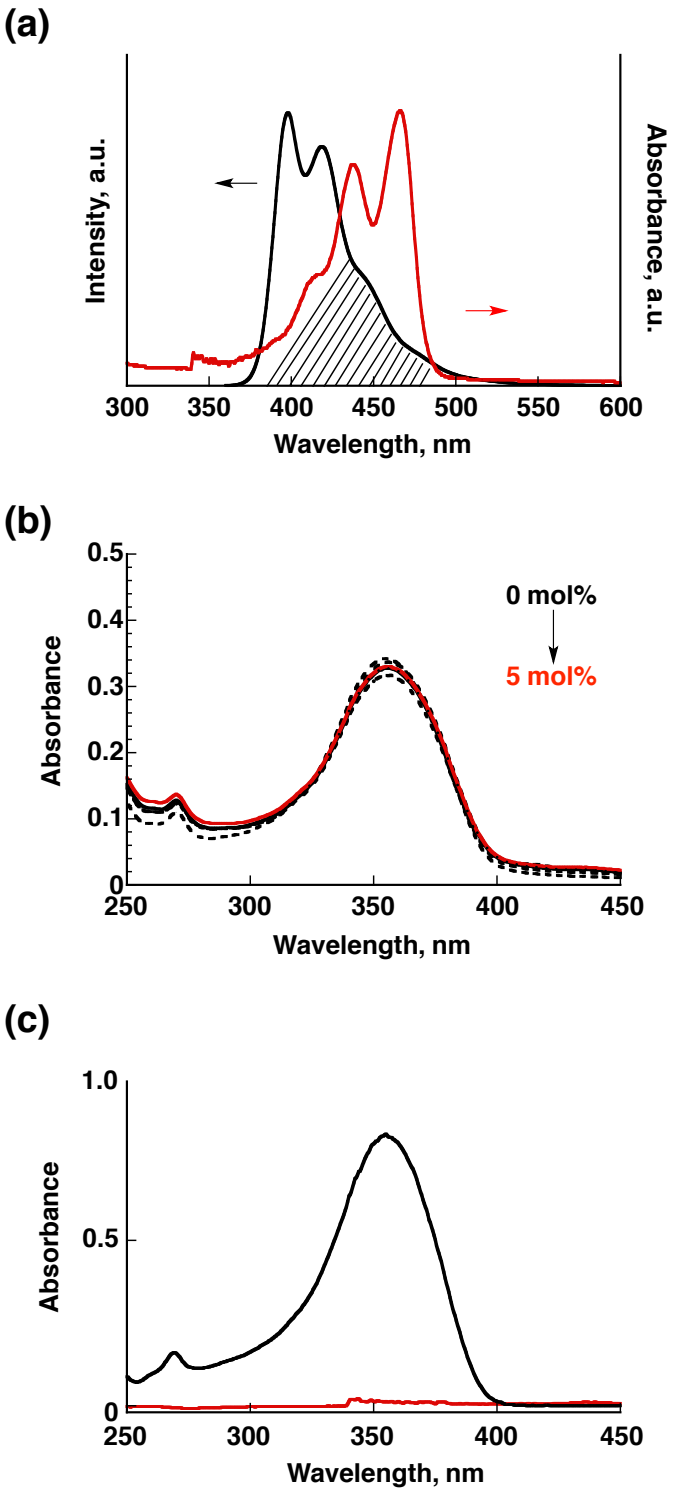

Figure 2-8. (a) Spectral overlap between absorption of **PS** energy acceptor (red) and emission of **OFN** energy donor (black) at room temperature (5×10^{-6} M, λ_{ex} = 355 nm, $J(\lambda) = 8.2 \times 10^{14}$ M^{-1} cm^{-1} nm^4); (b) UV/Vis absorption spectra of **OFN** in the absence and the presence of anionic dye **PS** (0–5 mol%); (c) comparison of individual absorption spectra of **OFN** (black line, [**OF**] = 5×10^{-6} M) and **PS** (red

line, 2×10^{-7} M, which is 4 mol% with respect to the **OFN** concentration), indicating that **OFN** energy donor can be selectively excited at 355 nm.

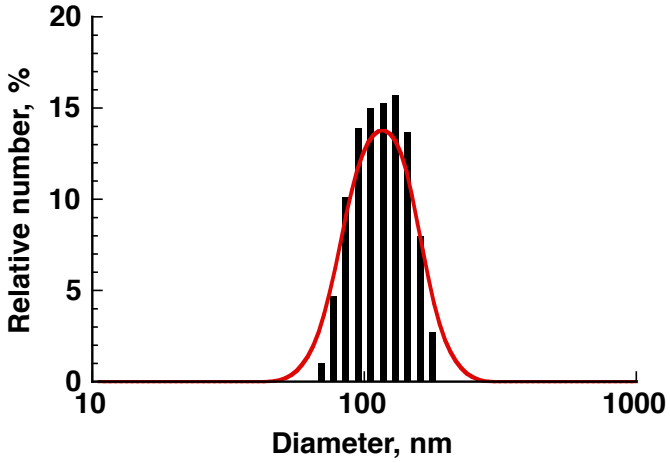

Figure 2-9. Particle size distribution profile of **OFN–PS** in the presence of 4 mol% **PS** obtained from DLS analysis. The average diameter is 105 ± 4 nm.

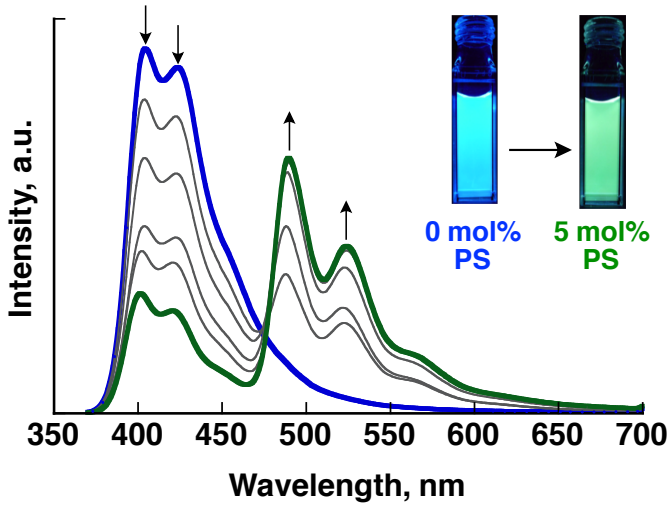

Figure 2-10. Fluorescence spectral changes of **OFN** suspensions upon addition of increasing amounts of **PS** (λ_{ex} = 355 nm). Insets: fluorescent color images of the nanoparticle suspension in the absence and presence of **PS** under 365 nm UV illumination.

The excitation spectra of **OFN–PS** in the presence of 4 mol% **PS** was performed and monitored at 485 nm (emission from **PS**) is consistent with the absorption of **OFN** (Figure 2-11). This results indicated that the emission from **PS** is originating from the absorption of **OFN**.

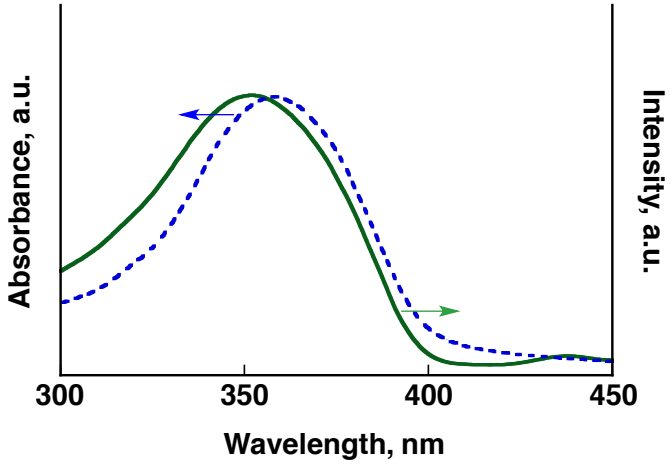

Figure 2-11. Excitation (green) and absorption spectra (blue) of **OFN–PS** suspension in the presence of 4 mol% **PS** (λ_{moni} = 485 nm) in aqueous medium.

Time-correlated single photon counting experiments (Figure 2-12) also support the fact that the interior and exterior particle FRET processes efficiently took place.

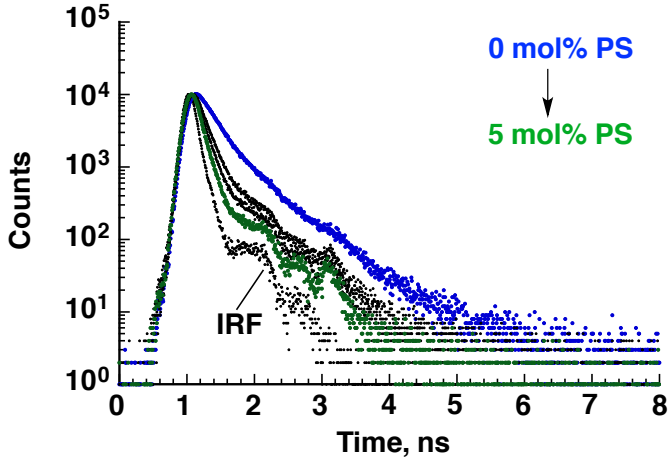

Figure 2-12. Lifetime decay profiles of **OFN–PS** suspension with increasing amounts (0–5 mol%) of **PS** (λ_{ex} = 375 nm, λ_{moni} = 420 nm; IRF: Instrumental Response Function).

It is noteworthy that a plot of the emission intensity against **PS** concentration showed saturation behavior above 2 mol% addition of **PS** ([**PS**] = 2×10^{-7} M), indicating the strong electrostatic attraction between **OFN** and **PS** with the association constant over 10^7 (Figure 2-13). Given that the size of **OFN** was evaluated to be ~100 nm, more than 10^5 of **OF** molecules contributed to the formation of one nanoparticle, indicating that [**OFN**] is calculated to be lower than 10^{-10} M; it is

surprising for us that even at such a concentration of **OFN**, anionic small molecule **PS** facilitated to interact with the surface.

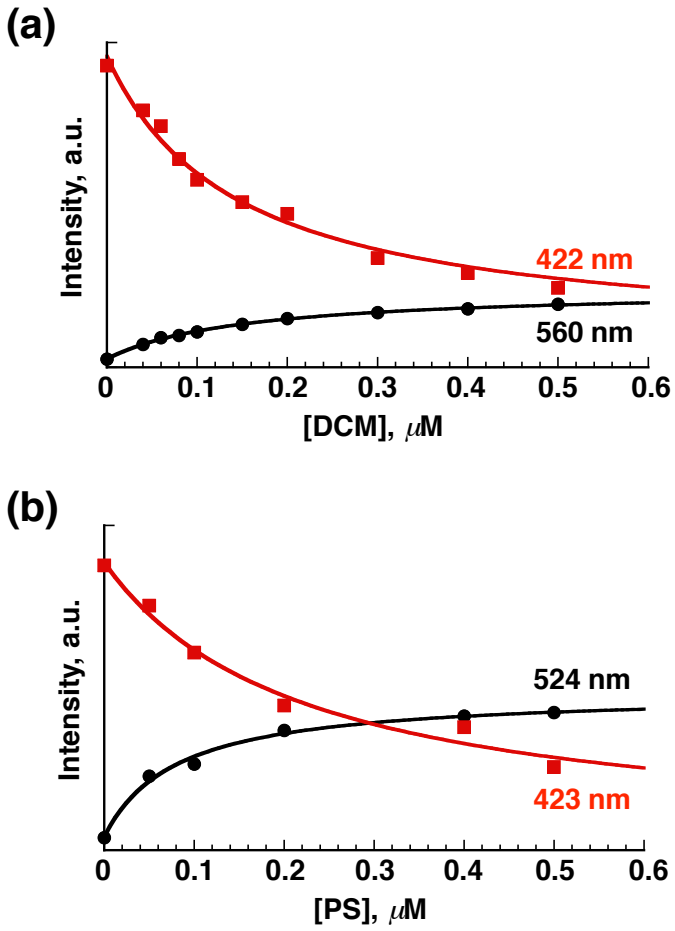

Figure 2-13. (a) Fluorescence intensity changes at 422 nm (red, from **OFN**) and 560 nm (black, from **DCM**) as a function of **DCM** concentration; (b) Fluorescence intensity changes at 423 nm (red, from **OFN**) and 524 nm (black, from **PS**) as a function of **PS** concentration.

It was also confirmed by utilizing a red emitting cationic dye that electrostatic interaction for exterior FRET is of importance and no FRET between **OFN** and the acceptor dye in bulk aqueous solution occurs, despite of comparable extent of the spectral integral with the case of **OFN**–**PS** (Figure 2-14).

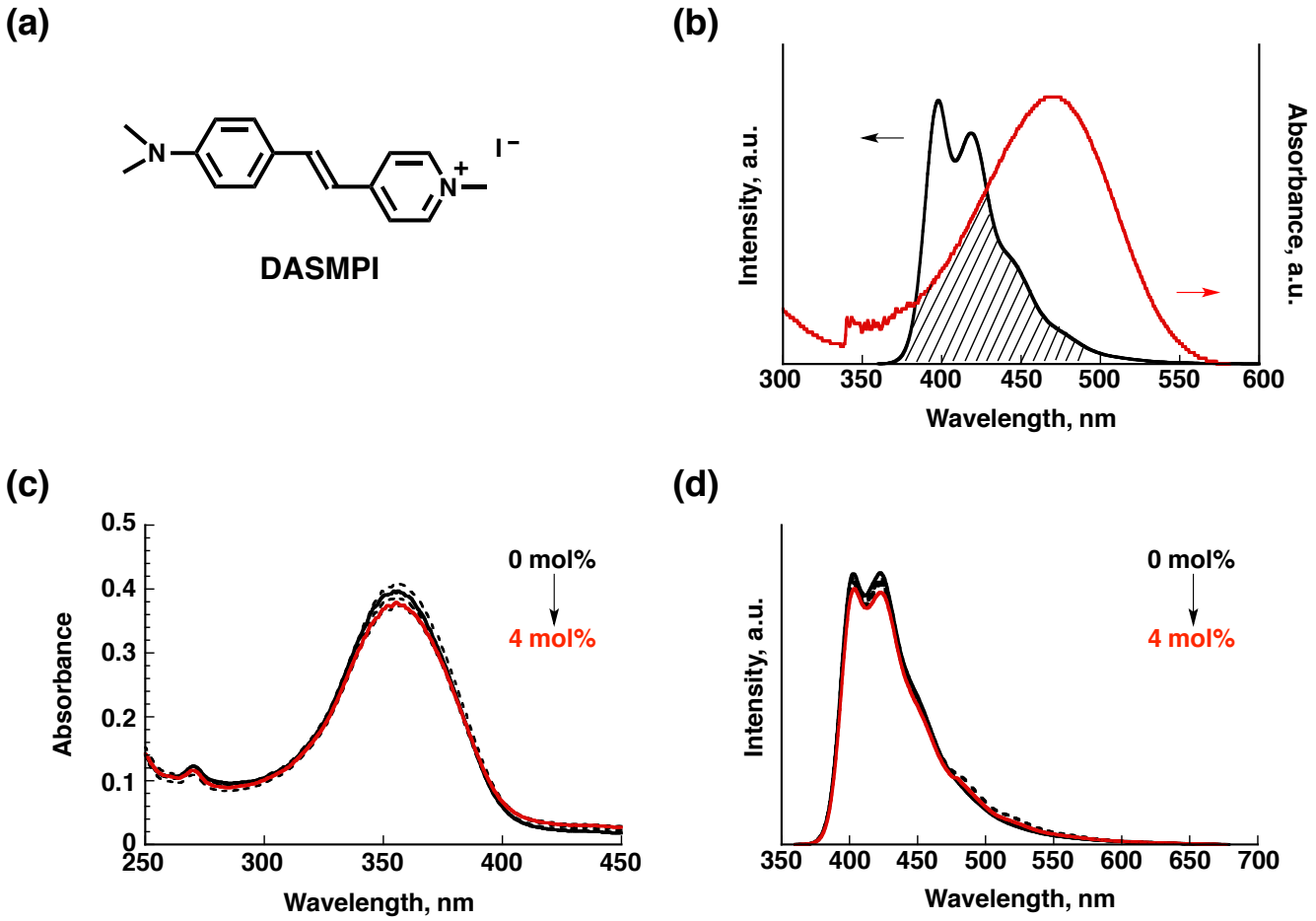

Figure 2-14. (a) Chemical structures of a cationic dye *trans*-4-[4-(Dimethylamino)styryl]-1-methylpyridinium iodide (**DASMPI**) as energy acceptor for comparison; (b) UV/Vis absorption spectra of the **OFN–DASMPI** suspension with increasing amounts of **DASMPI** (0–4 mol%); (c) Spectral overlap between absorption of **DASMPI** energy acceptor (red) and emission of **OFN** energy donor (black) at room temperature (5×10^{-6} M, λ_{ex} = 355 nm, $J(\lambda) = 8.6 \times 10^{14}$ M^{-1} cm^{-1} nm^4); (d) Corresponding fluorescence spectra of the **OFN–DASMPI** suspension (λ_{ex} = 355 nm).

Dual particle FRET

Given the interior and exterior FRET from the **OFN** scaffold to **DCM** and **PS**, one can expect efficient "dual FRET" without interference with each other (Scheme 2-8), which would lead to full-color generation including white.

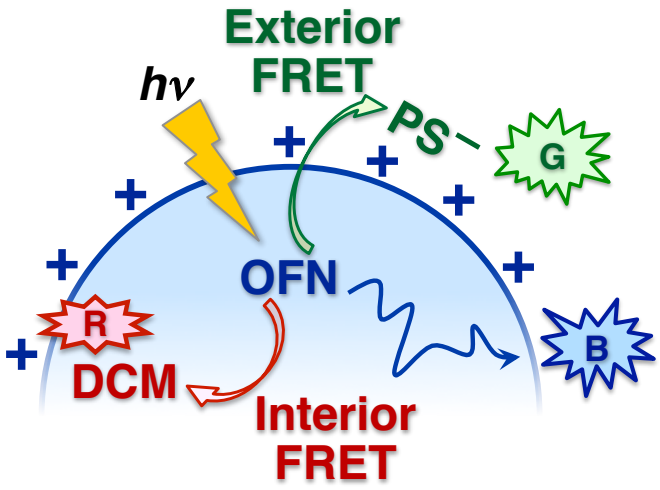

Scheme 2-8. The Schematic illustration of dual FRET in combination of interior and exterior particle FRET.

The RGB trichromophoric assembled nanoparticle system (**OFN–DCM–PS**) was thus prepared by adding **PS** into a pre-assembled **OFN–DCM** suspension (Scheme 2-9).

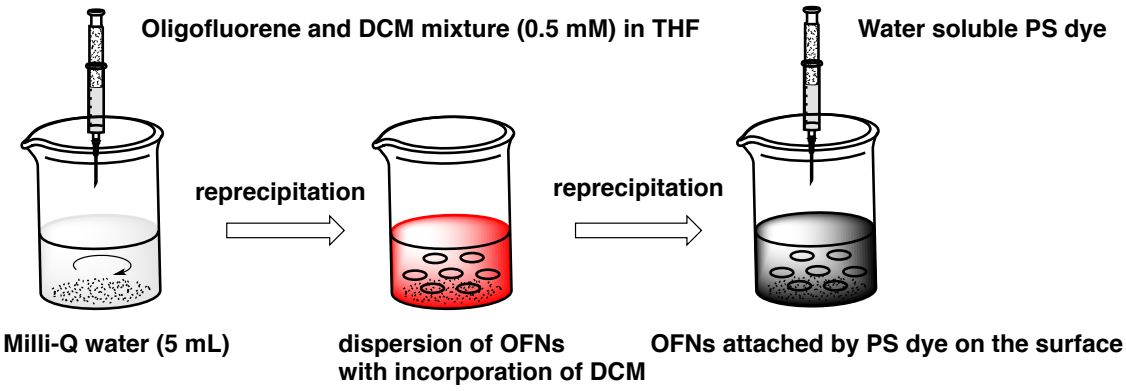

Scheme 2-9. The illustration of the preparation of co-assembled nanoparticle in corporation of **OFN** with **DCM** and **PS**.

The size and surface charge of **OFN–DCM–PS** were 105 nm and +5.1 mV, respectively (Figure 2-15), which are consistent with those of **OFN–PS**.

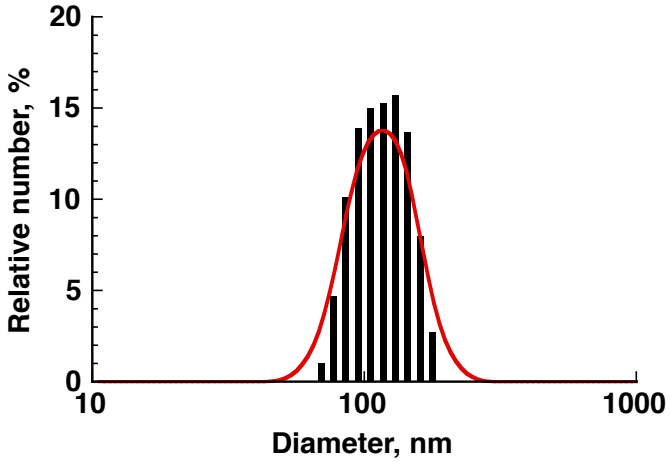

Figure 2-15. Particle size distribution profile of **OFN–DCM–PS** with **OF**:**DCM**:**PS** = 1:0.04:0.04 (mol/mol) obtained from DLS analysis. The average diameter is 105 ± 3 nm.

The addition of **PS** into a pre-assembled **OFN–DCM** (4 mol% **DCM**) suspension induced the decrease in emission intensity of **OFN** along with the appearance of emission peaks from **PS**, while the emission from **DCM** remained almost the same (Figure 2-16). When 0.5 mol% and 1 mol% **PS** were added to the **OFN–DCM** suspension, the exterior FRET efficiencies are calculated to be 12% and 29%, respectively, which are identical to the case of **OFN–PS,** where the FRET efficiencies are 13% (0.5 mol% **PS**) and 29% (1 mol% **PS**), respectively.

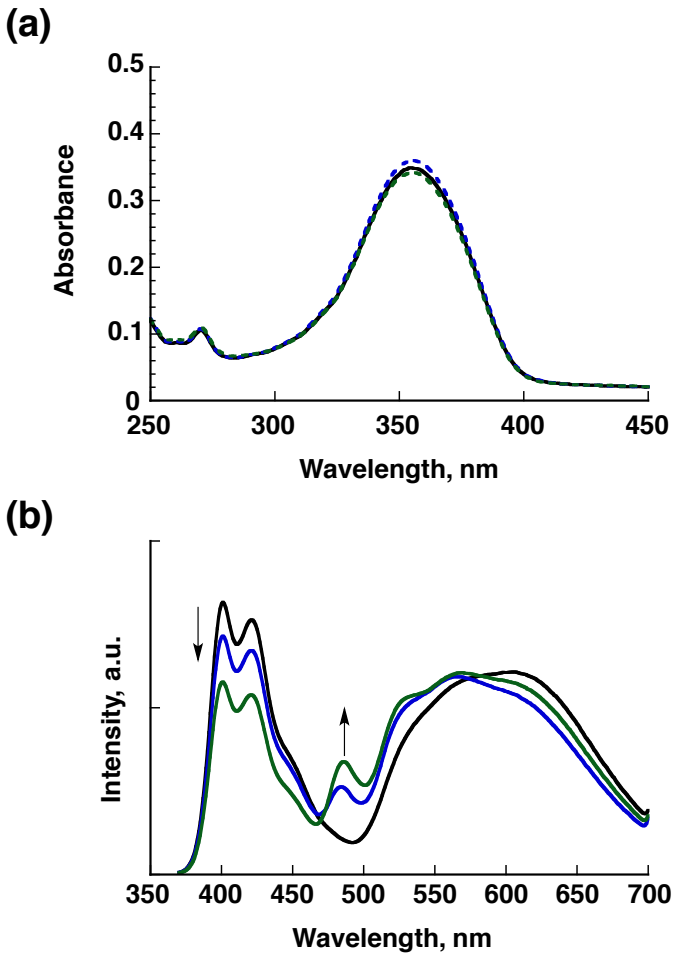

Figure 2-16. (a) Absorption and (b) corresponding fluorescence spectra (λ_{ex} = 355 nm) of **OF–DCM–PS** suspensions in various molar ratios: **OF**:**DCM**:**PS** = 1.0:0.04:0 (mol/mol, black), 1.0:0.04:0.005 (mol/mol, blue), 1.0:0.04:0.01 (mol/mol, green).

The excitation spectra of **OFN–DCM–PS** monitored at 485 nm (**PS** emission) and 600 nm (**DCM** emission) were consistent with the absorption spectrum of **OFN** (Figure 2-17). These results clearly revealed that each FRET event occurred independently and this system was free from sequential FRET, indicating that emission color can be fine-tuned by varying the ratio of the constituents.

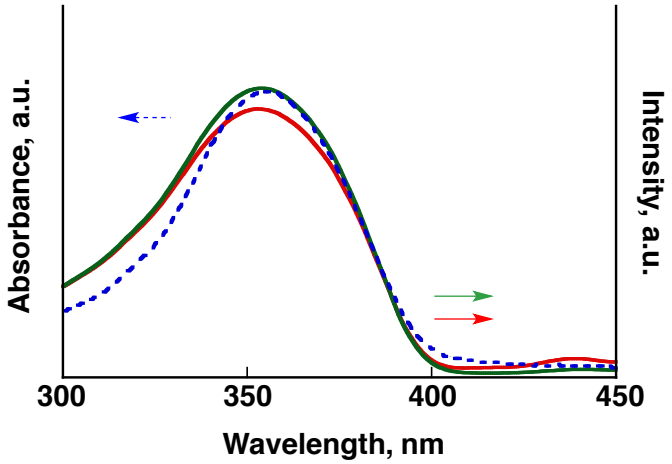

Figure 2-17. Normarized excitation spectra monitored at 485 nm (green) and 600 nm (red) and absorption spectrum (blue) of the nanoparticle suspension with **OF**:**DCM**:**PS** = 1.0:0.04:0.008 (mol/mol).

Indeed, full color luminescence tuning including blue, green, yellow, and red were readily achieved by the adjustment of relative molar ratio of tri-constituents as shown in Figures 2-18 and 2-19. When molar ratio of **OF**/**DCM**/**PS** was adjusted to 1:0.04:0.008, an ideal white emissive nanoparticle was obtained in aqueous solution with CIE coordinate of (0.32, 0.33), owing to almost equal contributions from tri-constituents covering the whole visible range. Such color tunable feature assisted by dual FRET was achieved even in film states when the resultant nanoparticles were embedded in polyvinyl alcohol matrix (**PVA**) (Figures 2-20 and 2-21).

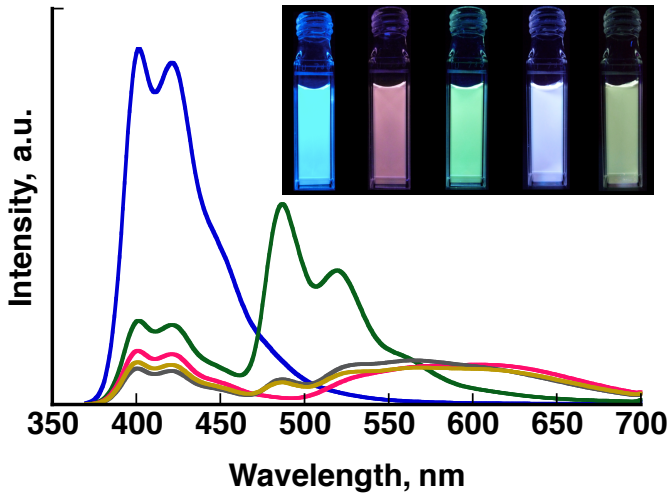

Figure 2-18. Fluorescence spectra of nanoparticle suspensions with various **OF**:**DCM:PS** molar ratios: from left to right, (1:0:0) blue, (1:0.04:0) red, (1:0:0.02) green, (1:0.04:0.008) white, (1:0.04:0.006)

yellow, (λ_{ex} = 355 nm); Inset: fluorescent color images of the nanoparticle suspensions under 365 nm UV-illumination.

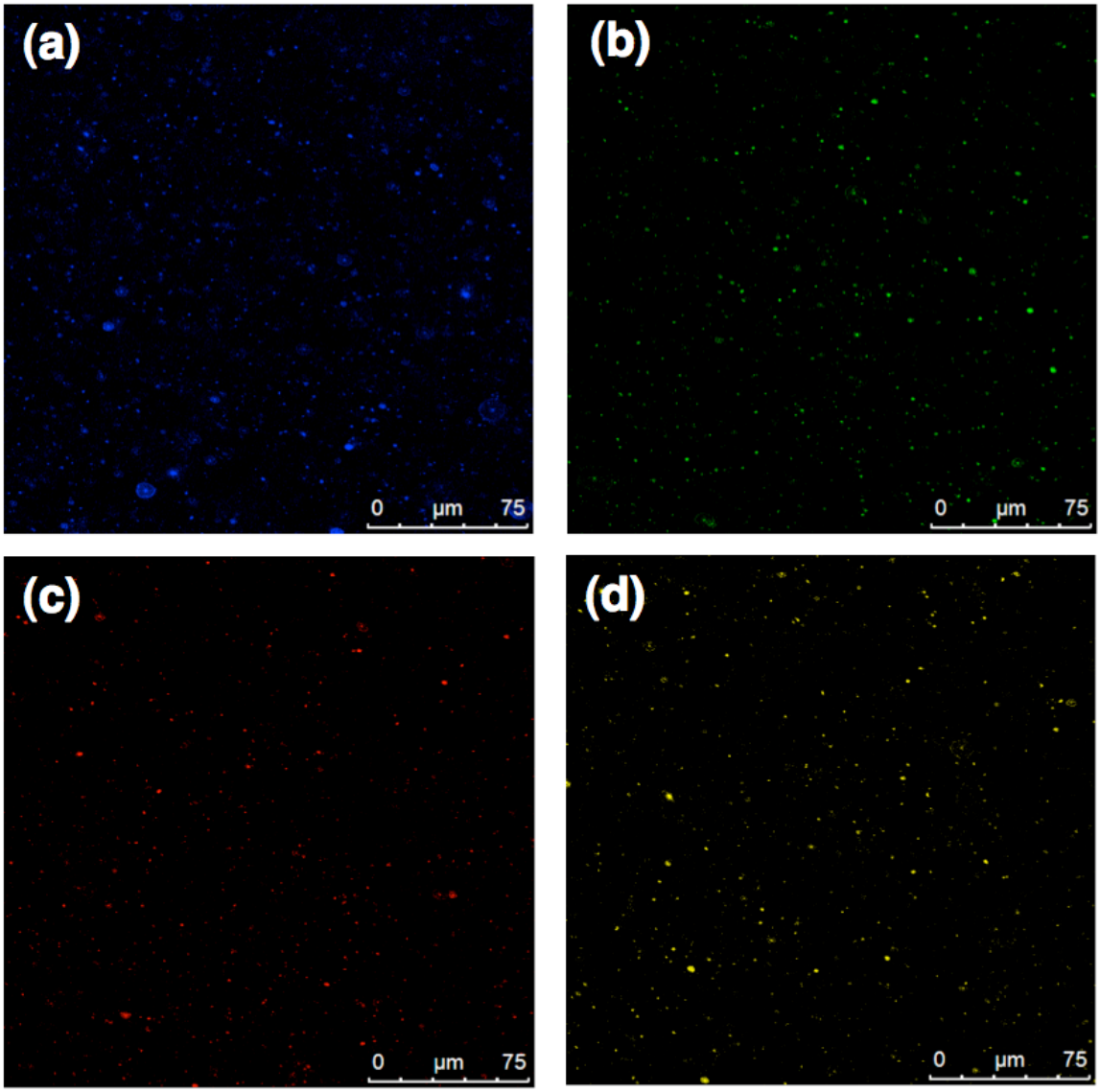

Figure 2-19. Fluorescence microscopic images (λ_{ex} = 355 nm) of (a) **OFN**; (b) **OFN–PS** (**OF**:**PS** = 1.0:0.04 mol/mol); (c) **OFN–DCM** (**OF**:**DCM** = 1.0:0.04 mol/mol); (d) **OFN–DCM–PS** (**OF**:**DCM**:**PS** = 1.0:0.04:0.01 mol/mol).

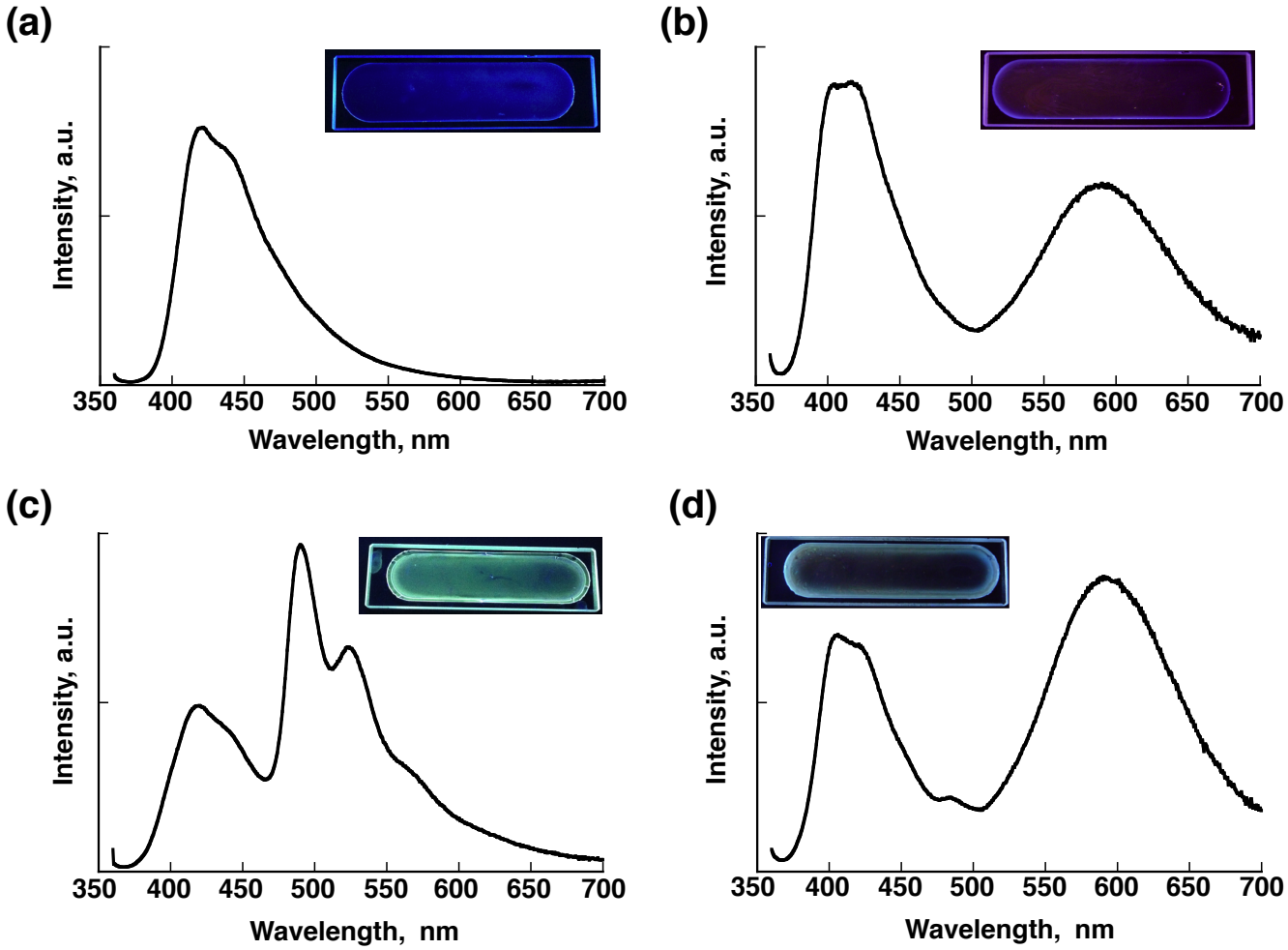

Figure 2-20. Fluorescence spectra of nanoparticle suspensions in **PVA** embedded films containing various **OF**:**DCM**:**PS** (mol/mol): (a) 1:0:0, blue; (b) 1:0.05:0, pink-red; (c) 1: 0:0.05, green; (d) 1:0.05:0.00625, white. The excitation wavelength is 355 nm. Insets: corresponding photo images of the films taken under 365 nm UV illumination.

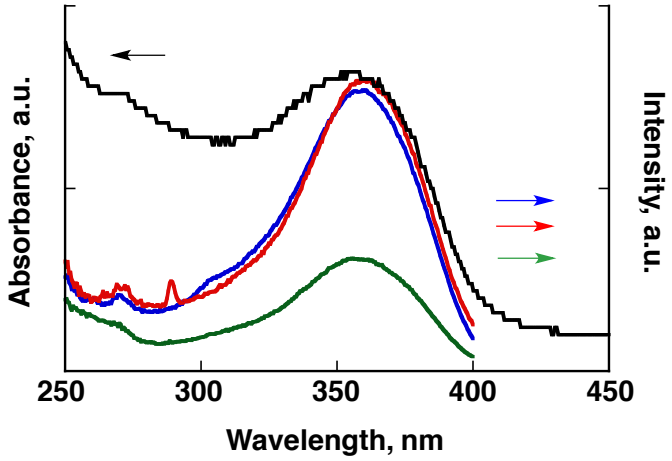

Figure 2-21. Normarized excitation spectra monitored at 419 nm (blue), 490 nm (green), 585 nm (red), and absorption spectrum (black) of nanoparticle suspension (**OF**:**DCM**:**PS** = 1:0.05:0.00625 mol/mol) embedded in the **PVA** polymer matrix.

Anionic bio-macromolecules sensing

Considering that FRET event is very sensitive to the spatial distance and orientation between energy-donor and acceptor,[15] perturbation to **PS** on the surface of **OFN–DCM–PS** would induce the change in exterior FRET efficiency, giving rise to the creation of sensory system in a ratiometric and fluorogenic way of detection; one can readily read out such events as visible changes of emissions (Scheme 2-10).

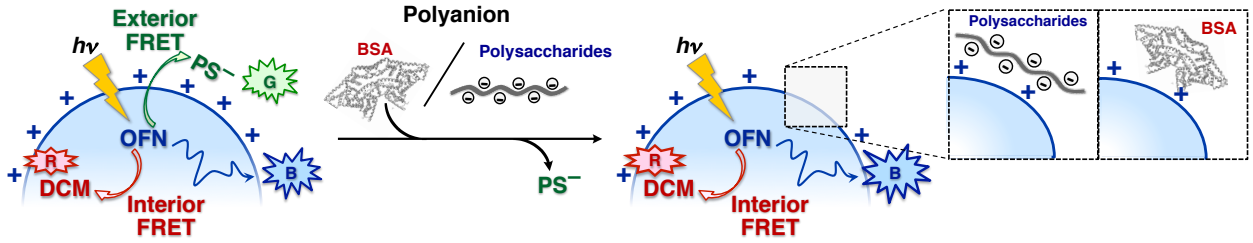

Scheme 2-10. Schematic illustration of the white emissive **OFN–DCM–PS** toward ratiometric and visual polyanion sensing. The **BSA** structure is taken from Protein Data Bank.

We deduce that white light emission has no interferential background in terms of colorfulness and thus subtle change in emission bands contributing to white would readily result in visible changes in addition to providing a ratiometric way of detection.[9c,10,16] We chose four anionic bio-macromolecules, namely bovine serum albumin (**BSA**), sodium hyaluronate (**NaHA**), chodroitin sulfate (**ChS**), and

heparin sodium (**HEP**)[17] as analytes to demonstrate highly sensitive and selective polyanion sensing. The structures of four analytes were shown in Scheme 2-11.

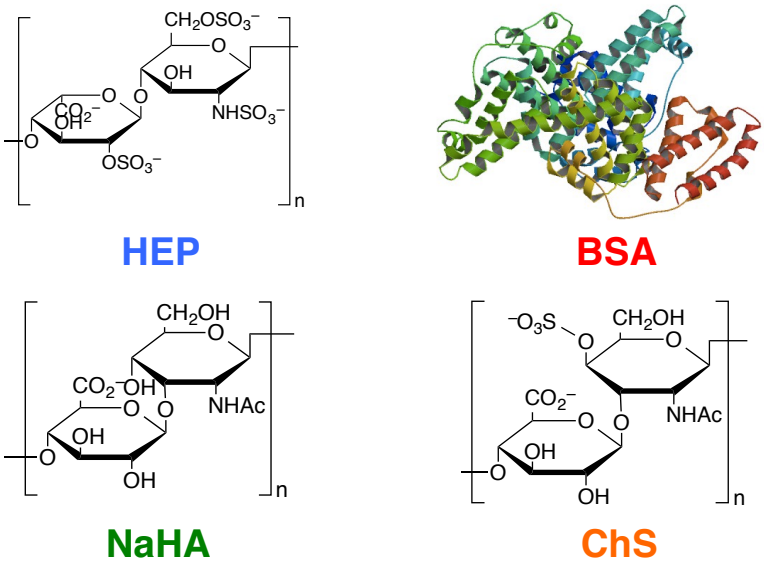

Scheme 2-11. The strutures of **HEP**, **BSA**, **NaHA** and **ChS**.

The charge density of four analytes are examined by Zeta-potential measurements. The results are summarized in Table 2-2.

Table 2-2. Zeta potential results of four anlaytes:

	BSA (mV)	**HEP** (mV)	**NaHA** (mV)	**ChS** (mV)
Entry 1	–9.51	–11.23	–19.05	–17.62
Entry 2	–10.94	–12.49	–19.68	–16.00
Entry 3	–11.03	–10.62	–19.92	–17.97
Average[a]	–10.49 ± 0.98	–11.45 ± 1.04	–19.55 ± 0.5	–17.20 ± 1.2

[a] Concentration of analytes is 5 mg/mL in PBS buffer solution. Each entry is repeated for three times.

Considering that the high ionic strength induced aggregation of nanoparticles by the cancellation of the cationic surface charge of nanoparticle, we set a white emissive **OFN–DCM–PS** suspension, **OF/DCM/PS** = 1:0.01:0.01 in a molar ratio ([**OF**] = 0.83×10^{-5} M), in buffer conditions (1.67 mM PBS, pH 7.2).

Upon gradual addition of **BSA** into the white emissive **OFN–DCM–PS**, the suppression of exterior FRET from **OFN** to **PS** –decrease in the emission intensity of **PS** and recovery of the emission from **OFN** with isosbestic points– was observed until reaching the saturation point, which is reversal of the situation for adding **PS** to **OFN–DCM** (Figure 2-22). It was reported that **BSA** has an ability to interact with **PS** with the association constant of 3.7×10^4 M^{-1},[18] however under the conditions we used here ([**PS**] = 0.83×10^{-7} M, [**BSA**] = $0 \sim 2 \times 10^{-6}$ M), the complex formation between **PS** and **BSA** is negligible; it is therefore reasonable to infer that the successful displacement of **PS** by anionic **BSA** took place in the sub mM range. Eventually emission color change from white to blue was noticeable by naked eyes.

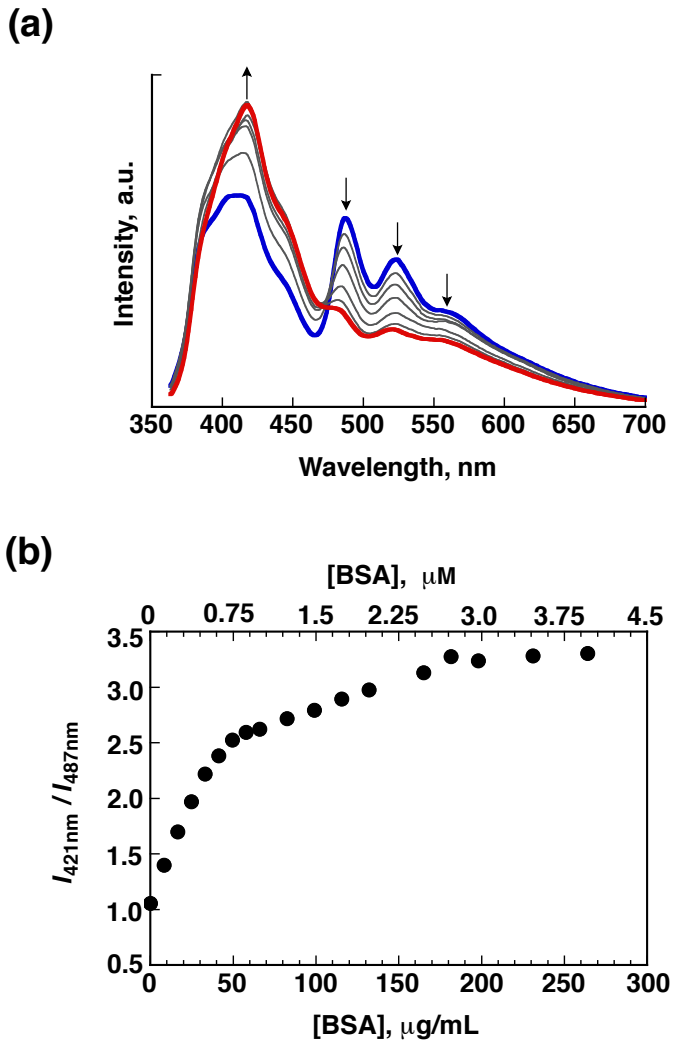

Figure 2-22. Fluorescence spectral changes of the white emissive **OFN–DCM–PS** (1:0.01:0.01) suspension upon addition of varying amounts of **BSA** in PBS buffer solution (pH = 7.2, λ_{ex} = 355 nm);

(b) Fluorescence intensities ratio change of **OF–DCM–PS** (1:0.01:0.01) suspension as a function of concentration of **BSA** in PBS buffer solution.

Circular dichroic analysis revealed that no denaturing of **BSA** occurred in the presence of the nanoparticle (Figure 2-23).

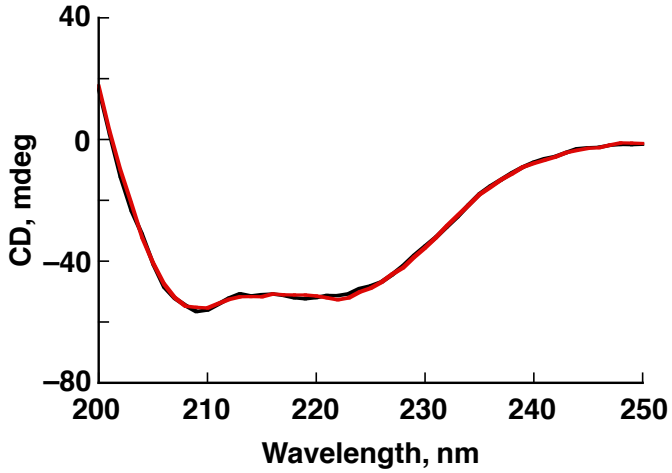

Figure 2-23. Circular Dichroic spectra of native **BSA** (black) and **OFN–BSA** (red) in 10 mM PBS buffer solution. ([**OFN**] = 0.83×10^{-5} M, [**BSA**] = 2×10^{-6} M)

Similar to the results from **BSA** sensing, displacement of **PS** upon addition of increasing amount of **HEP**, **NaHA** and **ChS** took place, leading to the suppression of exterior FRET from **OFN** to **PS** (Figures 2-24, 2-25 and 2-26). Typically, **PS** started to be expelled even at concentration of [**HEP**] = 30 ng/mL (Figure 2-24) and a plot of emission intensity *vs.* [**HEP**] changed and saturated at sub mg/mL range (Figures 2-24). Visible response from white to blue (390 ng/mL) via yellowish white (180 ng/mL) was conspicuous (Figure 2-24 inset).

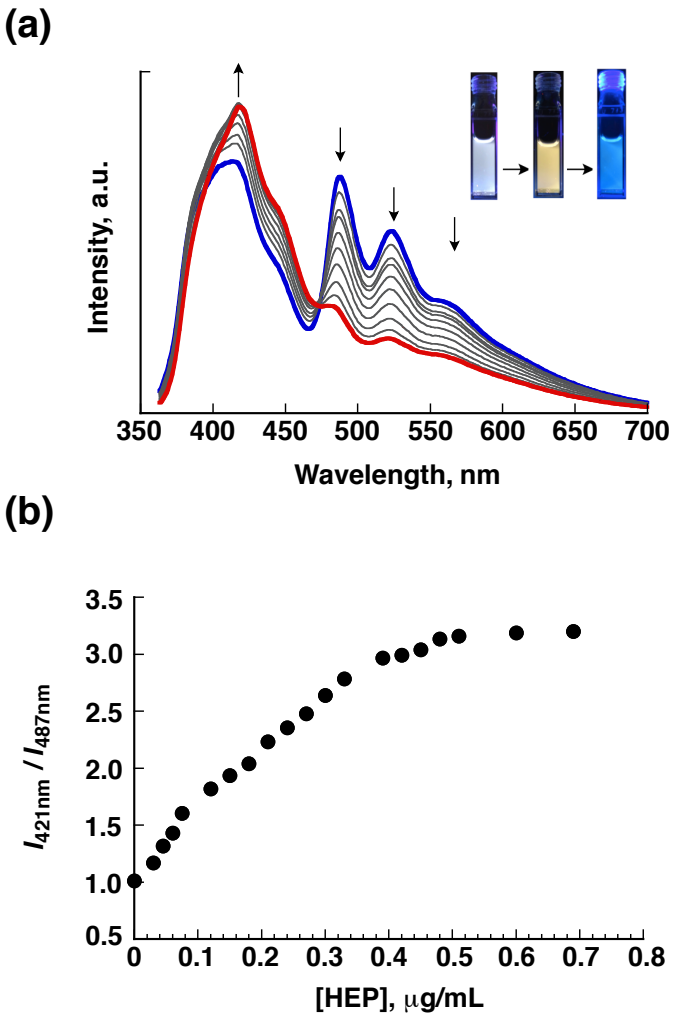

Figure 2-24. Fluorescence spectral changes of the white emissive **OFN–DCM–PS** (1:0.01:0.01) suspension upon addition of varying amounts of **HEP** in PBS buffer solution (pH = 7.2, λ_{ex} = 355 nm); (b) Fluorescence intensities ratio change of **OF–DCM–PS** (1:0.01:0.01) suspension as a function of concentration of **HEP** in PBS buffer solution.

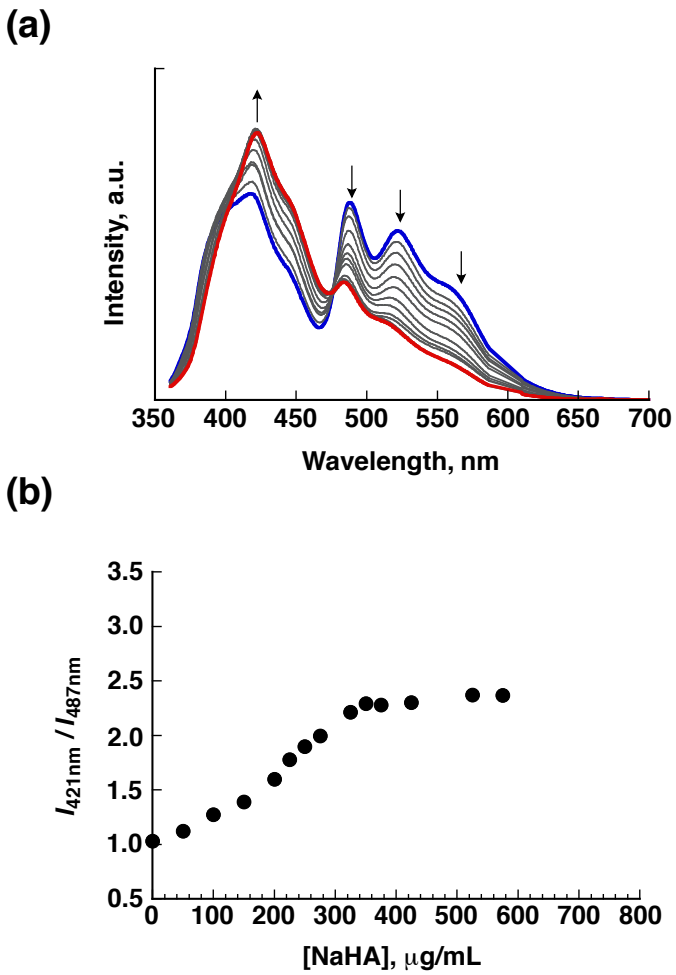

Figure 2-25. Fluorescence spectral changes of the white emissive **OFN–DCM–PS** (1:0.01:0.01) suspension upon addition of varying amounts of **NaHA** in PBS buffer solution (pH = 7.2, λ_{ex} = 355 nm); (b) Fluorescence intensities ratio change of **OF–DCM–PS** (1:0.01:0.01) suspension as a function of concentration of **NaHA** in PBS buffer solution.

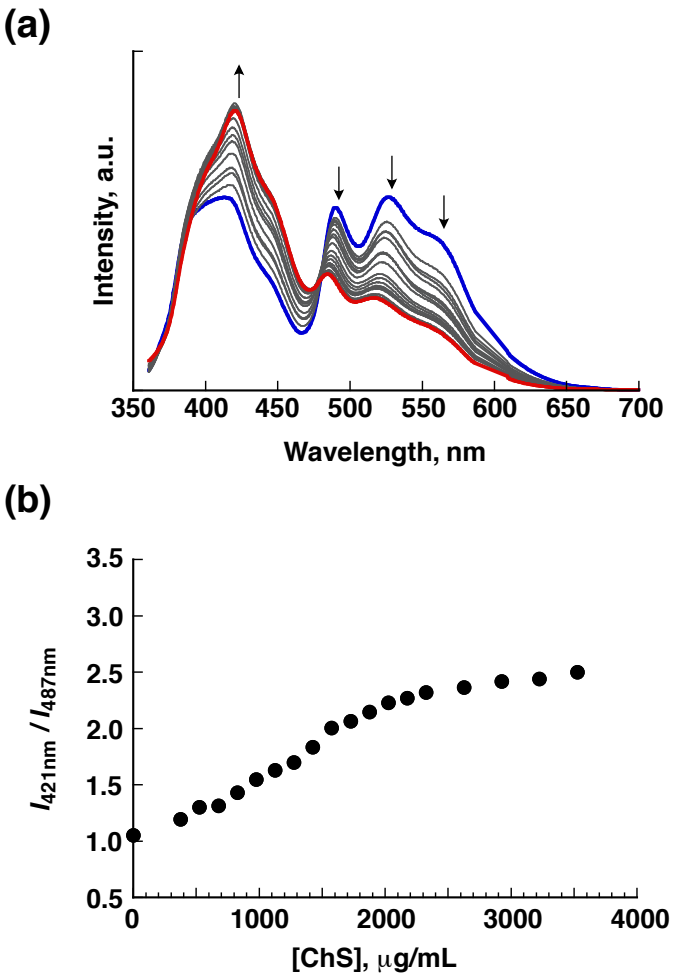

Figure 2-26. Fluorescence spectral changes of the white emissive **OFN–DCM–PS** (1:0.01:0.01) suspension upon addition of varying amounts of **ChS** in PBS buffer solution (pH = 7.2, λ_{ex} = 355 nm); (b) Fluorescence intensities ratio change of **OF–DCM–PS** (1:0.01:0.01) suspension as a function of concentration of **ChS** in PBS buffer solution.

The detection limit for **HEP** was calculated to be 8 ng/mL,[16f] while those for **BSA**, **NaHA** and **ChS** were estimated to be 2.4, 73.2, and 326.1 μg/mL, respectively (Figure 2-27). The high sensitivity and selectivity toward **HEP** can be explained by the polyelectrolyte effect between the positively-charged nanoparticle surface and **HEP** bearing the highest anionic charge density.[17,19,20] Considering that the visible response was monitored as a result of displacement of **PS** with analytes, it is surprising for us that **HEP** affinity to the cationic surface of **OFN–DCM–PS** would be comparable with those for heparin binding proteins and heparin binders.[17,21,22]

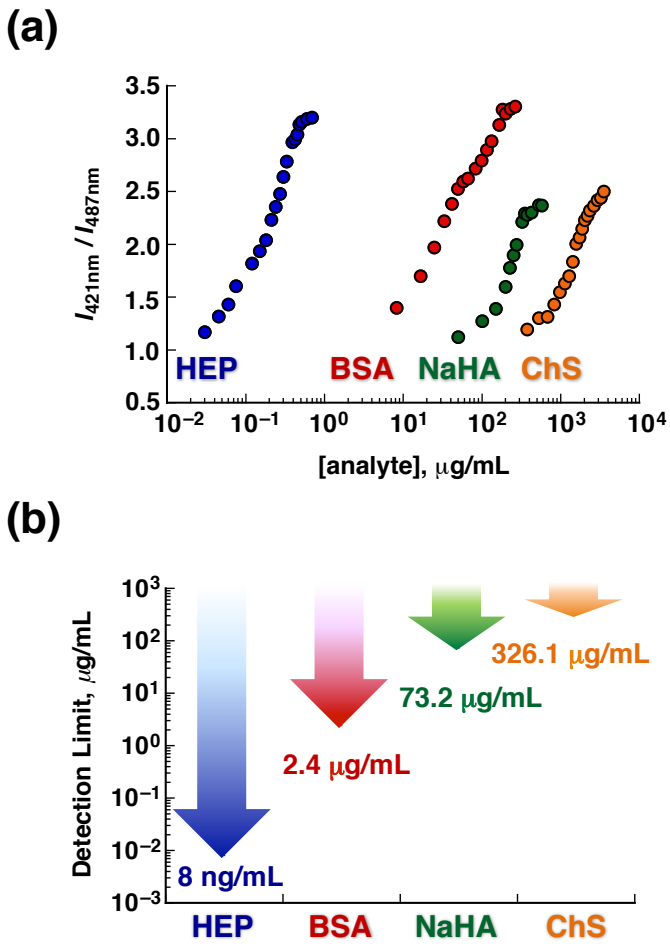

Figure 2-27. (a) Fluorescence intensity changes (I_{421nm}/I_{487nm}) of the nanoparticle suspension as a function of concentration of analytes in PBS buffer solution. (b) Detection limits for anionic analytes used herein.

The affinity of the white emissive nanoparticle toward **HEP** was compared with a conventional heparin binder, hexadimethrine bromide, as shown in Figure 2-28. No significant change was observed on the fluorecent spectrum of the **HEP**-attached nanoparticle upon addition of the heparin binder. This resut indicates that the white emissive nanoparticle has higher affinity toward **HEP** than the conventional heparin binder.

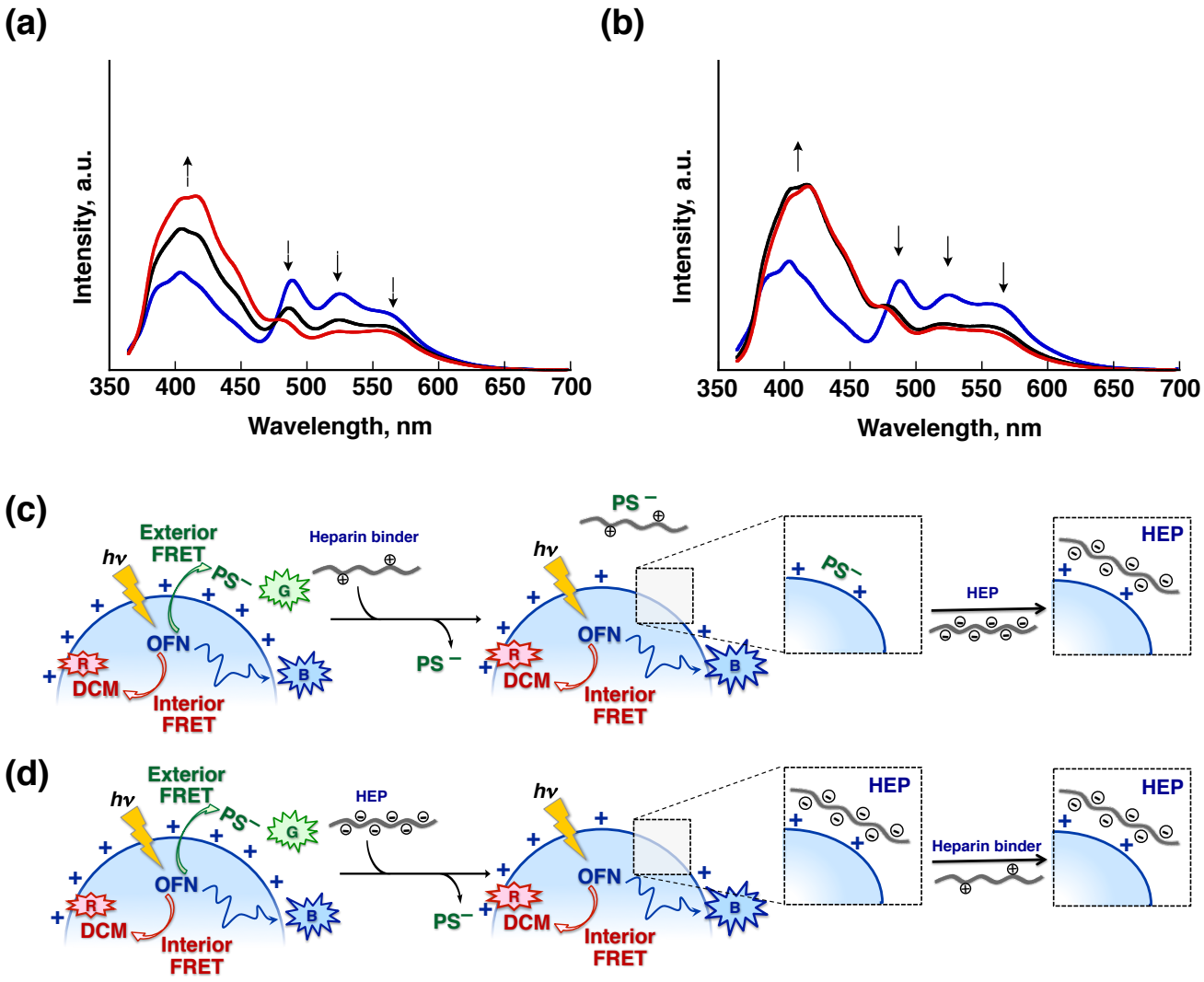

Figure 2-28. Fluorescence spectral changes of the white emissive **OFN–DCM–PS** (1:0.01:0.01) suspension upon addition of (a) 8.3 mM (based on the molecular weight of repeating unit) hexadimethrine bromide and then 0.53 mg/mL **HEP**; (b) 0.53 mg/mL **HEP** and then 8.3 mM hexadimethrine bromide in sequence, respectively (in PBS buffer solution, λ_{ex} = 355 nm). The proposed processes of (a) and (b) were illustrated in (c) and (d), respectively.

Conclusion

In summary, we reported a new RGB trichromophoric nanoparticle system, wherein an energy donor scaffold and two acceptor dyes are spatially organized to achieve interior and exterior dual FRET, generating full color emissions including white in aqueous medium and in **PVA** film. Furthermore, we have demonstrated that the cationic white emissive nanoparticle is useful for the construction of highly sensitive sensory system for polyanions with ratiometric and visible responses. The "white background" that we introduced here provides low background in terms of colorfulness but indeed has high emission background, it would, therefore, allow to screen inherent auto-fluorescence background appeared in biological sensing system.[23] The concepts in this paper would complement the displacement-based chemosensors and other sensing techniques existing currently. Introducing interactive sites toward specific analytes on the nanoparticle surface can increase the selectivity in a cooperative action of different interactions.

Experimental Section

Chemicals and Reagents.

All chemicals were purchased from Sigma-Aldrich, Kanto Chemical, Tokyo Chemical Industry, or Wako Pure Chemical Industries and used as received. Bovine Serum Albumin (**BSA**) was purchased from Sigma-Aldrich (the molecular weight is approximately 66 kDa). Heparin sodium (**HEP**) was purchased from Wako Pure Chemical Industries containing 100,000 units. Hyaluronic acid sodium salt (**NaHA**) from cockscomb and chondroitin sulfate sodium salt (**ChS**) were purchased from Tokyo Chemical Industry. Oligofluorene derivatives were synthesized according to the literature procedures.

General Method.

^{1}H NMR and ^{13}C NMR spectra were recorded on a JEOL ECS-400; chemical shifts were recorded in ppm relative to TMS (0 ppm). UV/Vis absorption spectra, fluorescence spectra were obtained on a Hitachi U-2900 spectrophotometer and a Hitachi F-7000 spectrophotometer, respectively. Fluorescence quantum yields were obtained on a Hamamatsu Photonics, Absolute PL Quantum Yield Measurement System, C9920-02G. Fluorescence lifetimes were measured using an IBH (FluoroCube) time correlated picosecond single photon counting (TCSPC) system. Samples were excited using a pulsed diode laser (NanoLED-11, <100 ps pulse duration) at a wavelength of 375 nm with a repetition rate of 1 MHz. Particle size analysis was carried out using a Photal DLS-8000HAL (Otsuka Electronics). Zeta-potentials were measured by using a ELSZ-1000Z (Otsuka Electronics) instrument. The standard deviation of the distribution in a single measurement was 6% and 10% for size and zeta potential measurements, respectively. Field-emission scanning electron microscopy (FE-SEM) observations of the samples were carried out using a Hitachi S-4800 at an accelerating voltage of 10 kV. Fluorescence microscopic images of nanoparticles were observed by a confocal laser scanning microscopy (Leica-microsystem TCS SP5). Circular dichroic (CD) spectroscopic analysis of **BSA** in phosphate-buffered saline (PBS) buffer solution (pH = 7.2) in the absence and the presence of **OFN** was performed on a JASCO J-725 using 10 mm path length cell in wavelength range of 200 nm–300 nm with a scan rate of 50 nm/min.

Synthesis of 9,9-Didodecylfluorene (1).

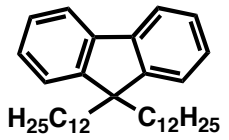

Fluorene (10 g, 60.2 mmol) was dissolved in anhydrous THF (100 mL) by stirring under argon. The reaction temperature was reduced to –78 ^{o}C by using a slush bath and stirring was continued for 15 minutes. 2.5 M *n*-BuLi solution in hexane (50 mL, 127 mmol) was added dropwise and the mixture was stirred at –78 ^{o}C for 45 minutes. 1–Bromododecane (32 g, 150 mmol) was then added dropwise followed by further stirring at –78 ^{o}C for 1 h. The solution was then allowed to slowly warm to room temperature and stirred for another 3 h. The mixture was poured into water and extracted with hexane. The organic extracts were washed with brine and dried over anhydrous Na_2SO_4. The solvent was removed under reduced pressure and the crude oily product was purified by column chromatography (silica gel, hexane). The pure product was obtained as colorless oil. Yield: 88%; ^{1}H NMR (600 MHz, $CDCl_3$): δ [ppm] 0.56–0.65 (m, 4H), 0.88 (t, J = 14.4Hz, 6H), 1.05–1.32(m, 36H), 1.89–1.92(m, 4H), 7.26–7.33 (m, 6H), 7.68–7.70 (d, 2H).

Synthesis of 2,7-Dibromo-9,9-Didodecylfluorene (2).

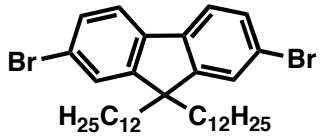

1 (8 g, 16 mmol) was dissolved in CH_2Cl_2 (80 mL) by stirring and the reaction vessel was covered with black paper to avoid light. I_2 (81 mg, 0.32 mmol) was added to the reaction mixture followed by the addition of bromine (1.8 mL, 34.5 mmol) in 30 mL of CH_2Cl_2. The reaction mixture was stirred at room temperature for 20 h. An aqueous solution of $NaHSO_4$ (15%) was added until the red color disappears. The organic layer was extracted with CH_2Cl_2, washed with water and dried over anhydrous Na_2SO_4. The solvent was removed under reduced pressure and the crude product was purified by column chromatography (silica gel, hexane). Yield: 85%; ^{1}H NMR (600 MHz, $CDCl_3$): δ [ppm] 0.55–0.62 (m, 4H), 0.88 (t, J = 14.4Hz, 6H), 1.03–1.32 (m, 36H), 1.89–1.92 (m, 4H), 7.44–7.48 (m, 4H), 7.50–7.52 (d, 2H).

Synthesis of 2,7-Bis(4,4,5,5-tetramethyl-1,3,2-dioxaborolan-2-yl)-9,9-Didodecylfluorene (3).

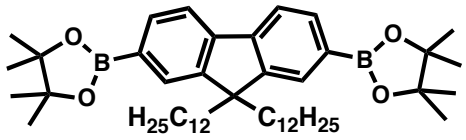

2 (5 g, 7.57 mmol) was dissovled in anhydrous THF (70 mL) by stirring under argon. The reaction temperature was reduced to –78 ^{o}C by using a slush bath and stirring was continued for 15 minutes. 2.5 M *n*-BuLi solution in hexane (6.35 mL, 15.9 mmol) was added dropwise and the mixture stirring was continued at –78 ^{o}C for 1 h. 2-Isopropoxy-4,4,5,5-tetramethyl-1,3,2-dioxaborolane (3.52 g, 18.92 mmol) was added rapidly to the reaction mixture and the resulting mixture was warmed to room temperature and stirred for 24 h. The mixture was poured into water and extracted with hexane. The organic layer was washed with brine and dried over anhydrous Na_2SO_4. The solvent was removed under reduced pressure and the crude product was purified by column chromatography (silica gel, 5% EtOAc-hexane) to provide the titile product as a white solid. Yield: 65%; ^{1}H NMR (600 MHz, $CDCl_3$): δ [ppm] 0.50–0.59 (m, 4H), 0.88 (t, J = 14.4Hz, 6H), 1.07–1.34 (m, 36H), 1.38 (s, 24 H), 1.89–1.98 (m, 4H), 7.71 (d, J = 7.8 Hz, 2H), 7.74 (s, 2H), 7.79 (d, J = 8.4 Hz, 2H).

Synthesis of 7-bromo-9,9-Didodecylfluorene-2-carbaldehyde (4).

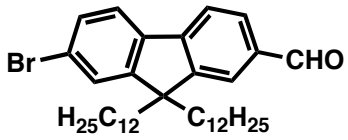

To a stirred solution of **2** (4 g, 6.06 mmol) in anhydrous ether (40 mL) at –78 ^{o}C, 2.5 M *n*-BuLi solution in hexane (2.68 mL, 6.7 mmol) was added dropwise under argon atmosphere and stirring was continued for 30 minuntes. The reaction mixture was then allowed to warm to room temperature and stirred at that temperature for another 30 min; it was cooled again to – 78 ^{o}C, followed by the addtion of DMF (1.2 mL, 10 mmol). The mixture was allowed to warm to room temperature gradually and stirred for 8 h. Aquous HCl solution (2 M, 50 mL) was added and stirring was continued for another 2 h. The mixture was extracted with ether and washed with water and brine. The organic extracts were dried over anhydrous Na_2SO_4 and the solvent was evaporated under reduced pressure. The crude product was purified by column chromatography (silica gel, 25% $CHCl_3$-hexane) to provide the title product as colorless liquid. Yield: 45%; ^{1}H NMR (600 MHz, $CDCl_3$): δ [ppm] 0.55–0.59 (m, 4H), 0.86 (t, J = 14.4Hz, 6H), 1.03–1.32 (m, 36H), 1.93–2.05 (m, 4H), 7.50–7.51 (m, 2H), 7.63 (d, J = 8.4Hz, 1H), 7.80 (d, J = 8.4 Hz, 1H), 7.85–7.87 (m, 2H).

Synthesis of 9,9,9',9',9",9"-Hexadodecyl-7,2';7',2"-terfluorene-2,7"-dicarbaldehyde (5).

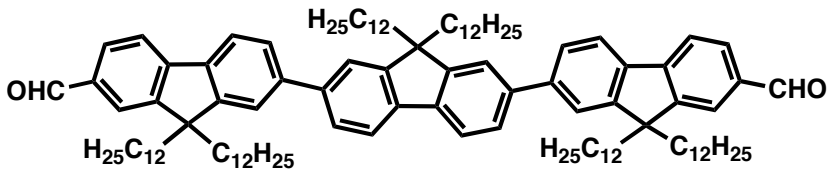

3 (1 g, 1.325 mmol) and **4** (1.62 g, 2.66 mmol), K_2CO_3 (1.83 g, 13.25 mmol) were weighed in a two necked RB flash. Air was removed from the flash by applying vacuum followed by filling with argon gas. The process was repeated for 3 times, then $Pd(PPh_3)_4$ (155.6 mg, 0.13 mmol) was added under argon counter flow followed by the addition of degassed and THF-H_2O (2:1) solvent mixture (40 mL). The reaction mixture was refluxed at 90 ^oC for 2 days, then poured into water and extracted with CH_2Cl_2 for 3 times. The combined organic fraction was dried over Na_2SO_4 and evaporated to dryness under reduced pressure. The crude product was purified by column chromatography (silica gel, $CHCl_3$-hexane) to provide the product as a glassy solid. Yield: 85%; ^1H NMR (600 MHz, $CDCl_3$): δ [ppm] 0.62–0.75 (m, 12H), 0.86 (t, J = 14.4Hz, 18H), 1.03–1.32 (m, 108H), 2.08–2.14 (m, 12H), 7.65–7.72 (m, 8H), 7.83 (d, J = 7.8Hz, 2H), 7.86–7.91 (m, 8H), 10.08 (s, 2H).

Synthesis of OF

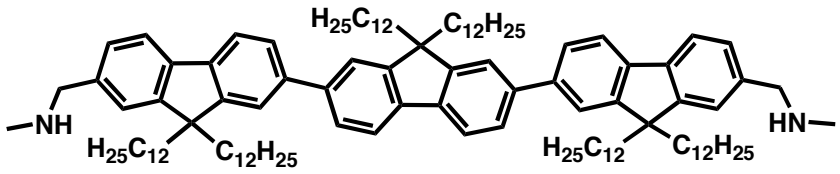

5 (50 mg, 0.032 mmol) was dissolved in $CH_3OH/CHCl_3$ mixture (1:1) in RB flask and methylamine (40 %, 6.367 mmol, 0.082 mmol, 6.83 μL) was added under argon at room temperature. The reaction was kept stirring overnight. A solution of sodium borohydride (3.1 mg, 0.082 mmol) was added dropwise into the mixture and was stirred for 4 h. Then the reaction mixture was poured into water and extracted with CH_2Cl_2 for 3 times. The combined organic fraction was dried over Na_2SO_4 and evaporated to dryness under reduced pressure. The crude product was purified by column chromatography (silica gel, 25% CH_2Cl_2-hexane) to provide the product as a yellow solid. Yield: 85%; ^1H NMR (600 MHz, $CDCl_3$): δ [ppm] 0.70–0.72 (m, 12H), 0.83 (t, 18H), 1.03–1.32 (m, 108H), 2.01–2.03 (m, 12H), 2.5 (d, 6H), 3.87 (d, 4H), 7.29-7.30 (m, 4H), 7.61-7.69 (m, 10H), 7.73-7.76 (d, 2H), 7.79-7.83 (d, 2H).

Preparation of Nanoparticle.

Organic nanoparticles in aqueous medium were prepared as follows: 5 mL water was taken in a 15 mL glass vial and stirred at 1500 rpm using a magnetic bead and stirrer. **OF** dissolved in THF was taken in a syringe and injected into the stirring water. Stirring was continued for another 1 minute to yield a stable nanoparticle suspension of **OFN**.

Preparation of Nanoparticle Composite for FRET Studies.

(i) **OFN–DCM**: Small quantities of a neutral dye (**DCM**, 0–5 mol%) in THF solution was dissolved into a THF solution of **OF**, keeping the **OF** concentration constant. This mixture solution (100 μL) was injected into water (5 mL) to afford **OFN–DCM** where **DCM** was encapsulated in the **OFN** scaffold.

(ii) **OFN–PS**: Adsorption of an anionic dye (**PS**) on the **OFN** surface was achieved by injecting water soluble **PS** at required concentrations into the **OFN** suspension, followed by stirring for three minutes. The mixture was kept at room temperature for another three minutes before measurements.

(iii) **OFN–DCM–PS**: The desired concentrations of water soluble **PS** were subsequently injected into a suspension of pre-prepared **OFN–DCM**, leading to the formation of a trichromophoric **OFN–DCM–PS** suspension. The mixture was kept at room temperature for another three minutes before measurements.

Fluorescence Titration Experiments for BSA.

The stock solutions of **BSA** (0.05 mM) was prepared in 10 mM phosphate-buffered saline (PBS) buffer solution. A 1 mL aquilot of 10 mM PBS buffer solution was added into 5 mL of the trichromophoric nanopartcile suspension **OFN–DCM–PS** (**OF**:**DCM**:**PS** = 1:0.01:0.01, mol/mol), 3 mL of which was transferred to a fluorescence cuvette and initial fluorescence was measured. The titration experiments were performed by progressively adding 5 μL aliquots of **BSA** stock solution to the cuvette and recording the spectral changes after each aliquots addtion.

Fluorescence Titration Experiments for HEP.

A 1 mL of 10 mM PBS buffer solution was added into 5 mL of the trichromophoric **OFN–DCM–PS** suspension (**OF**:**DCM**:**PS** = 1:0.01:0.01, mol/mol), 2 mL of which was transferred to a fluorescence cuvette and initial fluorescence was measured. The titration experiments were performed by adding

successive 5 μL aliquots of **HEP** stock solution (6 μg/mL) to the cuvette and recording the spectral changes after each aliquots addition.

Preparation of PVA Embedded Films.

Various molar ratio of **OFN–DCM–PS** suspension (1 mL) was injected into 5 mL of 10 wt% polyvinyl alcohol (**PVA**) aqueous solution under rapid stirring. The resultant mixture was drop-casted on a quartz plate and dried completely prior to fluorescent spectroscopic measurements.

Calculation of Spectral Overlap Integral.

The spectral overlap integral of the energy donor emission and the acceptor absorption, $J(\lambda)$, was calculated by using the equation below,[S2]

$$J(\lambda) = \frac{\int_0^{\alpha} F_D(\lambda)\varepsilon_A(\lambda)\lambda^4 d\lambda}{\int_0^{\alpha} F_D(\lambda) d\lambda}$$

where $F_D(\lambda)$ is the fluorescence intensity of the donor in the wavelength range $\lambda + \Delta\lambda$, and $\varepsilon_A(\lambda)$ is the extinction coefficient of the acceptor at λ.

Calculation of Efficiency and Rate Constant of Energy Transfer.

The efficiency (E) of energy transfer from the energy donor to the acceptor was evaluated from the donor fluorescence quenching profile by using the equation below,[S2]

$$E = 1 - \frac{I_{DA}}{I_D}$$

where I_D and I_{DA} are emission intensities of the donor in the absence and the presence of the acceptor, respectively.

Reference

1 *(a)* H. B. Wu, L. Ying, W. Yang, Y. Cao, *Chem. Soc. Rev.,* 2009, **38**, 3391; (*b*) Y. M. Yang, Q. Zhao, W. Feng, F. Y. Li, *Chem. Rev.,* 2013, **113**, 192; (*c*) N. H. Evans, P. D. Beer, *Angew. Chem. Int. Ed.,* 2014, **53**, 11716; (*d*) H. Q. Peng, L. Y. Niu, Y. Z. Chen, L. Z. Wu, C. H. Tung, Q. Z. Yang, *Chem. Rev.,* 2015, **115**, 7502; (*e*) J. S. Wu, B. Kwon, W. M. Liu, E. V. Anslyn, P. F. Wang, J. S. Kim, *Chem. Rev.* 2015, **115**, 7893; (*f*) L. You, D. J. Zha, E. V. Anslyn, *Chem. Rev.,* 2015, **115**, 7840.

2 (*a*) R. Abbel, R. van der Weegen, W. Pisula, M. Surin, P. Leclère, R. Lazzaroni, E. W. Meijer, A. P. H. J. Schenning, *Chem. Eur. J.,* 2009, **15**, 9737; (*b*) C. Vijayakumar, V. K. Praveen, A. Ajayaghosh, *Adv. Mater.,* 2009, **21**, 2059; (*c*) J. M. Malicka, A. Sandeep, F. Monti, E. Bandini, M. Gazzano, C. Ranjith, V. K. Praveen, A. Ajayaghosh, N. Armaroli, *Chem. Eur. J.,* 2013, **19**, 12991; (*d*) V. K. Praveen, C. Ranjith, N. Armaroli, *Angew. Chem. Int. Ed.,* 2014, **53**, 365.

3 (*a*) Y. L. Lei, Q. Liao, H. B. Fu, J. N. Yao, *J. Am. Chem. Soc.,* 2010, **132**, 1742; (*b*) C. Giansante, G. Raffy, C. Schäfer, H. Rahma, M. T. Kao, A. G. L. Olive, A. Del Guerzo, *J. Am. Chem. Soc.,* 2011, **133**, 316; (*c*) C. Giansante, C. Schäfer, G. Raffy, A. Del Guerzo, *J. Phys. Chem. C* 2012, **116**, 21706.

4 (*a*) A. Kaeser, A. P. H. J. Schenning, *Adv. Mater.,* 2010, **22**, 2985; (*b*) L. H. Feng, C. L. Zhu, H. X. Yuan, L. B. Liu, F. T. Lv, S. Wang, *Chem. Soc. Rev.,* 2013, **42**, 6620; (*c*) K. Li, B. Liu, *Chem. Soc. Rev.,* 2014, **43**, 6570; (*d*) J. Schill, A. P. H. J. Schenning, L. Brunsveld, *Macromol. Rapid Commun.,* 2015, **36**, 1306.

5 (*a*) S. P. Dudek, M. Pouderoijen, R. Abbel, A. P. H. J. Schenning, E. W. Meijer, *J. Am. Chem. Soc.,* 2005, **127**, 11763; (*b*) R. Abbel, C. Grenier, M. J. Pouderoijen, J. W. Stouwdam, P. E. L. G. Leclère, R. P. Sijbesma, E. W. Meijer, A. P. H. J. Schenning, *J. Am. Chem. Soc.,* 2009, **131**, 833; (*c*) R. Abbel, R. van der Weegen, E. W. Meijer, A. P. H. J. Schenning, *Chem. Commun.,* 2009, 1697; (*d*) X. Zhang, S. Rehm, M. M. Safont-Sempere, F. Würthner, *Nat. Chem,.* 2009, **1**, 623; (*e*) X. Zhang, D. Gorl, F. Würthner, *Chem. Commun.,* 2013, **49**, 8178.

6 (*a*) W. Ki, J. Li, G. Eda, M. Chhowalla, *J. Mater. Chem.* 2010, **20**, 10676; (*b*) K. V. Rao, K. K. R. Datta, M. Eswaramoorthy, S. J. George, *Angew. Chem. Int. Ed.* 2011, **50**, 1179; (*c*) K. V. Rao, K. K. R. Datta, M. Eswaramoorthy, S. J. George, *Chem. Eur. J.* 2012, **18**, 2184; (*d*) K. V. Rao, K. K. R. Datta, M. Eswaramoorthy, S. J. George, *Adv. Mater.* 2013, **25**, 1713; (*e*) V. K. Praveen, C. Ranjith, E. Bandini, A. Ajayaghosh, N. Armaroli, *Chem. Soc. Rev.* 2014, **43**, 4222.

7 (*a*) C. F. Wu, Y. L. Zheng, C. Szymanski, J. McNeill, *J. Phys. Chem. C* 2008, **112**, 1772; (*b*) L. Cerdán, E. Enciso, V. Martín, J. Bañuelos, I. López-Arbeloa, A. Costela, I. García-Moreno, *Nat. Photonics* 2012, **6**, 621; (*c*) J. Malinge, C. Allain, A. Brosseau, P. Audebert, *Angew. Chem. Int. Ed.* 2012, **51**, 8534; (*d*) I. Fischer, K. Petkau-Milroy, Y. L. Dorland, A. P. H. J. Schenning, L. Brunsveld, *Chem. Eur. J.* 2013, **19**, 16646; (*e*) A. Jana, K. T. Nguyen, X. Li, P. C. Zhu, N. S. Tan, H. Agren, Y. L. Zhao, *ACS Nano* 2014, **8**, 5939; (*f*) F. Tang, C. Wang, J. S. Wang, X. Y. Wang, L. D. Li, *ACS Appl. Mater. Interfaces* 2014, **6**, 18337; (*g*) M. Wu, X. J. Xu, J. S. Wang, L. D. Li, *ACS Appl. Mater. Interfaces* 2015, **7**, 8243.

8 (*a*) S. Kim, S. J. Yoon, S. Y. Park, *J. Am. Chem. Soc.* 2012, **134**, 12091; (*b*) T. O. McDonald, P. Martin, J. P. Patterson, D. Smith, M. Giardiello, M. Marcello, V. See, R. K. O'Reilly, A. Owen, S. Rannard, *Adv. Funct. Mater.* 2012, **22**, 2469; (*c*) S. S. Babu, M. J. Hollamby, J. Aimi, H. Ozawa, A. Saeki, S. Seki, K. Kobayashi, K. Hagiwara, M. Yoshizawa, H. Mohwald, T. Nakanishi, *Nat. Commun.* 2013, **4**, 1969; (*d*) S. Fery-Forgues, *Nanoscale* 2013, **5**, 8428; (*e*) A. Kaeser, I. Fischer, R. Abbel, P. Besenius, D. Dasgupta, M. A. J. Gillisen, G. Portale, A. L. Stevens, L. M. Herz, A. P. H. J. Schenning, *ACS Nano* 2013, **7**, 408; (*f*) P. Anees, S. Sreejith, A. Ajayaghosh, *J. Am. Chem. Soc.* 2014, **136**, 13233; (*g*) G. Kaur, T. Raj, N. Kaur, N. Singh, *Org. Biomol. Chem.* 2015, **13**, 4673.

9 (*a*) F. M. Ye, C. F. Wu, Y. H. Jin, Y. H. Chan, X. J. Zhang, D. T. Chiu, *J. Am. Chem. Soc.,* 2011, **133**, 8146; (*b*) C. Cordovilla, T. M. Swager, *J. Am. Chem. Soc.,* 2012, **134**, 6932; (*c*) J. Liang, K. Li, B. Liu, *Chem. Sci.,* 2013, **4**, 1377; (*d*) S. Rochat, T. M. Swager, *ACS Appl. Mater. Interfaces* 2013, **5**, 4488.

10 (*a*) E. Reinhard, E. A. Khan, A. O. Akyuz, G. Johnson, *Color Imaging: Fundamentals and Applications*, CRC Press, Florida, **2008**; (*b*) R. Nishiyabu, Y. Sugino, Y. Kubo, *Chem. Commun.* 2013, **49**, 9869.

11 (*a*) C. Vijayakumar, K. Sugiyasu, M. Takeuchi, *Chem. Sci.,* 2011, **2**, 291; (*b*) B. Balan, C. Vijayakumar, S. Ogi, M. Takeuchi, *J. Mater. Chem.,* 2012, **22**, 11224.

12 (*a*) H. Kasai, H. S. Nalwa, H. Oikawa, S. Okada, H. Matsuda, N. Minami, A. Kakuta, K. Ono, A. Mukoh, H. Nakanishi, *Jpn. J. Appl. Phys., Part 2* 1992, **31**, L1132; (*b*) H. Kasai, H. Kamatani, S. Okada, H. Oikawa, H. Matsuda, H. Nakanishi, *Jpn. J. Appl. Phys., Part 2* 1996, **35**, L221; (*c*) C. F. Wu, C. Szymanski, J. McNeill, *Langmuir* 2006, **22**, 2956.

13 Upon addition of trifluoroacetic acid to a solution of **OF**, no photoinduced electron transfer (PET) from *N*-methylaminomethyl groups to the oligofluorene backbone was observed, indicating that relatively low F_F arose not from PET but from amorphous packing among **OF** molecules in **OFN**.

14 Although **OFN–PS** are less stable than pristine **OFN**, they are stable, at least, for 7 h in aqueous medium.

15 (*a*) K. Lee, L. K. Povlich, J. Kim, *Analyst* 2010, **135**, 2179; (*b*) J. L. Fan, M. M. Hu, P. Zhan, X. J. Peng, *Chem. Soc. Rev.,* 2013, **42**, 29; (*c*) L. Yuan, W. Y. Lin, K. B. Zheng, S. S. Zhu, *Acc. Chem. Res.,* 2013, **46**, 1462.

16 (*a*) X. D. Wang, R. J. Meier, O. S. Wolfbeis, *Adv. Funct. Mater.,* 2012, **22**, 4202; (*b*) E. Ahmed, S. W. Morton, P. T. Hammond, T. M. Swager, *Adv. Mater.,* 2013, **25**, 4504; (*c*) S. Maiti, K. Das, P. K. Das, *Chem. Commun.,* 2013, **49**, 8851; (*d*) S. Rochat, T. M. Swager, *J. Am. Chem. Soc.,* 2013, **135**, 17703; (*e*) C. F. Wu, D. T. Chiu, *Angew. Chem. Int. Ed.,* 2013, **52**, 3086; (*f*) F. Du, Y. Min, F. Zeng, C. Yu, S. Wu, *Small*, 2013, **10**, 964.

17 (*a*) Z. L. Zhong, E. V. Anslyn, *J. Am. Chem. Soc.,* 2002, **124**, 9014; (*b*) A. T. Wright, Z. L. Zhong, E. V. Anslyn, *Angew. Chem. Int. Ed.,* 2005, **44**, 5679; (*c*) K. Y. Pu, B. Liu, *Macromolecules* 2008, **41**, 6636; (*d*) K. Y. Pu, B. Liu, *Adv. Funct. Mater.,* 2009, **19**, 277; (*e*) R. Y. Zhan, Z. Fang, B. Liu, *Anal. Chem.,* 2010, **82**, 1326; (*f*) Q. Dai, W. M. Liu, X. Q. Zhuang, J. S. Wu, H. Y. Zhang, P. F. Wang, *Anal. Chem.,* 2011, **83**, 6559; (*g*) S. M. Bromfield, E. Wilde, D. K. Smith, *Chem. Soc. Rev.,* 2013, **42**, 9184.

18 S. Naveenraj, M. R. Raj, S. Anandan, *Dyes Pigm.,* 2012, **94**, 330.

19 (*a*) L. Muhl, S. P. Galuska, K. Öörni, L. Hernández-Ruiz, L. C. Andrei-Selmer, R. Geyer, K. T. Preissner, F. A. Ruiz, P. T. Kovanen, S. M. Kanse, *FEBS J.* 2009, **276**, 4828; (*b*) R. Y. Zhan, Z. Fang, B. Liu, *Anal. Chem.,* 2010, **82**, 1326.

20 J. C. Sauceda, R. M. Duke, M. Nitz, *ChemBioChem,* 2007, **8**, 391.

21 (*a*) R. Martinez-Manez, F. Sancenon, *Chem. Rev.,* 2003, **103**, 4419; (*b*) B. T. Nguyen, E. V. Anslyn, *Coord. Chem. Rev.,* 2006, **250**, 3118; (*c*) M. Kitamura, S. H. Shabbir, E. V. Anslyn, *J. Org. Chem.,* 2009, **74**, 4479; (*d*) V. Kumar, E. V. Anslyn, *J. Am. Chem. Soc.,* 2013, **135**, 6338; (*e*) V. Kumar, E. V. Anslyn, *Chem. Sci.,* 2013, **4**, 4292; (*f*) S. M. Bromfield, P. Posocco, C. W. Chan, M. Calderon, S. E. Guimond, J. E. Turnbull, S. Pricl and D. K. Smith, *Chem. Sci.,* 2014, **5**, 1484; (*g*) S. M. Bromfield and D. K. Smith, *J. Am. Chem. Soc.,* 2015, **137**, 10056; (*h*) B. Roy, T. Noguchi, D. Yoshihara, T. Yamamoto, J. Sakamoto, S. Shinkai, *Phys. Chem. Chem. Phys.,* 2016, **18**, 13239.

22 I. Capila, R. J. Linhardt, *Angew. Chem. Int. Ed.,* 2002, **41**, 391.

23 H. Szelke, S. Schübel, J. Harenbergb, R. Kramer, *Chem. Commun*., 2010, **46**, 1667.

Appendix:

^{1}H NMR of **OF** in $CDCl_3$ (400 MHz)

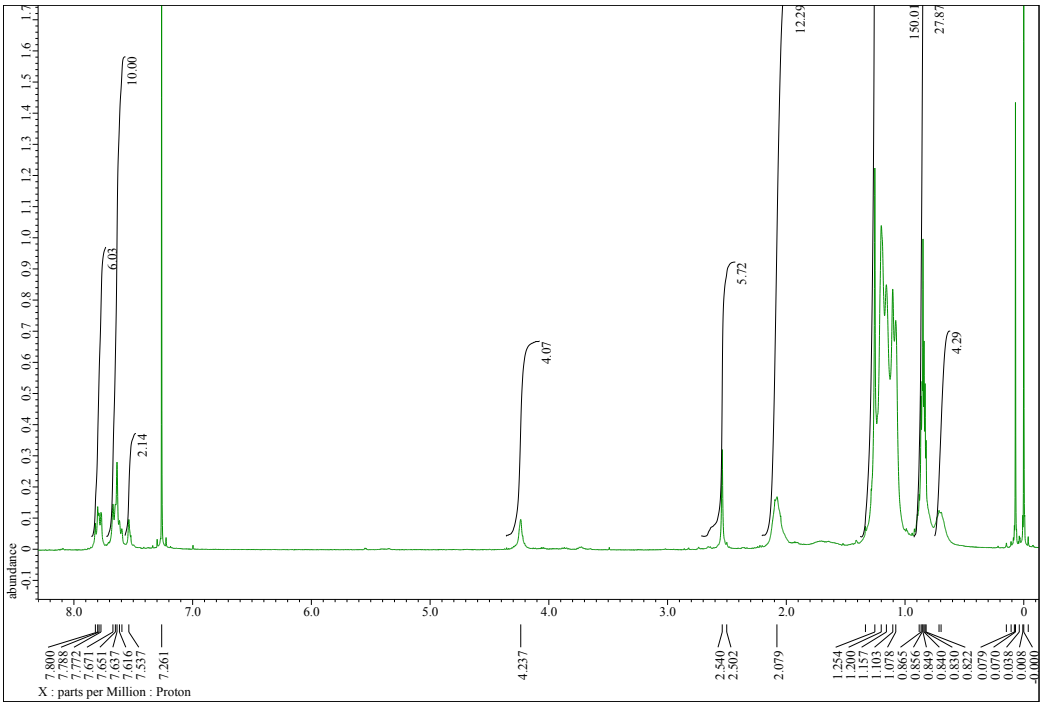

^{13}C NMR of **OF** in $CDCl_3$ (100 MHz)

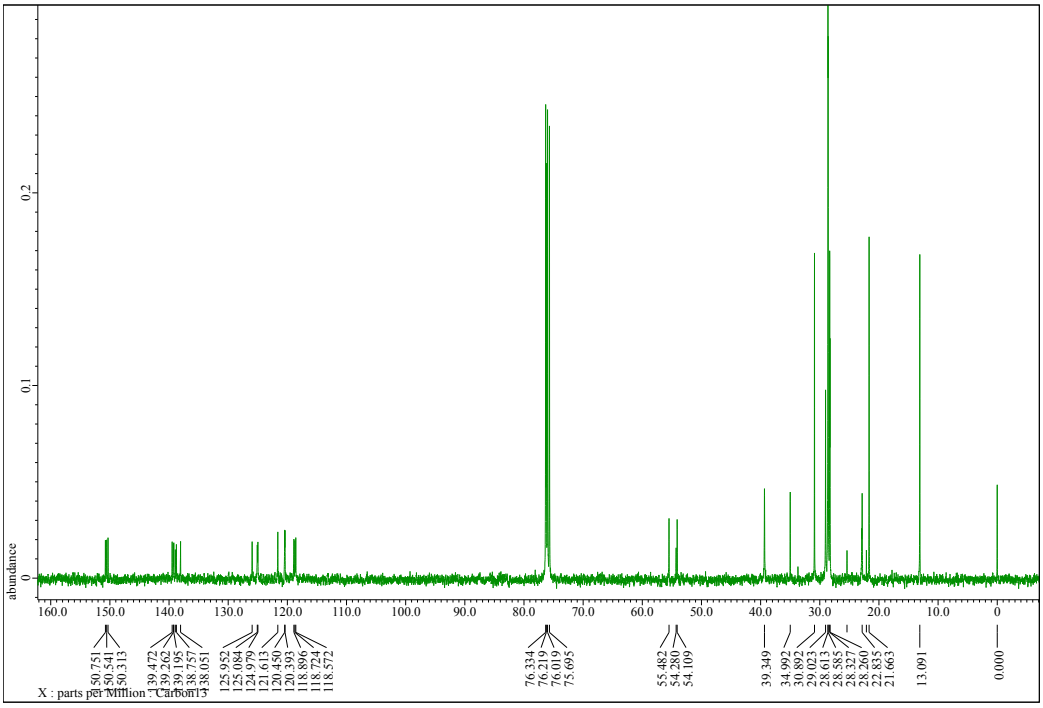

Chapter 3. Multiple Emissions from Indenofluorenedione in Solution and in Polymer Film

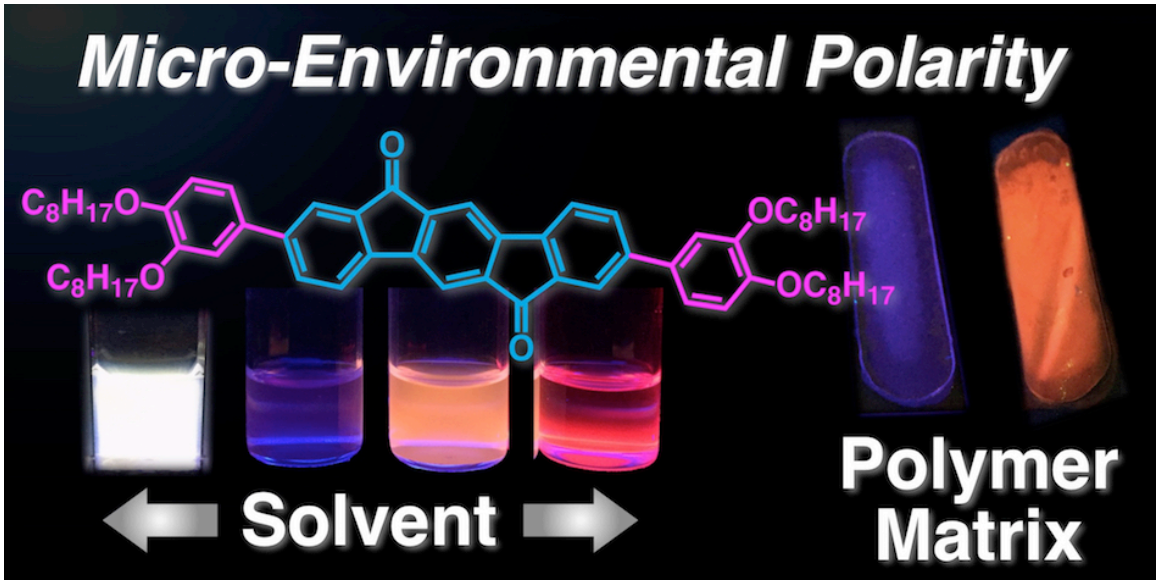

Abstract

A new indenofluorenedione derivative (**IFO**) with D–A–D framework was synthesized, of which the multiple fluorescent channels can be controllably switched by changing solvent and polymer matrix in broad visible range, exhibiting multi-emission including white. It was also demonstrated that **IFO** embedded in polystyrene matrix is sensitive to environmental polarity, thus exhibiting the emission colour changes upon exposure to polar organic solvents.

Introduction

Multicolour organic luminescent materials have attracted extensive attentions due to their potential applications in flexible full-colour displays, the next-generation lighting and bioimaging.[1] Compared with multicomponent molecular emitters, a single organic molecule eliciting multiple luminescences has many advantages such as no inherent phase separation, excellent colour stability, reproducibility and easy fabrication.[2] So far, several strategies have been proposed in this research area, that mainly rely on use of multiple channels or multiple signaling pathways such as an excimer or exciplex,[3] excited-state intramolecular proton transfer[4] and intra-/inter-molecular charge transfer states.[5] Among the above, a single molecule comprising electron-donor (D) and acceptor (A) units can be one of the simple and promising candidates for new colour tuneable fluorophores, because one can utilize emission from an intramolecular charge transfer (**ICT**) transition state.[6,7] The **ICT** state, however, becomes a non-switchable deactivation pathway in many cases, resulting in showing red-shifted fluorescence.[7a] Therefore, a **ICT** molecule with blue emission arising from locally excited state (**LE**) is still limited, thus hampering to design a single organic emitter with multiple emissions for the generation of white emission.

In this chapter, we report a new indenofluorenedione-based fluorophore (**IFO**) (Scheme 3-1), which exhibits multiple luminescence including white. Indenofluorenedione is a rigid and planar π-conjugated molecule with electron-accepting ability, in which the n-π^* and π-π^* transition states lie very close to each other in non-polar solvents, and π-π^* transition state is expected to be dominant in polar solvents.[8,9] By introducing the alkoxy side chains (weak electron-donor), the D–A–D π-skeleton of **IFO** affords other deactivation pathways via intra-/inter-molecular **ICT** states, leading to multiple fluorescent channels.[10] Compared to the fluorenone counterpart (**FO**; Scheme 1a), which is known to be non-emissive materials with

special sensitivity towards solvent polarity,[9,6c] **IFO** has an extended π-conjugated structure, enabling broad emission in visible range. We found that **IFO** indeed exhibits blue emission in dimethylformamide (DMF), orange in methylcyclohexane (MCH), and red in *p*-xylene, resulting from the **LE–ICT** state switching property. The **LE–ICT** state switching[11] of **IFO** can be also achieved in different polymer matrixes, resulting in multi-fluorescent polymer films.

Results and discussions

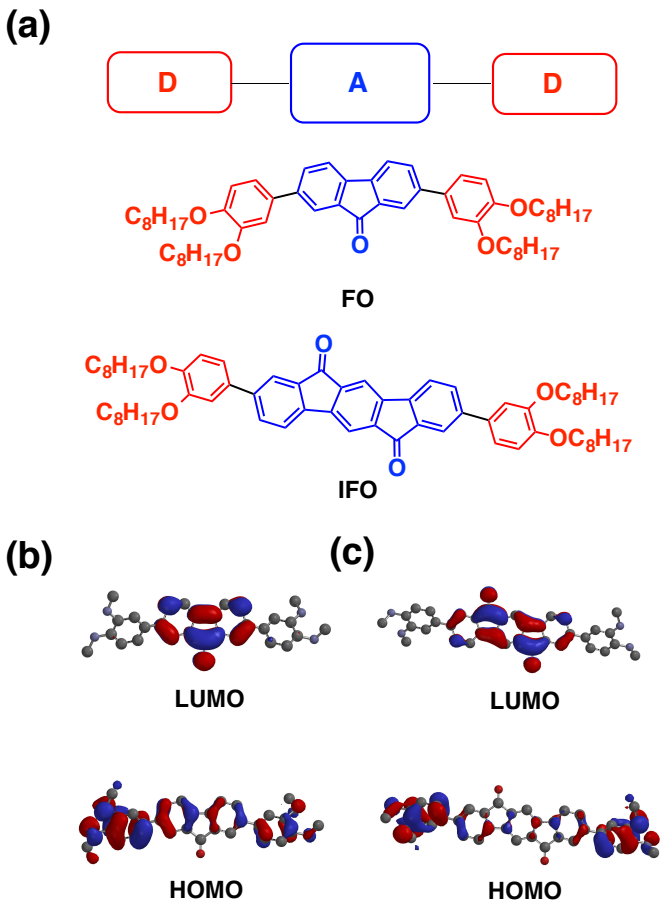

Scheme 3-1. (a) Chemical structures of **FO** and **IFO** with donor–acceptor–donor arrangement; **HOMO** and **LUMO** of (b) **FO** and (c) **IFO** calculated at B3LYP/6-31G* level. The dodecyl groups are replaced by ethyl groups for simplicity.

The **FO** and **IFO** molecules were characterized by ^{1}H NMR, ^{13}C NMR and MALDI/TOF-MS measurements. According to the DFT calculation (Schemes 3-1b and 3-1c), the HOMO of **IFO**

is mostly delocalized on the electron-donating moiety and the LUMO is delocalized on the electron-accepting moiety. Photophysical properties of **IFO** in methylcyclohexane (MCH), dichloromethane (DCM), tetrahydrofuran (THF), DMF and *p*-xylene were summarized in Table 3-1.[12]

The absorption spectrum of **IFO** consists of three peaks at 319 nm, 369 nm and 530 nm (Figure 3-1); the peaks at 319 and 369 nm correspond to π-π* transition of the indenofluorenedione core, which is consistent with the reported results.[8] The absorbance of **IFO** at 369 nm is proportional to the concentration in the range from 5 μM to 40 μM in DCM, THF, DMF and *p*-xylene (Figure 3-2), indicating that there is no aggregates in the ground state under the experimental conditions. The absorption around at 530 nm can be assigned to **ICT** absorption; indeed when increasing the polarity of solvents from MCH to DMF, it showed positive solvatochromic shift (Figure 3-1).

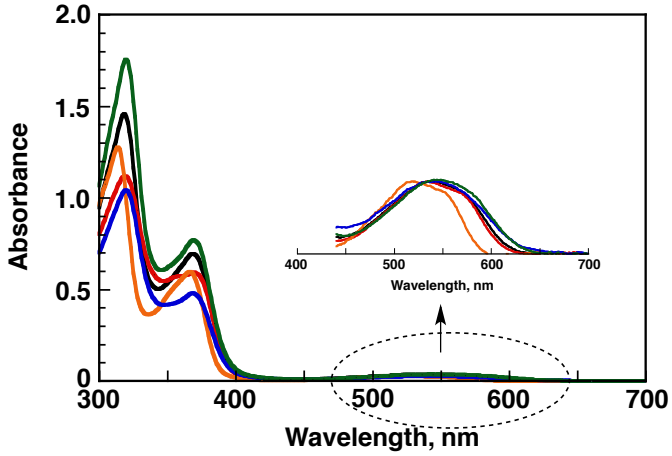

Figure 3-1. Absorption spectra of **IFO** (20 μM) in MCH (orange), *p*-xylene (red), THF (black), DCM (green), DMF (blue) at 298K.

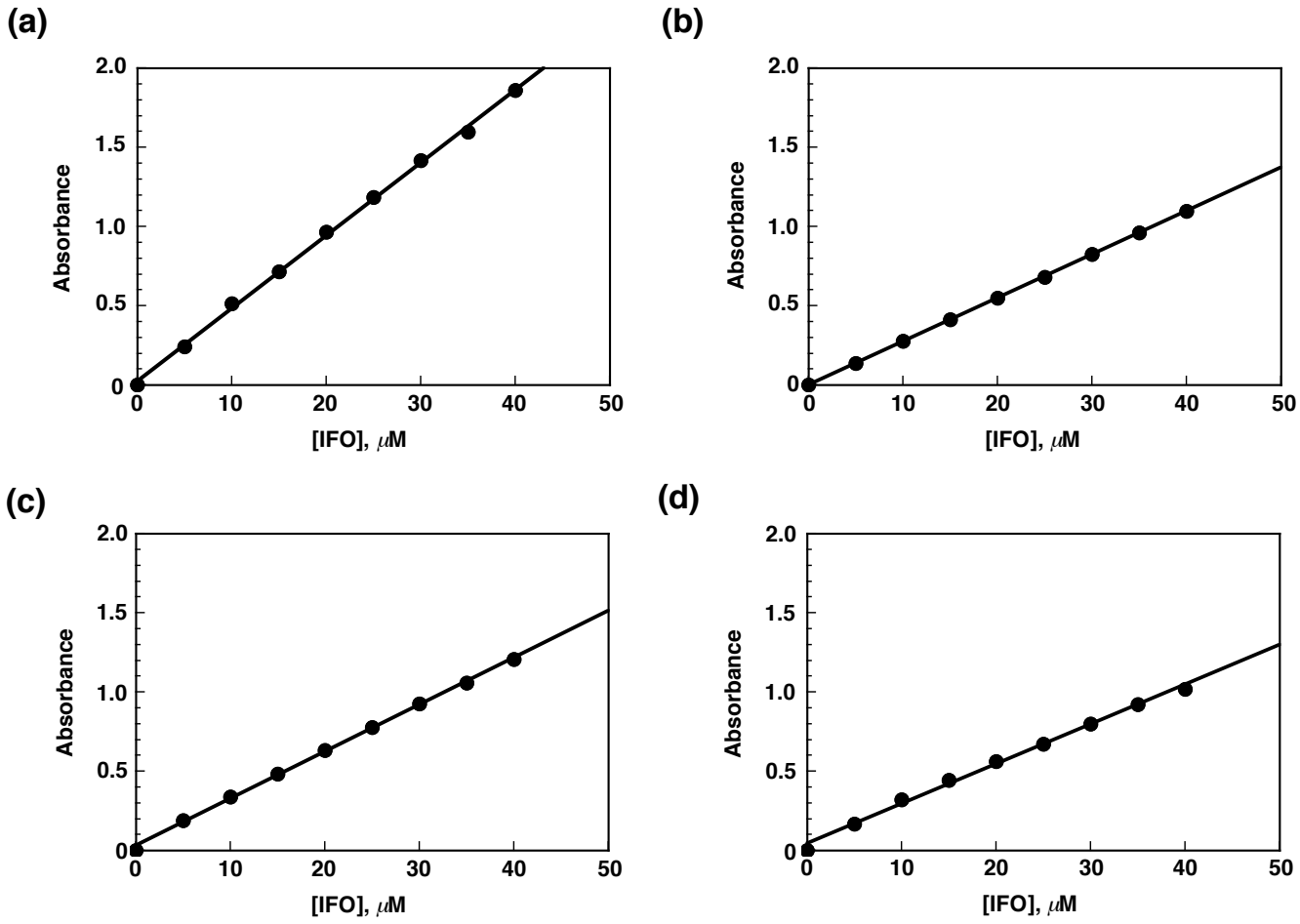

Figure 3-2. The absorbance at 369 nm as a function of concentration of **IFO** in (a) DCM, (b) THF, (c) *p*-xylene and (d) DMF.

In stark contrast to the typical solvatochromic behaviours of conventional **ICT** molecules that fluorescence is progressively red-shifted in correlation with the solvent polarity,[7a] the **IFO** showed unusual solvatochromic behaviour. In polar solvent like DMF, a fluorescent band at 436 nm was observed, which is attributable to the transition from **LE**, S_1–S_0,[13] while two low-energy emission peaks at 530 nm and 610 nm were observed in non-polar solvent like *p*-xylene (Figure 3-3).

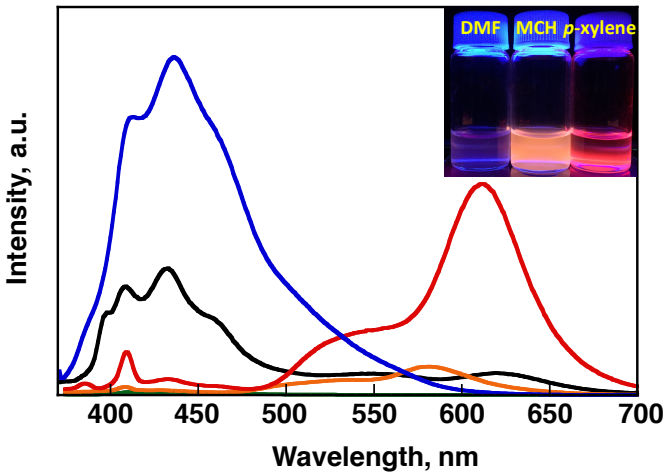

Figure 3-3. Fluorescence spectra of **IFO** in various solvents. (black: THF, green: DCM, orange: MCH, red: *p*-xylene, blue: DMF). [**IFO**] = 20 μM Excitation wavelength is 355 nm. (Inset: photographs under irradiation with 365 nm UV–lamp)

In order to assign the two emission peaks observed at longer wavelengths, the concentration dependence of fluorescence spectra of **IFO** was performed in *p*-xylene (Figure 3-4). The solution of each concentration was excited at the wavelength, where the absorbance is around 0.2. We found that the fluorescent intensity at 610 nm is constant throughout the different concentrations (5 μM to 40 μM).

On the other hand, the fluorescent intensity at 530 nm slightly increased along with increasing the **IFO** concentration (Figure 3-4). These results indicate that fluorescent emissions at 530 and 610 nm in *p*-xylene are originating from the intermolecular events at the excited state and intramolecular charge transfer bands, respectively. The both charge transfer bands exhibited red shifts when medium changed from *p*-xylene to MCH. The three emissions from **LE** (436 nm) and charge transfer states (555 and 619 nm) were observed in THF (Figure 3-3).

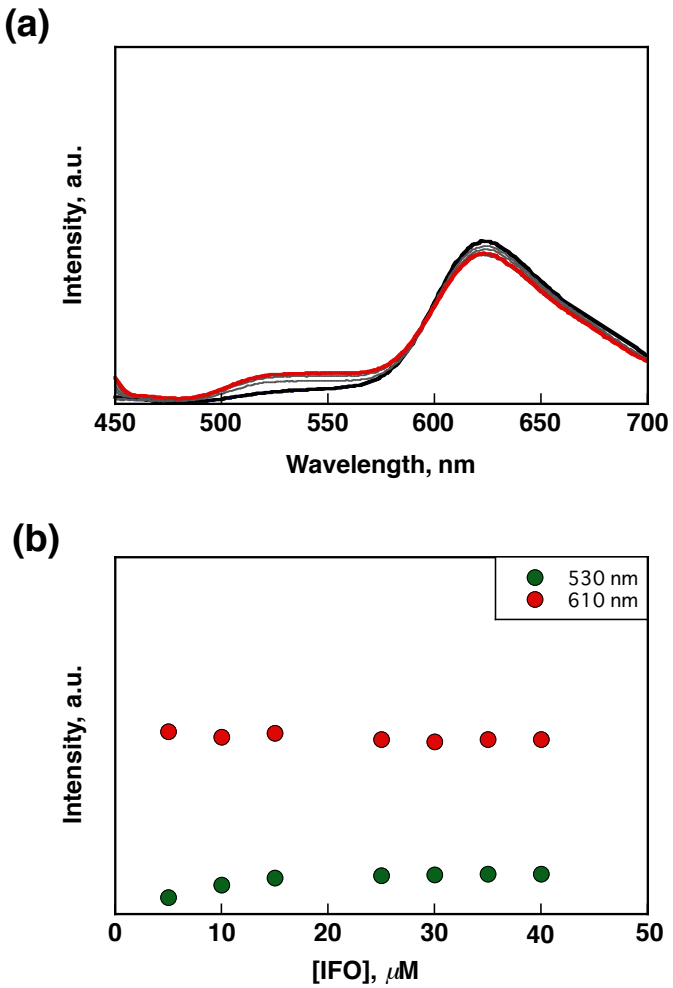

Figure 3-4. (a) Concentration dependence of fluorescence spectra of **IFO** in *p*-xylene in the range of 5 μM to 40 μM (from black line to red line); (b) fluorescent intensity as a function of **IFO** concentration.

The excitation spectra in various solvents were identical to the corresponding absorption spectrum (Figure 3-5).

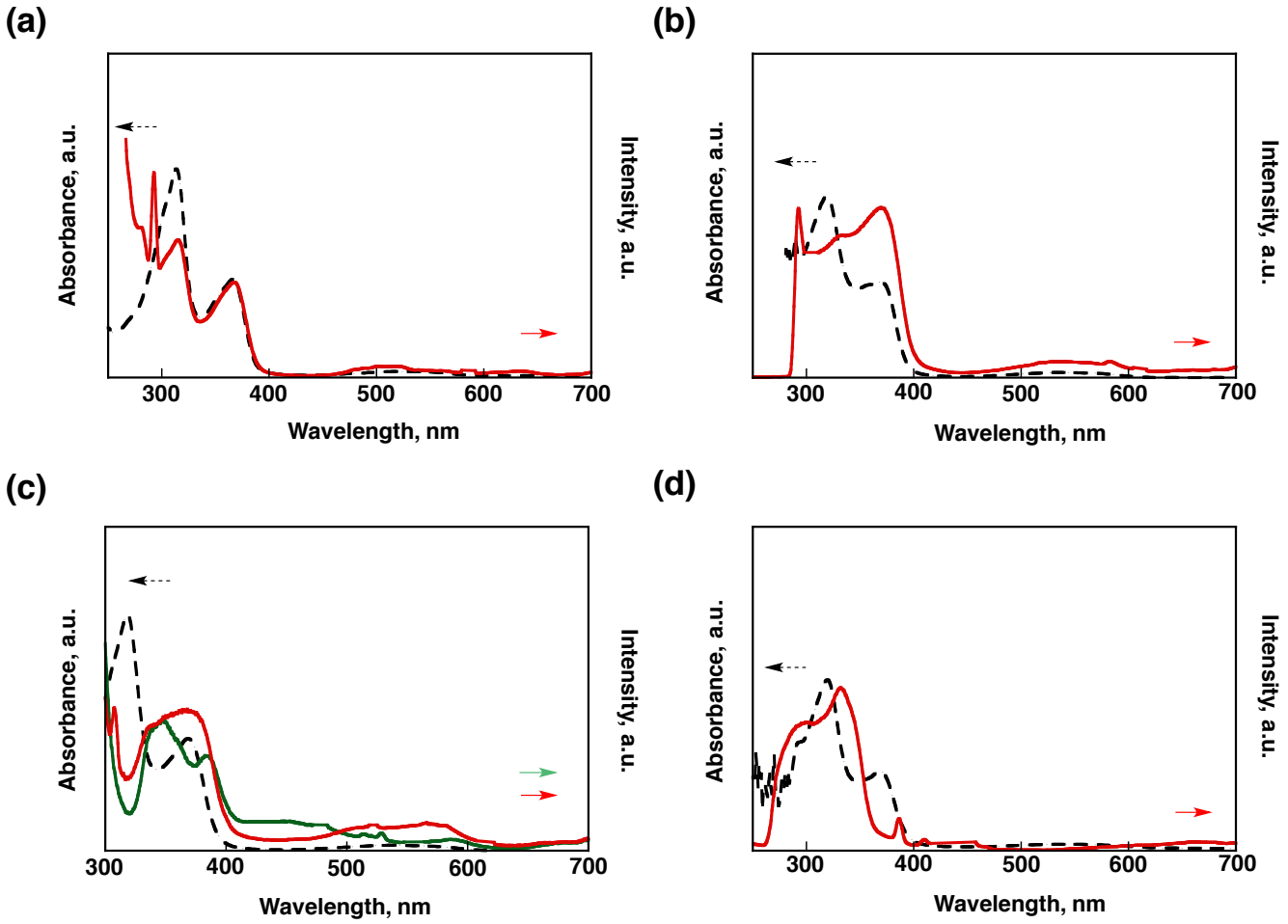

Figure 3-5. Excitation spectra of **IFO** (19 μM) measured in (a) MCH (λ_{moni} = 586 nm), (b) *p*-xylene (λ_{moni} = 610 nm), (c) THF (green λ_{moni} = 555 nm, red λ_{moni} = 618 nm) and (d) in DMF (λ_{moni} = 437 nm) dash lines are the corresponding absorption spectra.

Table 3-1. Photophysical data of **IFO** and **FO** in various solvents.

	solvent	λ_{abs} (nm) [a] (ε 10^4 M^{-1} cm^{-1})	λ_{em} [b] (nm)	τ [c] ns	Φ_F [d] (%)
IFO	MCH	367 (2.9)	585	5.3	3.3
	p-xylene	370 (2.9)	610	1.8	3.2
	THF	369 (2.7)	436/619	1.2/0.5	0.7
	DMF	369 (2.5)	436	3.4	2.2
FO	MCH	341 (3.2)	523	7.3	23
	p-xylene	345 (3.2)	546	3.9	13
	THF	345 (3.2)	557	1.3	13
	DMF	347 (2.9)	422/571	2.4/1.3	3.3

[a] Absorption maxima of π-π* transition; [b] Emission maxima upon excitation at 355 nm for **IFO** and 345 nm for **FO**; [c] Fluorescent lifetimes calculated as average lifetimes; [d] Absolute fluorescence quantum yields determined by a calibrated integrating sphere system.

We inferred that in MCH and *p*-xylene, the S_0–S_1 transition is n-π* forbidden transition. Consequently, the excited deactivation pathway of **IFO** would be switched onto the intra- and inter-molecular **CT** channels (Scheme 3-2), leading to the low-energy fluorescence with solvent-dependent characteristics (Table 3-1).

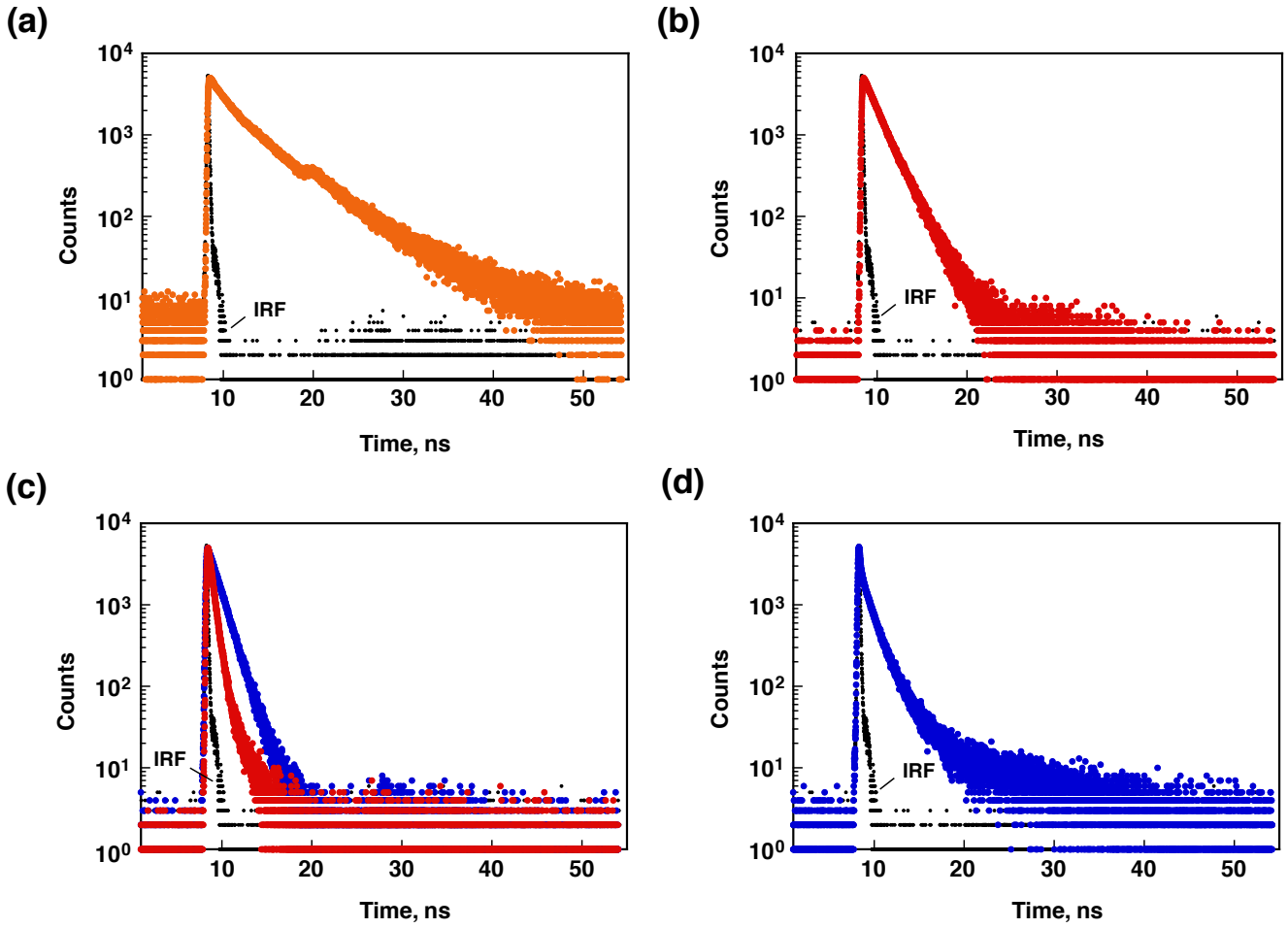

Figure 3-6. Fluorescence lifetime decay profiles of **IFO** measured in (a) MCH (λ_{moni} = 585 nm), (b) *p*-xylene (λ_{moni} = 610 nm), (c) THF (blue λ_{moni} = 420 nm, red λ_{moni} = 619 nm) and (d) DMF (λ_{moni} = 435 nm) at 298K. Excitation wavelengths are 375 nm. IRF: Instrumental Response Function.

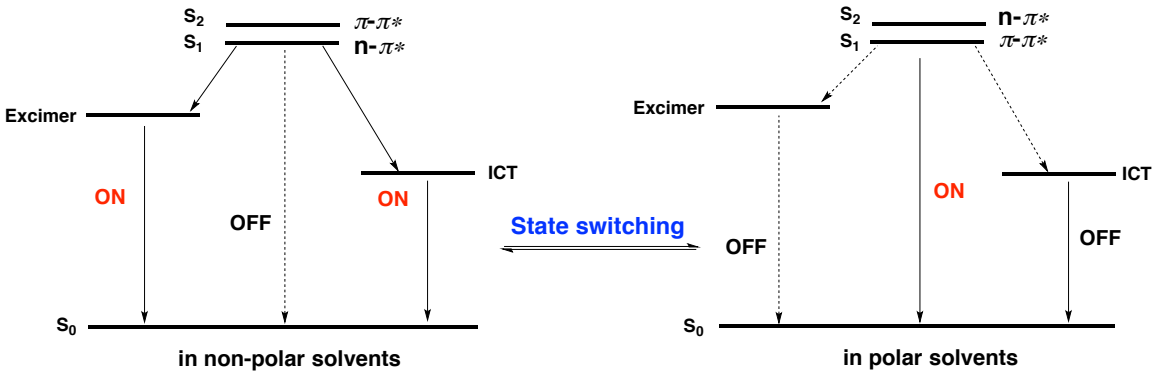

Scheme 3-2. Plausible deactivation mechanism for our designed system in polar and non-polar media.

The large dipole moment variation between the ground state and excited state of **IFO** is responsible for large Stokes shift observed in MCH (218 nm) and *p*-xylene (240 nm). Interestingly, in polar medium like DCM, THF and DMF, the character of the lowest excited state of **IFO** changed to allowed π-π^* transition (Scheme 3-2). In this case, the **CT** band was not as favourably active as in non-polar solvents probably because of weak electron donating ability of dialkoxyphenyl groups.[14] Instead, the **LE** with π-π^* character would play a major role in excited state deactivation mechanism. Thus, multiple fluorescent deactivation pathways of **IFO** can be switched by varying polarity of solvents. Commensurate with structural similarity, **FO** exhibits similar solvatochromic behaviour (Figure 3-7), but the extended π-conjugation length of **IFO** enables us to tune emission colours in wider range, particularly complementary blue (in DMF) and red (in *p*-xylene).

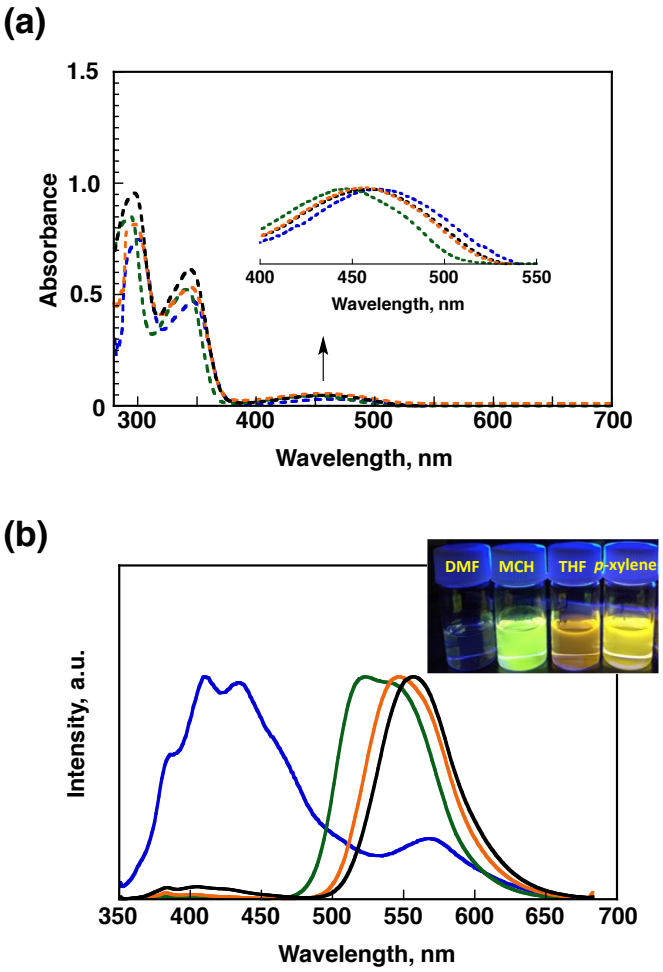

Figure 3-7. (a) Absorption and (b) emission spectra of **FO** (15 μM) measured in DMF (blue), MCH (green), *p*-xylene (orange) and THF (black) at 298K. Excitation wavelengths are 345 nm. The

intensities were normalized at the emission maximum. Inset: photographs under irradiation with 365 nm UV–lamp.

The lifetime of **IFO** and **FO** in various solvents were examined and shown in the Figures 3-6 and 3-8.

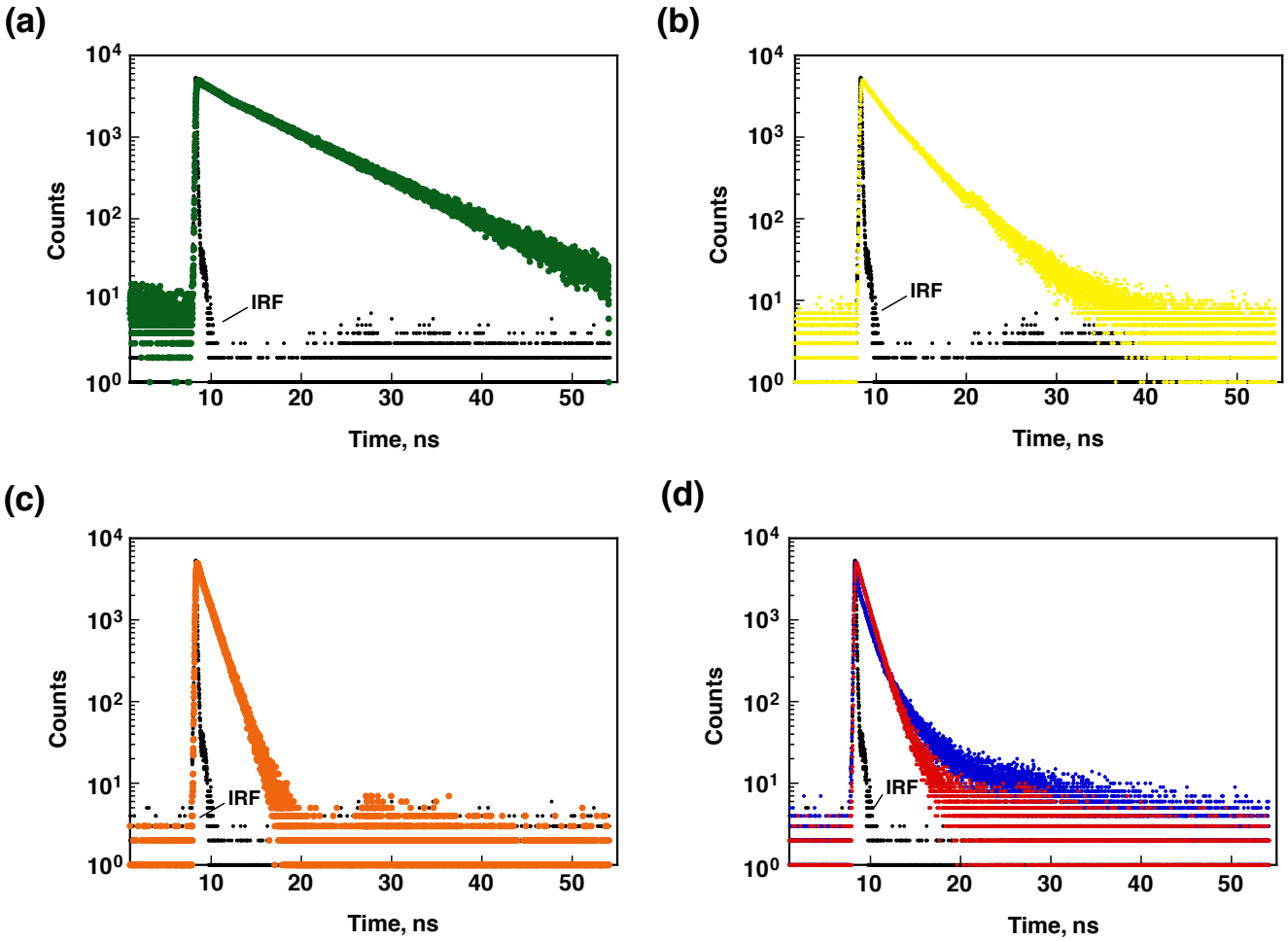

Figure 3-8. Fluorescence lifetime decay profiles of **FO** measured in (a) MCH (λ_{moni} = 523 nm), (b) *p*-xylene (λ_{moni} = 546 nm), (c) THF (λ_{moni} = 557 nm) and (d) DMF (blue λ_{moni} = 420 nm, red λ_{moni} = 570 nm) at 298 K. Excitation wavelengths are 375 nm. IRF: Instrumental Response Function.

The excitation spectra in various solvents were identical to the corresponding absorption spectrum (Figure 3-9).

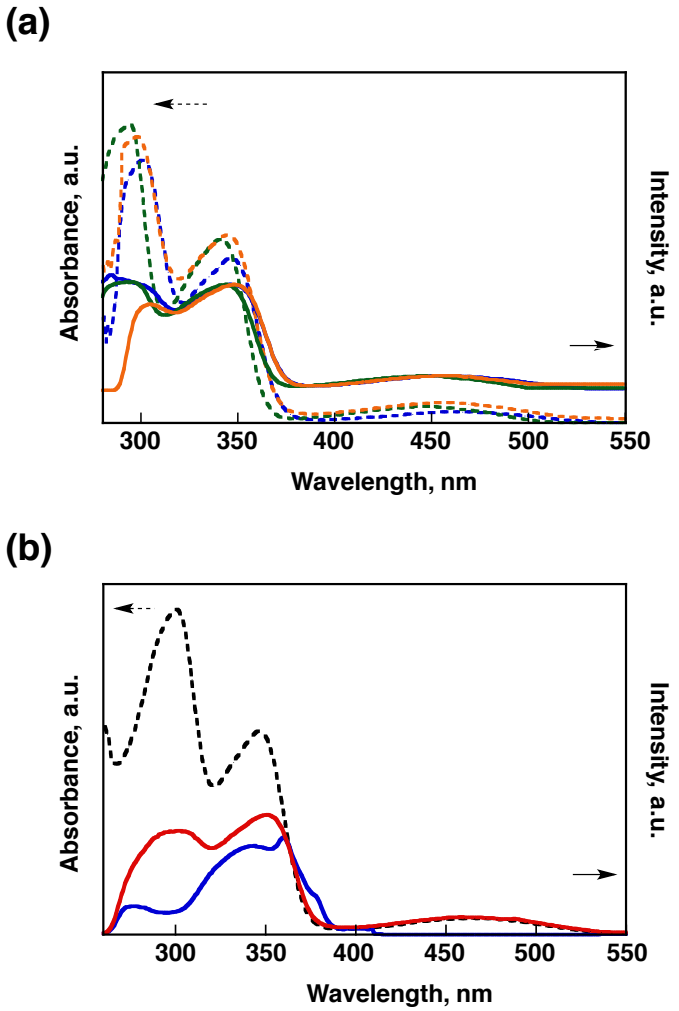

Figure 3-9. Excitation spectra of **FO** (15 μM) measured in (a) MCH (black, λ_{moni} = 520 nm), *p*-xylene (blue λ_{moni} = 547 nm), THF (green λ_{moni} = 557 nm) and (b) DMF (blue λ_{moni} = 422 nm, red λ_{moni} = 570 nm) dash lines are the corresponding absorption spectra.

Such unusual solvatochromic behaviour inspires us to generate white emission in binary solvent mixtures. The desirable amount of **IFO** was added into binary solvents of DMF and *p*-xylene under varying ratios. The final concentration of **IFO** was kept identical to be 20 μM. All the solvent combinations showed similar absorption spectra. However, the fluorescence was tunable and determined by the number of polar solvent molecules in close proximity to the **IFO** molecule.[15] As shown in Figure 3-10, upon gradual addition of DMF into *p*-xylene, the low-energy fluorescent band at 610 nm was progressively decreased along with the increase of high-energy fluorescent band at 436 nm. Strikingly, when the ratio of DMF: *p*-xylene was tuned to 1:4 (v/v), white emission was obtained with CIE of (0.35, 0.32) as shown in Figure 3-10b.[16]

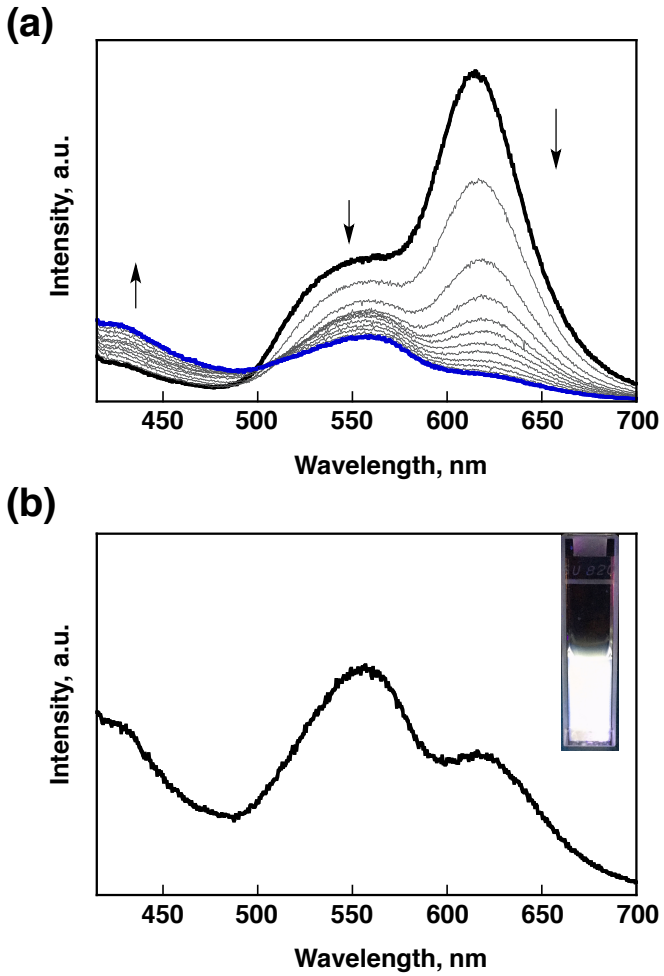

Figure 3-10. (a) Fluorescence spectral change of **IFO** (20 μM) in binary solvents system (DMF and *p*-xylene) in the presence of 0% DMF (black line) to 50% DMF (blue line). Excitation wavelength is 355 nm. (b) White light emission of **IFO** in binary solvent system with DMF: *p*-xylene = 1:4 (v/v). Inset: a photograph under irradiation with 365 nm lamp.

Additionally, such multicolour emissions can be achieved when **IFO** encounters with surrounding polymer matrixes having different polarities.[17] The polysulfone (**PSF**) and polystyrene (**PS**) were chosen as host polymer matrixes to examine fluorescent properties. The **IFO** doped **PS** and **PSF** films were fabricated by using drop casting from a $CHCl_3$ solution containing **IFO** (1 wt%) onto the surface of quartz cells. The low doping level ensured that **IFO** was molecularly dispersed into polymer matrix without the formation of aggregates. The emission spectra and photographic images of **IFO**-doped-**PS** and -**PSF** films were shown in Figure 3-11. The emission colours are identical to those observed in solution. The fluorescent

maximum of **IFO** embedded in **PS** is located at 598 nm, showing red emissive colour with CIE of (0.23, 0.20). While the polymer matrix changed to **PSF**, the emission maximum is dramatically hypsochromic shifted to 393 nm exhibiting blue emission with CIE of (0.31, 0.25). This result indicates that **IFO** exhibits high sensitivity towards microenvironments surrounding **IFO** molecule.

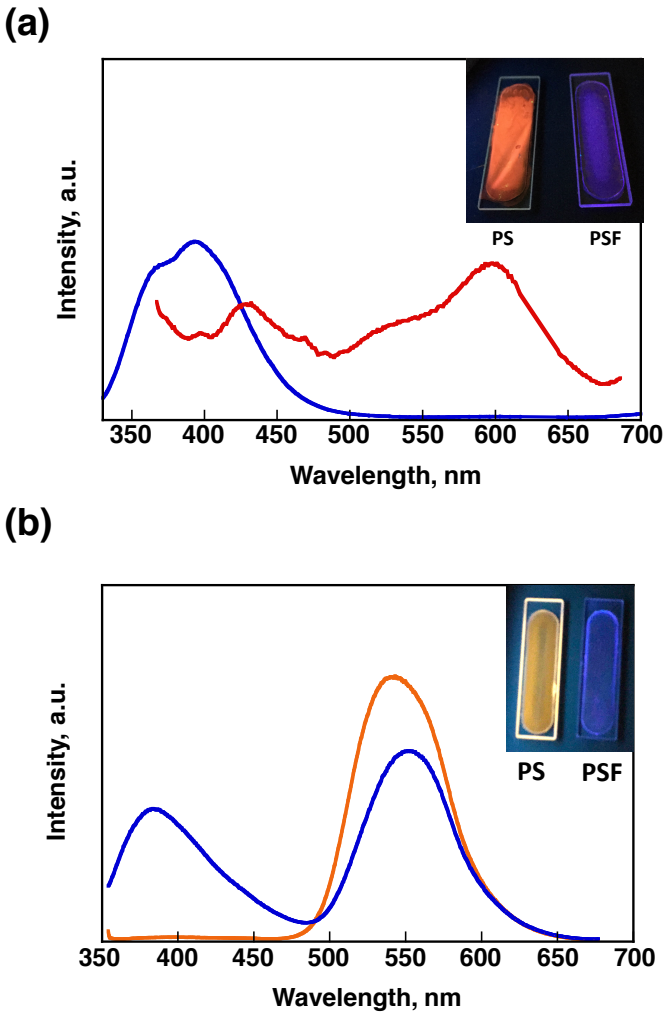

Figure 3-11. (a) Fluorescence spectra of **IFO** doped in **PS** (red line) and **PSF** (blue line) as host matrixes fabricated by drop casting of $CHCl_3$ solution containing the corresponding **IFO** (1 wt%). Excitation wavelength is 315 nm for **PSF** film and 355 nm for **PS** film. Inset: Corresponding photographs under irradiation with UV–lamp. (b) Fluorescence spectra of **FO** film doped in polystyrene (orange) and polysulfone (blue) as host matrixes fabricated by drop casting of $CHCl_3$ solution containing 1 wt% **FO**. Excitation wavelengths are 345 nm. Inset: corresponding

photograph under irradiation with 365 nm UV–lamp.

The excitation spectra of **IFO**-doped and **FO**-doped **PS** and **PSF** were identical to the corresponding absorption spectrum (Figure 3-12).

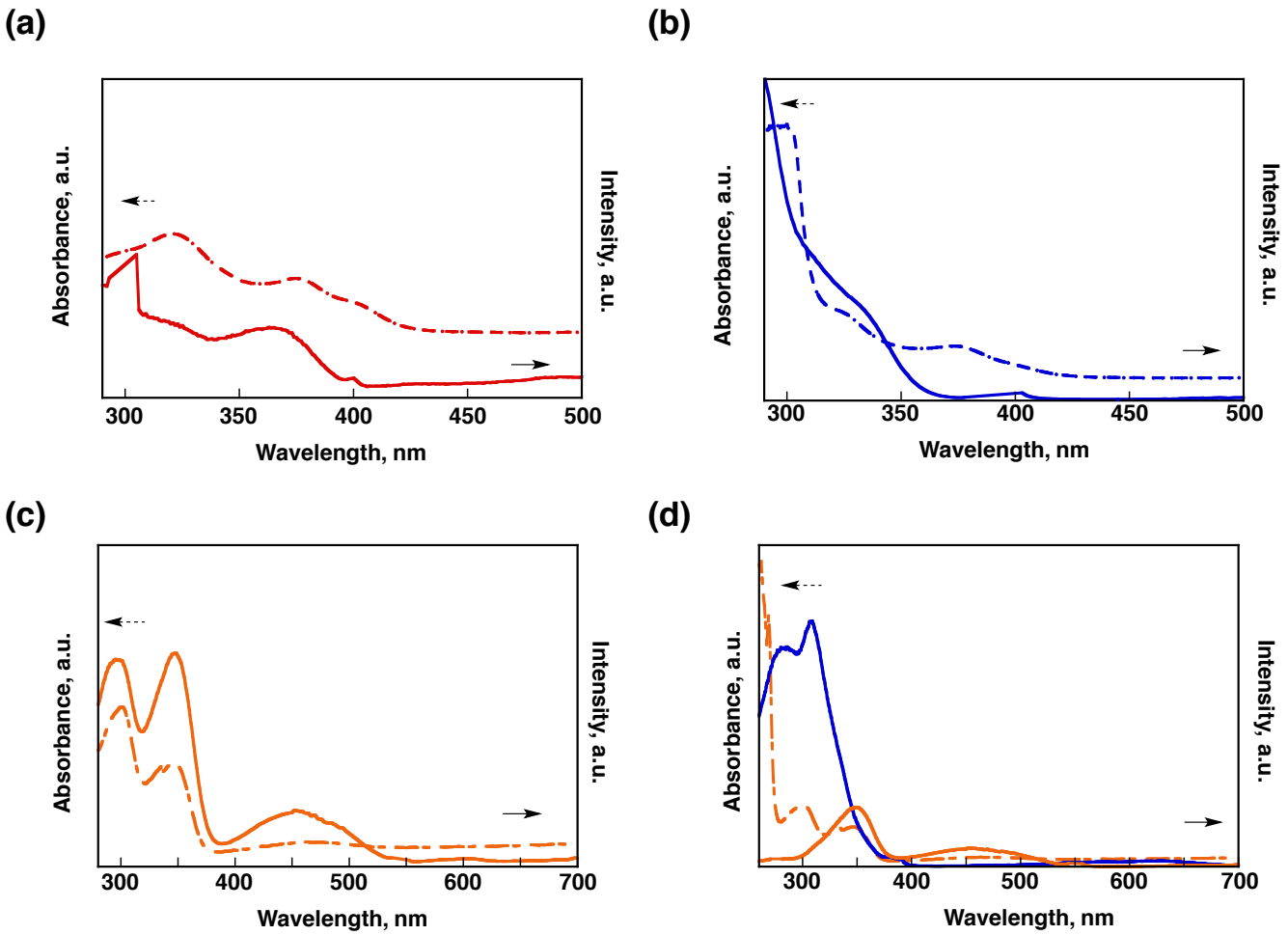

Figure 3-12. Excitation spectra of **IFO** film doped in (a) polystyrene (λ_{moni} = 598 nm) and (b) polysulfone (λ_{moni} = 393 nm) as host matrixes containing 1 wt% **IFO**. The dash lines are the corresponding absorption spectra. Excitation spectra of **FO** film doped in (c) polystyrene (λ_{moni} = 545 nm) and (d) polysulfone (blue λ_{moni} = 385 nm, orange λ_{moni} = 550 nm) as host matrixes containing 1 wt% **FO**. The dash lines are the corresponding absorption spectra.

We further utilized the **IFO**-doped **PS** film to study the feasibility of selective detection of common organic solvents, in which **IFO** is able to act as an indicator. The organic solvents were placed onto **IFO** embedded **PS** film and resulting luminescent colour change was monitored after 10 min. The **IFO**-doped **PS** film showed distinct colour change from red to

blue upon exposure to acetonitrile, ethyl acetate and methanol probably because of large polarity of solvents into **PS** matrix. In contrast to the above, no visible response towards MCH, DCM, $CHCl_3$, THF and toluene was observed (Figure 3-13). Such discriminated response is consistent with the results obtained in solution.

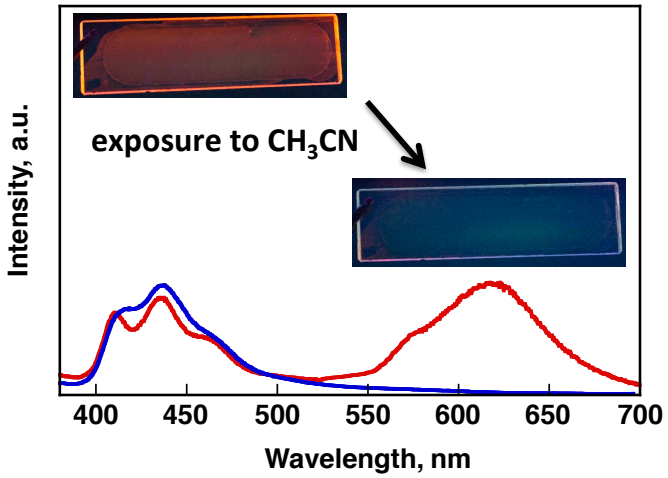

Figure 3-13. Fluorescence spectral change of **IFO** doped **PS** film before (red line) and after exposure to acetonitrile (blue line), excitation wavelength is 355 nm. Inset: corresponding fluorescent images of **IFO** doped **PS** films before and after acetonitrile exposure.

Conclusions

In conclusion, we have successfully demonstrated that a newly designed electron D–A–D fluorophore, **IFO**, presented multiple fluorescence channels that can be switched depending on micro-environmental polarity such as solvent and polymer matrix. We believe that our molecular design would help and extend the limited design concept of **ICT** molecules towards stimuli-responsive and full-colour emissive materials.

Experimental Section

Materials.

All chemicals were purchased from Sigma-Aldrich, Kanto Chemical, Tokyo Chemical Industry, or Wako Pure Chemical Industries and used as received. The anhydrous DMF, anhydrous THF, *p*-xylene and methylcyclohexene (MCH) spectroscopic grade (Wako Pure Chemical Industries, Ltd.) were used for analysis. polysulfone (**PSF**) (M_w is 60 kDa) and polystyrene (**PS**) (M_w is 350 kDa) were used as host polymer matrixes. Fluorenone derivatives (**IFO** and **FO**) were synthesized according to the literature procedures shown below.

General Method.

^{1}H NMR and ^{13}C NMR spectra were recorded on a JEOL ECS-400; chemical shifts were recorded in ppm relative to TMS (0 ppm for ^{1}H NMR as an internal standard). UV-Vis absorption and fluorescence spectra were obtained on a Hitachi U-2900 spectrophotometer and a Hitachi F-7000 spectrophotometer, respectively. Fluorescence quantum yields were obtained on a Hamamatsu Photonics, Absolute PL Quantum Yield Measurement System, C9920-02G. Fluorescence lifetimes were measured using an IBH (FluoroCube) time correlated picosecond single photon counting (TCSPC) system. Samples were excited using a pulsed diode laser (NanoLED-11, <100 ps pulse duration) at a wavelength of 375 nm with a repetition rate of 1 MH.

Synthetic Route of IFO and FO.

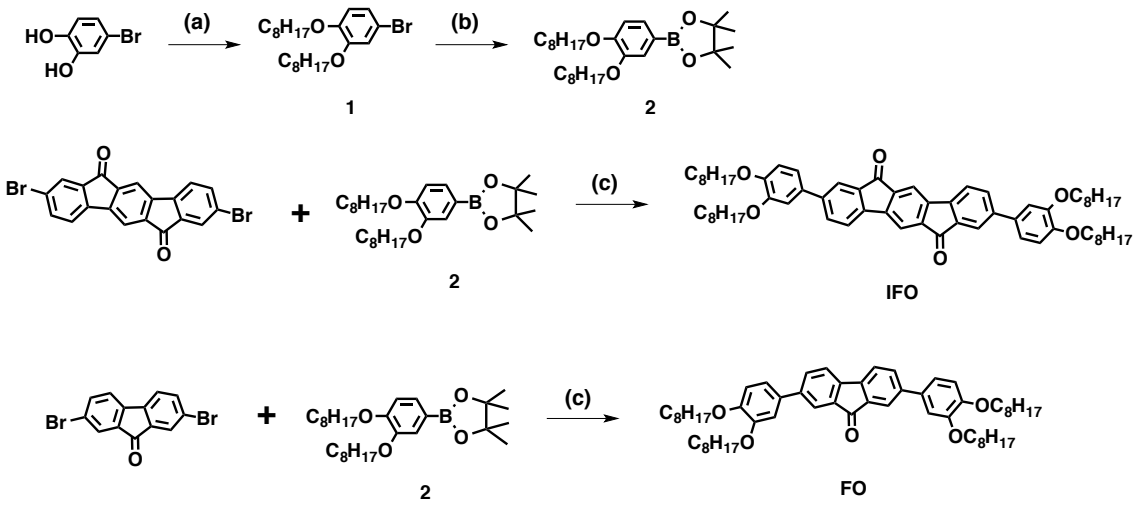

Reagents and conditions: (a) $C_8H_{17}Br$, CH_3CN, K_2CO_3, reflux, 2 days; (b) *n*-BuLi, THF, –78 °C, 2-isopropoxy-4,4,5,5-tetramethyl-1,3,2-dioxaborolane, –78 °C to r.t.; (c) $Pd(PPh_3)_4$, Na_2CO_3, toluene, H_2O, EtOH, reflux, overnight.

Synthesis of 1. 4-Bromocatechol (5 g, 26.45 mmol) and K_2CO_3 (22 g, 158.7 mmol) were dissolved in acetonitrile (100 mL) and the mixture was heated to reflux for 1 hour. Then 1-bromooctane (12.77 g, 66.13 mmol) was added and the mixture was kept refluxed for 2 days with vigorous stirring. After cooling, the mixture was poured into water and extracted with Et_2O for three times. The combined organic layers were washed with 2 M NaOH, dried over anhydrous $MgSO_4$ and concentrated to give pale brown solids. The crude products were freed from the residual 1-bromooctane by distillation and purified by column chromatography (silica gel) with hexane: DCM (2:1) as the eluent, affording the pure product as a white solid. (10.1 g, 93% yield). ^{1}H NMR ($CDCl_3$, 400 MHz, TMS, 298 K): δ 0.84-0.95 (m, 6H), 1.29-1.34 (m, 20H), 1.74-1.85 (m, 4H), 3.91-4.0 (m, 4H), 6.72-6.75 (d, 1H, J = 6.6 Hz), 6.97-7.01 (m, 2H) ppm. ^{13}C NMR ($CDCl_3$, 100 MHz, TMS, 298 K): δ 14.09, 22.66, 25.97, 29.13, 29.25, 29.33, 29.35, 31.81, 69.37, 69.53, 112.77, 115.14, 116.91, 123.41, 148.36, 150.03. MALDI/TOF-MS: m/z = 413.44 (calc. = 413.56).

Synthesis of 2. Compound **1** (5 g, 12.1 mmol) was dissolved in anhydrous THF (65 mL) by stirring under argon. The reaction temperature was reduced to –78 °C by using a slush bath (ethyl acetate/liq. N_2) and continued stirring for 10 minutes. 2.65 M *n*-BuLi solution in hexane (5.5 mL) was added

dropwise and the mixture was stirred at –78 °C for 1 h. 2-isopropoxy-4,4,5,5-tetramethyl-1,3,2-dioxaborolane (6.75 g, 36.3 mmol) was added rapidly to the reaction mixture, and the resulting mixture was warmed to room temperature and stirred overnight. The mixture was poured into water and extracted with ether. The organic layer was washed with brine and dried over anhydrous $MgSO_4$. The solvent was removed under reduced pressure and the crude product was purified by column chromatography (silica gel) with hexane: $CHCl_3$ = 2:1 as eluent to provide the pure product as liquid. (3.93 g, 71% yield). ^{1}H NMR ($CDCl_3$, 400 MHz, TMS, 298 K): δ 0.86-0.90 (m, 6H), 1.25-1.29 (m, 16H), 1.31 (s, 12H), 1.33-1.37 (m, 4H), 1.78-1.85 (m, 4H), 3.97-4.04 (m, 4H), 6.86-6.88 (d, 1H, J = 8 Hz), 7.29 (s, 1H), 7.37-7.39 (d, 1H, J = 7.8 Hz) ppm. ^{13}C NMR ($CDCl_3$, 100 MHz, TMS, 298 K): δ 14.09, 22.66, 24.84, 25.98, 26.04, 29.17, 29.26, 29.28, 29.38, 31.83, 68.84, 69.20, 83.54, 112.64, 119.34, 128.58, 148.47, 151.91. MALDI/TOF-MS: m/z = 460.51 (calc. = 460.67).

Synthesis of IFO. A 50 mL two-necked round bottom flask was charged with 2,8-dibromoindeno[1,2-b]fluorene-6,12-dione (856.2 mg, 1.95 mmol) and compound **2** (1.97 g, 4.28 mmol), sodium carbonate (1.24 g, 11.67 mmol), and evacuated and back-filled with Ar gas three times. Then 9.0 mL of dry toluene, 3.0 mL EtOH and 3.0 mL water which were already deaerated for 30 min were added under Ar. The mixture was stirred vigorously and refluxed at 90°C, tetrakis(triphenylphosphine)palladium (224.8 mg, 0.2 mmol) was then added to the reaction mixture. After the stirring was continued for 24 hours, the mixture was then allowed to cool to room temperature and the solvent was evaporated by reduced pressure. Water was poured into the reaction mixture and extracted by DCM for three times, the combined organic layer was washed by brine and dried over anhydrous $MgSO_4$. The crude product was purified by column chromatography (silica gel) with hexane: $CHCl_3$ (1:1) as the eluent, affording the pure product as a dark blue solid (736 mg, 45%). ^{1}H NMR ($CDCl_3$, 400 MHz, TMS, 298 K): δ 0.87-0.91 (m, 12H), 1.30-1.35 (m, 40H), 1.82-1.88 (m, 8H), 4.03-4.10 (m, 8H), 6.95-6.97 (d, 2H, J = 8 Hz), 7.15-7.17 (m, 4H), 7.58-7.60 (d, 2H, J = 7.6 Hz), 7.73-7.76 (d, 2H, J = 8 Hz), 7.83 (s, 2H), 7.89 (s, 2H), ppm. ^{13}C NMR ($CDCl_3$, 100 MHz, TMS, 298 K): δ 14.10, 22.67, 26.05, 29.29, 29.39, 31.83, 69.31, 69.52, 112.44, 113.89, 115.93, 119.37, 120.89, 122.72, 132.34, 133.29, 134.65, 139.63, 141.68, 142.60, 145.66, 149.47, 149.51, 193.04. MALDI/TOF-MS: m/z = 947.91 (calc. = 947.35). Anal. Calcd for $C_{64}H_{82}O_6$•H_2O: C, 79.63; H, 8.77. Found: C, 80.02; H, 8.65.

Synthesis of FO. A 50 mL two-necked round bottom flask was charged with 2,7-dibromo-9-fluorenone (400 mg, 1.17 mmol) and compound **2** (1.18 g, 2.58 mmol), sodium carbonate (0.74 g, 7

mmol), and evacuated then back-filled with Ar gas three times. Then 12.0 mL of dry toluene, 3.0 mL EtOH and 3.0 mL water which were already deaerated for 30 min were added under Ar. The mixture was stirred vigorously and refluxed at 90°C, tetrakis(triphenylphosphine)palladium (40.58 mg, 0.1 mmol) was then added to the reaction mixture. After the stirring was continued for 24 hours, the mixture was then allowed to cool to room temperature and the solvent was evaporated by reduced pressure. Water was poured into the reaction mixture and extracted by DCM for three times, the combined organic layer was washed by brine and dried over anhydrous $MgSO_4$. The crude product was purified by column chromatography (silica gel) with hexane: $CHCl_3$ (2:1) as the eluent, affording the pure product as orange powder (680.7 mg, 69% yield). ^{1}H NMR ($CDCl_3$, 400 MHz, TMS, 298 K): δ 0.87-0.91 (m, 12H), 1.25-1.34 (m, 32H), 1.81-1.88 (m, 8H), 4.03-4.10 (m, 8H), 6.95-6.97 (d, 2H, J = 8 Hz), 7.15-7.17 (m, 4H), 7.55-7.57 (d, 2H, J = 7.6 Hz), 7.68-7.69 (d, 2H, J = 7.2 Hz), 7.87 (s, 2H), ppm. ^{13}C NMR ($CDCl_3$, 100 MHz, TMS, 298 K): δ 14.20, 22.77, 26.15, 29.39, 29.49, 31.92, 69.42, 69.60, 76.77, 77.10, 77.41, 112.58, 114.04, 119.40, 120.68, 122.71, 132.82, 132.93, 135.24, 142.07, 142.07, 142.70, 149.43, 149.55, 194.27. MALDI/TOF-MS: m/z = 845.41 (calc. = 845.26). Anal. Calcd for $C_{57}H_{80}O_5 \bullet H_2O$: C, 79.31; H, 9.57. Found: C, 79.56; H, 9.45.

Preparation of IFO-doped and FO-doped films.

The **IFO** (2 mg) or **FO** (2 mg) and polysulfone (**PSF**) or polystyrene (**PS**) (200 mg) were dissolved in 2 mL of $CHCl_3$, and the solution was drop-casted onto the surface of quartz cell. The transparent polysulfone or polystyrene films of the **IFO** were obtained by slow evaporation of $CHCl_3$.

Acetonitrile detection by the IFO-doped PS film.

The **IFO** doped **PS** film was fabricated by drop casting from a $CHCl_3$ solution containing **IFO** (1 wt%) onto the surface of quartz cells until complete evaporation of $CHCl_3$. Pipette drops (*ca.* 80 μL) of organic solvents (MCH, DCM, $CHCl_3$, THF and toluene, acetonitrile, ethyl acetate and methanol) were placed onto the **IFO**-embedded **PS** film and resulting luminescent color change was monitored after 10 min.

Reference

1. (*a*) H. B. Wu, L. Ying, W. Yang and Y. Cao, *Chem. Soc. Rev.*, 2009, **38**, 3391; (*b*) H. B. Wu, G. J. Zhou, J. H. Zou, C. L. Ho, W. Y. Wong, W. Yang, J. B. Peng and Y. Cao, *Adv. Mater.*, 2009, **21**, 4181; (*c*) K. T. Kamtekar, A. P. Monkman and M. R. Bryce, *Adv. Mater.*, 2010, **22**, 572; (*d*) G. M. Farinola and R. Ragni, *Chem. Soc. Rev.*, 2011, **40**, 3467.
2. (*a*) J. Y. Li, D. Liu, C. W. Ma, O. Lengyel, C. S. Lee, C. H. Tung and S. Lee, *Adv. Mater.*, 2004, **16**, 1538; (*b*) Y. Liu, M. Nishiura, Y. Wang and Z. M. Hou, *J. Am. Chem. Soc.*, 2006, **128**, 5592; (*c*) G. L. Tu, C. Y. Mei, Q. G. Zhou, Y. X. Cheng, Y. H. Geng, L. X. Wang, D. G. Ma, X. B. Jing and F. S. Wang, *Adv. Funct. Mater.*, 2006, **16**, 101; (*d*) M. J. Park, J. Kwak, J. Lee, I. H. Jung, H. Kong, C. Lee, D. H. Hwang and H. K. Shim, *Macromolecules*, 2010, **43**, 1379; (*e*) M. G. Han, Y. Tian, Z. Yuan, L. Zhu and B. W. Ma, *Angew. Chem. Int. Ed.*, 2014, **53**, 10908; (*f*) Q. Y. Yang and J. M. Lehn, *Angew. Chem. Int. Ed.*, 2014, **53**, 4572; (*g*) C. K. Zhou, Y. Tian, Z. Yuan, M. G. Han, J. Wang, L. Zhu, M. S. Tameh, C. Huang and B. W. Ma, *Angew. Chem. Int. Ed.*, 2015, **54**, 9591.
3. (*a*) J. Y. Hu, Y. J. Pu, G. Nakata, S. Kawata, H. Sasabe and J. Kido, *Chem. Commun.*, 2012, **48**, 8434; (*b*) J. Y. Hu, Y. J. Pu, Y. Yamashita, F. Satoh, S. Kawata, H. Katagiri, H. Sasabe and J. Kido, *J. Mater. Chem. C*, 2013, **1**, 3871; (*c*) Z. Chen, X. K. Liu, C. J. Zheng, J. Ye, C. L. Liu, F. Li, X. M. Ou, C. S. Lee and X. H. Zhang, *Chem. Mater.*, 2015, **27**, 5206; (*d*) X. K. Liu, Z. Chen, J. Qing, W. J. Zhang, B. Wu, H. L. Tam, F. R. Zhu, X. H. Zhang and C. S. Lee, *Adv. Mater.*, 2015, **27**, 7079; (*e*) E. Ravindran, S. J. Ananthakrishnan, E. Varathan, V. Subramanian and N. Somanathan, *J. Mater. Chem. C*, 2015, **3**, 4359.
4. (*a*) J. Seo, S. Kim and S. Y. Park, *J. Am. Chem. Soc.*, 2004, **126**, 11154; (*b*) S. Park, O. H. Kwon, S. Kim, S. Park, M. G. Choi, M. Cha, S. Y. Park and D. J. Jang, *J. Am. Chem. Soc.*, 2005, **127**, 10070; (*c*) S. Park, J. E. Kwon, S. H. Kim, J. Seo, K. Chung, S. Y. Park, D. J. Jang, B. M. Medina, J. Gierschner and S. Y. Park, *J. Am. Chem. Soc.*, 2009, **131**, 14043; (*d*) J. E. Kwon and S. Y. Park, *Adv. Mater.*, 2011, **23**, 3615; (*e*) H. Shono, T. Ohkawa, H. Tomoda, T. Mutai and K. Araki, *ACS Appl. Mater. Inter.*, 2011, **3**, 654; (*f*) K. C. Tang, M. J. Chang, T. Y. Lin, H. A. Pan, T. C. Fang, K. Y. Chen, W. Y. Hung, Y. H. Hsu and P. T. Chou, *J. Am. Chem. Soc.*, 2011, **133**, 17738; (*g*) N. Suzuki, A. Fukazawa, K. Nagura, S. Saito, H. Kitoh-Nishioka, D. Yokogawa, S. Irle and S. Yamaguchi, *Angew. Chem. Int. Ed.*, 2014, **53**, 8231.
5. (*a*) K. C. Moss, K. N. Bourdakos, V. Bhalla, K. T. Kamtekar, M. R. Bryce, M. A. Fox, H. L. Vaughan, F. B. Dias and A. P. Monkman, *J. Org. Chem.*, 2010, **75**, 6771; (*b*) X. H. Jin, C. Chen, C. X. Ren, L. X. Cai and J. Zhang, *Chem. Commun.*, 2014, **50**, 15878; (*c*) X. C. Wang, L. Zhao, S. Y.

Shao, J. Q. Ding, L. X. Wang, X. B. Jing and F. S. Wang, *Macromolecules*, 2014, **47**, 2907; (*d*) Y. I. Park, O. Postupna, A. Zhugayevych, H. Shin, Y. S. Park, B. Kim, H. J. Yen, P. Cheruku, J. S. Martinez, J. W. Park, S. Tretiak and H. L. Wang, *Chem. Sci.*, 2015, **6**, 789; (*e*) E. Yamaguchi, C. G. Wang, A. Fukazawa, M. Taki, Y. Sato, T. Sasaki, M. Ueda, N. Sasaki, T. Higashiyama and S. Yamaguchi, *Angew. Chem. Int. Ed.*, 2015, **54**, 4539; (*f*) S. K. Park, I. Cho, J. Gierschner, J. H. Kim, J. H. Kim, J. E. Kwon, O. K. Kwon, D. R. Whang, J. H. Park, B. K. An and S. Y. Park, *Angew. Chem. Int. Ed.*, 2016, **55**, 203.

6. (*a*) G. Qian, B. Dai, M. Luo, D. B. Yu, J. Zhan, Z. Q. Zhang, D. G. Ma and Z. Y. Wang, *Chem. Mater.*, 2008, **20**, 6208; (*b*) J. L. Wang, Q. Xiao and J. Pei, *Org Lett*, 2010, **12**, 4164; (*c*) P. J. Homnick, J. S. Tinkham, R. Devaughn and P. M. Lahti, *J. Phys. Chem. A*, 2014, **118**, 475; (*d*) X. F. Lu, S. H. Fan, J. H. Wu, X. W. Jia, Z. S. Wang and G. Zhou, *J. Org. Chem.*, 2014, **79**, 6480.
7. (*a*) N. J. Turro, V. Ramamurthy and J. C. Scaianon, *Modern Molecular Photochemistry of Organic Molecules*, University Science Books, Sausalito, 2010; (*b*) N. J. Turro, V. Ramamurthy and J. C. Scaiano, *Photochem Photobiol*, 2012, **88**, 1033.
8. H. Usta, A. Facchetti and T. J. Marks, *Org. Lett.*, 2008, **10**, 1385.
9. (*a*) L. Biczok, T. Berces and F. Marta, *J. Phys. Chem.*, 1993, **97**, 8895; (*b*) J. L. Jamison, L. Davenport and B. W. Williams, *Chem. Phys. Lett.*, 2006, **422**, 30; (*c*) L. A. Estrada, J. E. Yarnell and D. C. Neckers, *J. Phys. Chem. A*, 2011, **115**, 6366; (*d*) M. Shigeta, M. Morita and G. Konishi, *Molecules*, 2012, **17**, 4452; (*e*) I. Ghosh, A. Mukhopadhyay, A. L. Koner, S. Samanta, W. M. Nau and J. N. Moorthy, *Phys. Chem. Chem. Phys.*, 2014, **16**, 16436.
10. B. H. Jhun, K. Ohkubo, S. Fukuzumi and Y. You, *J. Mater. Chem. C*, 2016, **4**, 4556.
11. M. S. Kwon, J. H. Jordahl, A. W. Phillips, K. Chung, S. Lee, J. Gierschner, J. Lahann and J. Kim, *Chem. Sci.*, 2016, **7**, 2359.
12. The photophysical properties of **IFO** are investigated in $CHCl_3$, DCM, DMF, THF, MCH and *p*-xylene due to their good solubility and variation of polarity. In DCM and $CHCl_3$, **IFO** is non-emissive.
13. No additional fluorescent peaks were observed in DMF when the concentration of **IFO** was increased from 5 μM to 40 μM.
14. (*a*) S. I. Hintschich, C. Rothe, S. M. King, S. J. Clark and A. P. Monkman, *J Phys. Chem. B*, 2008, **112**, 16300; (*b*) X. C. Wang, L. Zhao, S. Y. Shao, J. Q. Ding, L. X. Wang, X. B. Jing and F. S. Wang, *Polym. Chem.*, 2014, **5**, 6444.
15. J. Do, J. Huh and E. Kim, *Langmuir*, 2009, **25**, 9405.

16. The absolute quantum yield Φ_F is determined to be 2.5%.

17. (*a*) J. Bang, U. Jeong, D. Y. Ryu, T. P. Russell and C. J. Hawker, *Adv. Mater.*, 2009, **21**, 4769; (*b*) J. Lee, H. T. Chang, H. An, S. Ahn, J. Shim and J. M. Kim, *Nat. Commun.*, 2013, **4**, 2461; (*c*) S. Furukawa, H. Shono, T. Mutai and K. Araki, *ACS Appl. Mater. Inter.*, 2014, **6**, 16065.

Appendix:

^{1}H NMR of **IFO** (400 MHz, in $CDCl_3$)

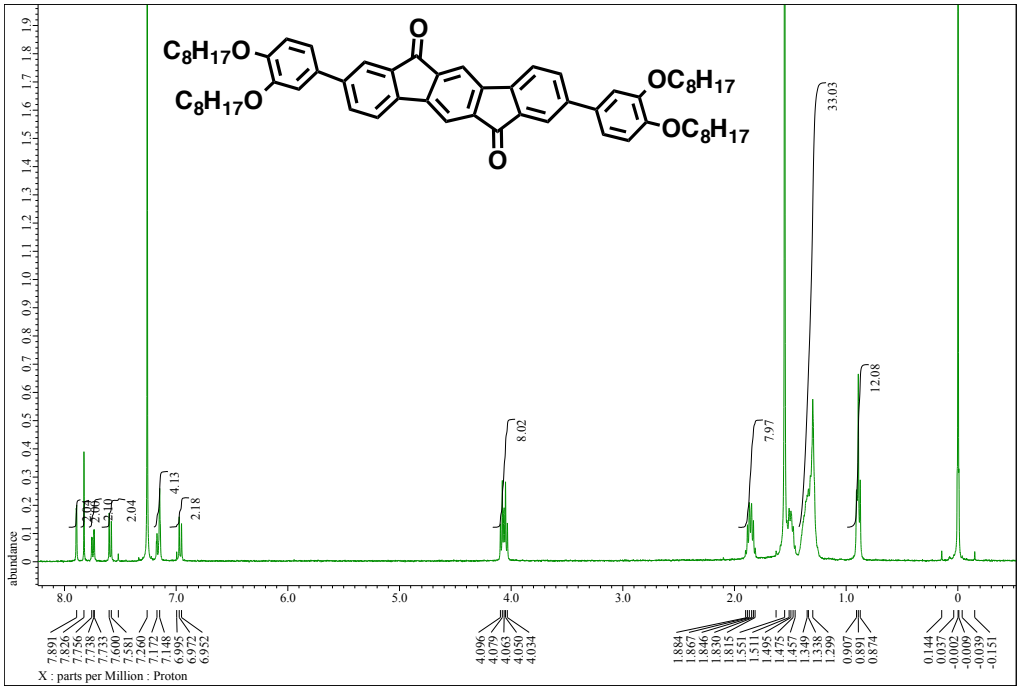

^{13}C NMR of **IFO** (100 MHz, in $CDCl_3$)

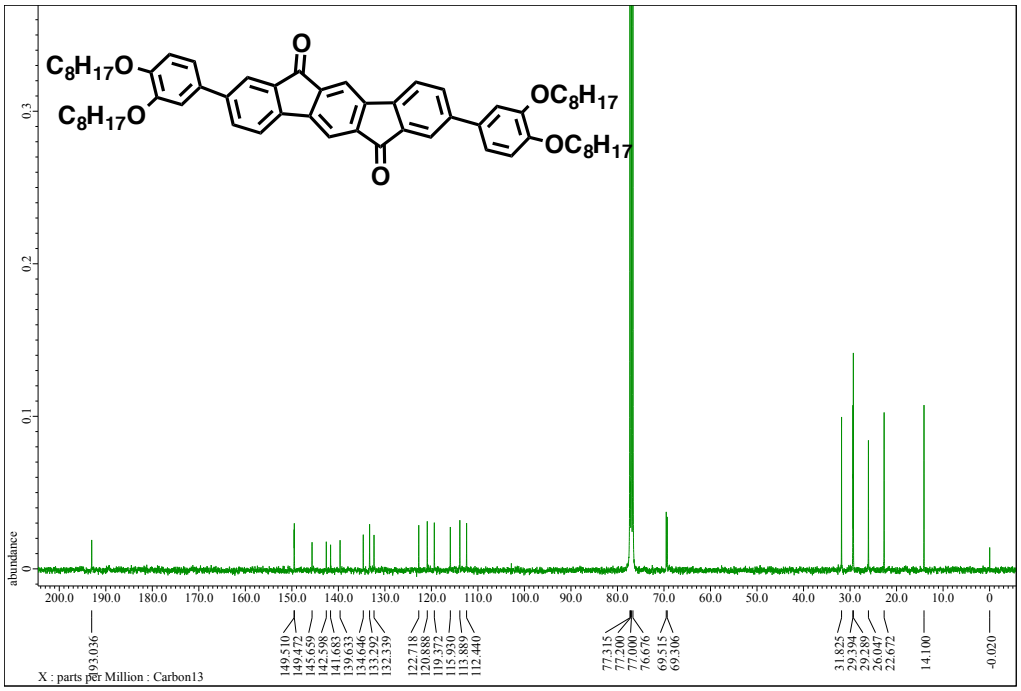

^{1}H NMR of **FO** (400 MHz, in $CDCl_3$)

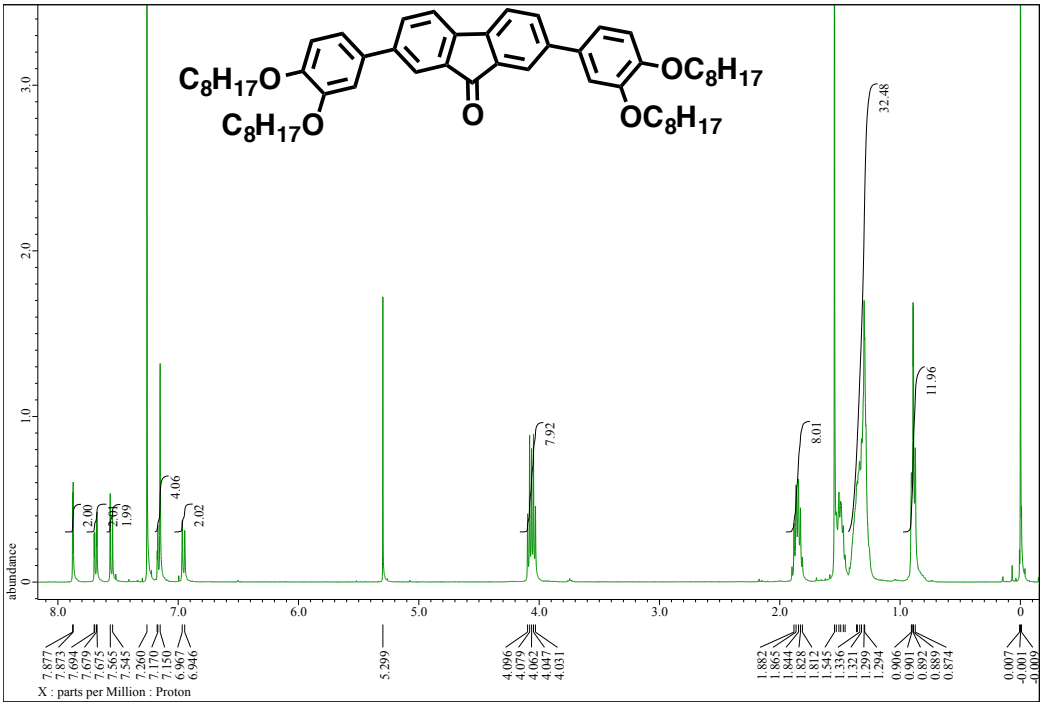

^{13}C NMR of **FO** (100 MHz, in $CDCl_3$)

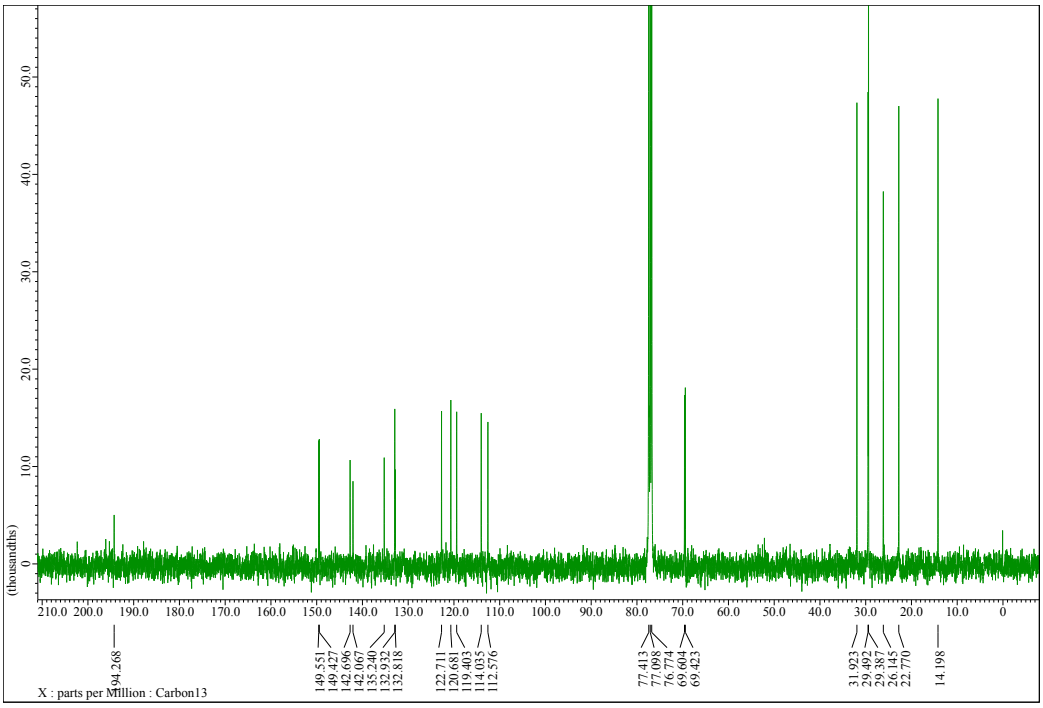

Conclusions

This thesis has focused on control over the deactivation pathways and supramolecular organizations of fluorene-based materials by rational molecular design strategies to achieve fluorene-based functional materials aiming at exploring unique photo-physical properties and interesting functionalities.

In chapter 1, the novel and unexpected phenomenon has been described that metal-free pure organic fluorene derivative bearing the bromide and aldehyde groups (**Br–FL–CHO**) was demonstrated experimentally and theoretically to exhibit phosphorescence in conventional organic solvents and embedded in polymer matrixes at room temperature. The spectroscopic techniques, time-resolved photoluminescence studies and quantum chemical calculations have been utilized to investigate the photophysical properties of **Br–FL–CHO**. The characteristic features of phosphorescence have been observed and confirmed as evident from dioxygen-quenching emission and long luminescent lifetime. The introduction of different substitutes into fluorene core provided a better understanding of the relationship between structural modification and observed photophysical properties of a given system, indicating that the combination of bromine and aldehyde groups are responsible for facilitating phosphorescence in solution at room temperature. Moreover, the electronic structures for the ground state, excited singlet and triplet states of related compounds were studied using TD-DFT calculation to illustrate the plausible mechanism of the observed phenomenon, which is in accordance with experimental results.

In chapter 2, a new RGB trichromophoric nanoparticle system with white emission assisted by dual FRET was constructed for highly sensitive fluorogenic dectection of polyanions. This system is consisting of blue emitting cationic oligofluorene nanoparticle (B), a red emitting neutral dye (R) and a green emitting anionic dye (G). By taking advantage of nano-structural architecture of oligofluorene nanoparticles, we are able to spatially organize two acceptor dyes interior and exterior of nanoparticle separately. The red emitting dye was encapsulated into the oligofluorene nanoparticles participating in interior FRET, while the green emitting anionic dye was adsorbed on the positively-charged surface of the nanoparticles by electrostatic interactions to undergo exterior FRET. Distinct two signaling pathways are free from sequential FRET, which allowed us to generate full-color emission especially white in aqueous medium and film state. Furthermore, the characteristic white emissive trichromophoric nanoparticle was applied for poly-anions sensing in aqueous medium, wherein

nanoparticle exhibited ratio-metric and drastic visible response upon addition of poly-anions such as bovine serum albumin and heparin with the low detection limit of mg/mL and ng/mL, respectively.

In chapter 3, the new donor-acceptor-donor type fluorophore, **IFO**, having indenofluorenedione chromophore as an electron-accepting unit with dialkoxyphenyl groups as weak electron donating moieties was synthesized and investigated. In stark contrast to the typical solvatochromic behaviors of conventional **ICT** molecules that fluorescence is progressively red-shifted in correlation with the solvent polarity, **IFO** showed unusual solvatochromic behavior: blue emission was observed in dimethylformamide (DMF), orange in methylcyclohexane (MCH), and red in *p*-xylene. Fluorescent channels, namely the locally excited and **ICT** states, can be controllably switched on and off by solvent induction, resulting in environmental polarity sensitive multi-luminescence. Furthermore, **IFO** also showed high sensitivity towards micro-environmental polarity even when **IFO** was embedded in the polymer matrix. The visible discrimination of polar solvents such as acetonitrile, ethyl acetate and methanol from common organic solvents was successfully demonstrated.

Fluorene-based π-conjugated systems are quite attractive for a wide diversity of accessible structures towards various applications. With unique molecular designs, preminary results presented in this thesis would not only provide a new strategy for the design of new fluorene-based functional materials especially with unique photo-physical properties, but also afford the development of nanostructural architectures with potential applications in bio-related sensing or imaging and dioxygen-sensors based on purely organic phosphors under ambient conditions can be expected in the near future.

Major achievements of this thesis are as follows:

List of publications

(1) Phosphorescence from pure organic fluorene derivative in solution at room temperature
J. Xu, A. Takai, Y. Kobayashi, M. Takeuchi*, *Chem. Commun.*, 2013, **49**, 8447-8449.
(**Highlighted as Inside Front Cover of the issue)**

(2) Red-Green-Blue trichromophoric nanoparticles with dual fluorescence resonance energy transfer: highly sensitive fluorogenic response toward polyanions
J. Xu, A. Takai, M. Takeuchi*
Chem.-Eur. J. 2016, **in press**. (DOI: 10.1002/chem.201602759)

(3) Multiple emissions from indenofluorenedione in solution and in polymer film
J. Xu, A. Takai, M. Takeuchi* *RSC Adv.*, 2016, **6**, 80867–80871.

Presentations at International Conferences:

Poster presentations:
(1) J. Xu, A. Takai, M. Takeuchi
"Full Color Fluorescence from RGB Trichromophoric Nanoparticle System Assisted by Dual FRET in Aqueous Medium towards Visual Bio-sensing" 12th International Symposium on Functional π Electron Systems, Settle, WA, USA. July 19-24, 2015.
(2) J. Xu, M. Takeuchi
"Full Color Fluorescence from RGB Trichromophoric Nanoparticle System Assisted by Dual-FRET in Aqueous Medium toward Visual Bio-sensing" The 10th SPSJ International Polymer Conference (IPC 2014), Tsukuba, Dec. 2-4, 2014.
(3) J. Xu, M. Takeuchi
"Control over Energy Transfer Pathways Using Surface-Charged Nanoparticles of Oligofluorene toward Color Tunable Sensors" The π-System Figuration for Rising Generation, Atami, Nov. 21-22, 2014.
(4) J. Xu, M. Takeuchi

"Phosphorescence from Pure Organic Fluorene Derivative in Solution at Room Temperature" The π-System Figuration for Rising Generation, Atami, Nov. 21-22, 2014.

(5) J. Xu, A. Takai, M. Takeuchi

"Full Color Fluorescence from RGB Trichromophoric Nanoparticle System Assisted By Dual-FRET in Aqueous Medium towards Visual Bio-sensing" NIMS Conference 2014, Tsukuba, July 1-3, 2014.

(6) J. Xu, M. Takeuchi

"Full Color Fluorescence from RGB Trichromophoric Nanoparticle System Assisted by Dual FRET in Aqueous Medium towards Visual Bio-sensing" CEMS International Symposium on Supramolecular Chemistry and Functional Materials, Tokyo, Dec. 15-17, 2013.

(7) J. Xu, A. Takai, M. Takeuchi

"Phosphorescence from Pure Organic Fluorene Derivative in Solution at Room Temperature" NIMS Conference 2013, July 01-03, 2013.

(8) J. Xu, A. Takai, M. Takeuchi

"Phosphorescence from Pure Organic Fluorene Derivative in Solution at Room Temperature" The 6th MANA International Symposium 2013, Tsukuba, Feb. 27-Mar. 01, 2013.

(9) J. Xu, A. Takai, M. Takeuchi

"Phosphorescence Emission from Pure Organic Materials in Solution at Ambient Temperature" The 12th International Kyoto Conference on New Aspects of Organic Chemistry, Kyoto, Nov. 12-16, 2012.

Oral presentations:

J. Xu, M. Takeuchi

"Control over Energy Transfer Pathways Using Surface-Charged Nanoparticles of Oligofluorene toward Color Tunable Sensors" The π-System Figuration for Rising Generation, Atami, Nov. 21-22, 2014.

Acknowledgments

The author would like to express her deepest respect and gratitude to Prof. Masayuki Takeuchi for his continuous guidance, support and encouragement through her PhD study.

The author would like to thank Prof. Kazushi Miki, Prof. Masanobu Naito from NIMS and Prof. Yohei Yamamoto from University of Tsukuba for nice discussions and comments.

The author is also great grateful to Prof. Kazunori Sugiyasu and Dr. Atsuro Takai for their valuable suggestions and directional leading. Thank you for all the members in Prof. Masayuki Takeuchi's group for their kind help, valuable discussion on these research projects and friendship.

The author acknowledges financial support from National Institute for Materials Science (NIMS) for Junior Researcher and Japan Society for the Promotion of Science (JSPS) for Yong Scientist.

Finally, the author appreciates the tremendous supports from her family and friends.

Tsukuba, Japan

August 2016

Jinjia XU

Department of Materials Science and Engineering

Graduate School of Pure and Applied Sciences

University of Tsukuba, Japan